A Kinetic Treatment of a Perpendicular Gradient in Field-aligned Flow in a Thermally Anisotropic Plasma

Robert S. Spangler

Thesis submitted to the College of Arts and Sciences at
West Virginia University
In partial fulfillment of the requirements for the degree of

Masters of Science
in
Physics

E. E. Scime, Ph. D., chair
M.E. Koepke, Ph.D.
G. Ganguli, Ph.D.

Department of Physics

ABSTRACT

The linearized dispersion relation describing waves in a plasma having a uniform magnetic field, uniform density, and inhomogeneous parallel (to the magnetic field) flow [G. Ganguli, M.J. Keskinen, H. Romero, R. Heelis, T. Moore, and C. Pollock, *J. Geophys. Res., 99,* 8873 (1994)] is generalized to include thermal anisotropy, a key feature existing in many space and laboratory plasmas. The effects of ion thermal anisotropy on the ion acoustic mode is examined. The growth rate of the ion acoustic mode is shown to increase with $T_{i\perp}/T_{i\|}$, and the real frequency at which the maximum growth rate occurs is shown to upshift significantly. The angle that an ion acoustic wave propagates is also shown to depend on $T_{i\perp}/T_{i\|}$. A limited examination of the effects of ion thermal anisotropy on the ion cyclotron mode is presented. The growth rate of the ion cyclotron mode in the presence of inhomogeneous flow is shown to increase with $T_{i\perp}/T_{i\|}$ and the real frequency is not significantly affected. Also presented is a generalized calculation of perturbed distribution functions [Sarfaty, M., S. DeSouza Machado, F. Skiff, *Phys. Plasmas*, 3, 4316, (1996); Skiff, F., *IEEE Transactions of Plasma Science*, 20, 701 (1992)] to include shear in field-aligned flow. Without shear, the first order perturbed distribution as a function of $v_{\|}$ is independent of the orientation of the wavevector in the plane perpendicular to the background magnetic field. A method of determining the wavevector components present in a plasma with shear in the parallel flow is suggested.

ACKNOWLEDGEMENTS

It brings me pleasure to thank several people for their help, both active and passive, in my research. I thank my parents for putting up with me for all these years. I'm glad that something came from all the years of seemingly random endeavors that they endured with great patience and encouragement. I thank my grandparents, who took the time to hike with me and had the wisdom not to tell me that leprechauns don't exist. I thank my advisor, Dr. Earl Scime, for having the energy and motivation to train a theorist. He deserves applause for his ability to use his background and love of science to motivate others and allow me to develop as a person. He is an optimist when it comes to interactions with others, and I believe it is for good reason. I am greatly indebted to Dr. Gurudas Ganguli. Only with his guidance and kindness was this research even remotely possible. He showed me the importance and elegance of doing things the easy way. I thank Dr. Valeriy Gavrishchaka for sharing his computational feats with me. I thank Dr. Mark Koepke for his animated chalkboard plasma wave illustrations. I extend thanks to Dr. Boyd Edwards for entertaining lectures and to John Kline for several informative discussions about the nature of perturbed distribution functions and computer coding. Dr. Matt Balkey has made a world of difference in my time here by being a fun guy and a great friend. I'm glad you could show me down the Big Sandy! I thank April Moncrief for her patience and her ability to reorganize my piles of papers into fewer piles. Much of this work was supported by the Naval Research Laboratory, whose hospitality is greatly appreciated. I'd also like to thank Kahlil Gibran for enhancing my delight in the world around me.

TABLE OF CONTENTS

I. MOTIVATION

A predictive capability of the near Earth environment has long been a cherished goal for the space physics community. This goal, however, is yet to be realized. The primary reason for this is that the exploration of the near Earth space environment, which is essentially a plasma medium subject to external forcing, has been a challenging endeavor. In particular, the Earth's auroral region is found to be highly turbulent with enhanced wave activity, plasma heating, heavy ion out-flow, and other dynamic processes. Therefore, the understanding of the plasma processes accompanying auroral phenomena has been a major goal in contemporary space physics research. Early space-probe measurements lacked fine resolution in time and space so physics at smaller scale sizes, such as wave-particle interactions and spatial inhomogeneities, remained under-resolved. This was significant since many of the properties of a collisionless plasma medium are influenced by wave-particle interactions. With the advent of modern space probes, such as Viking, Freja, FAST, AMICIST, Auroral Turbulence-2, etc., high-resolution observations of auroral phenomena became possible. A major revelation from these missions was that the auroral region is highly structured with spatial scale sizes as small as a few ion gyroradii. Localized static (or quasi-static) electric fields both perpendicular [*Ivchenko et al*., 1999; *Marklund et al*., 1994; *Mishin and Forster*, 1995] and parallel [*Ergun et al.*, 1998] to the magnetic field were found to be collocated with waves and coherent structures as well as with enhanced ion temperatures [*Andre et al.*, 1990; 1998; *Lynch et al.*, 1996; *Norqvist et al.*, 1998; *Knudsen et al*., 1998]. Clearly, the understanding of the cause and effect of the observed waves and their correlation with small-scale structures and ion heating became an important topic of research.

One topic that received considerable theoretical and experimental attention was the investigation of the role of inhomogeneous perpendicular (to the background magnetic field) electric fields in both space and laboratory plasmas. Because of the $\boldsymbol{E} \times \boldsymbol{B}$ drift in a plasma, an inhomogeneous, perpendicular electric field results in a perpendicular gradient in the perpendicular flow. Motivated by space observations [*Mozer et al*., 1981], a general kinetic theory that included a perpendicular localized electric field [*Ganguli et al*., 1985a; 1985b; 1988] was developed at the Naval Research Laboratory. The theory predicted the existence of a new branch of plasma oscillations that could explain the observation of ion-cyclotron like modes and the associated ion heating in the presence of paired electrostatic shocks [*Mozer et*

al., 1977]. Although the early laboratory experiments [*Sato et al*., 1986; *Alport et al*., 1986] focused on how inhomogeneities could be responsible for discrepancies between the experimental data and theoretical predictions for the current driven ion cyclotron mode, later experiments were designed specifically to investigate the predictions of the generalized theoretical model [*Koepke et al.*, 1994, 1998, 1999; *Amatucci et al.*, 1994; 1996], and were successful. Detailed application of the transverse electric field model to space plasmas followed [*Gavrishchaka*, 1996, 1997]. A review of these early activities can be found in *Ganguli* [1997].

While perpendicular, localized electric fields account for a number of observed features in the auroral region, others, such as observations of localized field-aligned flows correlated with ion-acoustic-like features in wave specta, remain unexplained. Localized field-aligned flows were added to the kinetic model [*Ganguli et al.*, 1994; *Ganguli* et al., 1999], and detailed applications of the theoretical model to space plasmas were produced [*Gavrishachaka et al.*, 1998; 1999*; Ganguli et al.*, 1988].

Application of the general kinetic formalism of *Ganguli et al*. [1994] to a typical ionospheric plasma [*Gavrishachaka et al.*, 1998; 1999] predicted that a gradient in the parallel flow lowers the threshold current for the ion-acoustic mode below that of the ion-cyclotron mode and allows it to propagate even when the ion temperature (T_i) exceeds the electron temperature (T_e). This was a major departure from the classical characteristics of the ion-acoustic modes as discussed by *Kindel and Kennel* [1971]. The physical consequences of velocity shear can be understood from the simplified shear modified dispersion relation for the ion acoustic mode [*Gavrishachaka et al.*, 1998]

$$\omega = k_z c_s \sigma + i\left(\text{Landau Resonance Terms}\right) \tag{1}$$

where

$$\sigma^2 = 1 - \frac{k_y}{k_z}\frac{dV_0}{dx}\frac{1}{\Omega_i}.$$

Here $V_{di}(x)$ is the inhomogeneous flow along the magnetic field (B_0) in the z direction, k_y and k_z are wave numbers in the y and z directions, $\omega = \omega_r + i\gamma$ is the complex wave frequency, and $c_s = (T_e/m_i)^{1/2}$ is the sound speed. For no shear ($\mathrm{d}V_{di}/\mathrm{d}x = 0$), the classical ion acoustic limit is recovered. If $\sigma^2 < 0$, then the narrowband instability around $\omega_r = 0$ in the drifting ion frame

[*D'Angelo*, 1965] is recovered. The $\sigma^2 > 0$ regime was first addressed by *Gavrishachaka et al.*, [1998]. For $\sigma^2 > 1$, shear increases the parallel phase speed (ω_r/k_z) of the ion acoustic mode (see Equation 1) and leads to a broadband frequency spectrum in the sub-cyclotron range. For a sufficiently large σ, the phase speed can be increased so much that ion Landau damping is greatly reduced. This leads to a much lower threshold for the ion acoustic mode and it can grow even for $T_i \geq T_e$ [*Gavrishachaka et al.*, 1998]. For wave propagation nearly perpendicular to B_0 ($k_y/k_z >> 1$), the magnitude of shear, i.e., dV_{di}/dx, needed to reduce the instability threshold is very small. This result may provide an explanation for the frequent observation of ion-acoustic like waves in ionospheric plasma where $T_i \sim T_e$ [*Knudsen and Wahlund,* 1998; *Wahlund et al.*, 1994a; 1994b; 1998]. Confirmation of a key theoretical prediction for the $\sigma^2 > 1$ case was reported by a recent laboratory experiment at the University of Iowa. They reported the spontaneous generation of ion-acoustic-like waves in a Q-machine plasma for which $T_i \sim T_e$ [*Agrimson et al.*, 2001]. Additional observations of ion-acoustic-like waves in the presence of inhomogeneous field-aligned flow in a Q-machine were reported at West Virginia University [Teodorescu et al., 2001].

Another unresolved issue concerning the FAST data is correlation of localized parallel ion beams (perpendicular gradients in the field-aligned flow) with large-amplitude ion cyclotron waves having broadband frequency spectra [*Ergun et al.*, 1998; *Mcfadden et al.*, 1998]. Although there has long been evidence of shear in parallel flows in the auroral ionosphere [*Kintner*, 1976; *Potemra et al.*, 1978; *Heelis et al.*, 1984], recent FAST observations provide evidence of strong shear ($dV_0/dx \sim \Omega_{O+}$) [*McFadden et al.*, 1998; *Amatucci*, 1999]. Extending the model for the ion-acoustic waves to large transverse shear magnitudes, *Gavrishachaka et al.*, [2000] found that in addition to the ion-acoustic waves, a shear in the parallel ion flow can also give rise to instabilities at multiple ion cyclotron harmonics. Thus, the parallel velocity shear mechanism could also explain FAST observations of large-amplitude ion cyclotron waves, especially in the upward current region of the auroral ionosphere [*Ergun et al.*, 1998] where evidence of strong shear exists.

Before discussing the specific details of this work, it is useful to review the general formalism of *Ganguli et al.*, [1994], including the effects of spatial inhomogeneities, or perpendicular gradients, in the field aligned flow. First consider a simple locally linear flow (i.e., $V_{0\alpha}(x) = V_{0\alpha} + (dV_{0\alpha}/dx)\, x$, where $V_{0\alpha}$ and $(dV_{0\alpha}/dx)$ are constants and α represents the species) with no equilibrium electric field. Also, for simplicity, let $dV_{0i}/dx = dV_{0e}/dx \equiv dV_0/dx$.

Transform to the ion frame (i.e., $V_{0i} = 0$) so that V_{0e} represents the relative electron-ion parallel drift. In the local limit these assumptions lead to the dispersion relation given by [*Gavrishchaka et al*., 1998; 1999],

$$1 + \sum_n \Gamma_n(b) F_{ni} + \tau(1 + F_{0e}) + k^2 \lambda_{Di}^2 = 0 \tag{2}$$

$$F_{0e} = \left(\frac{\omega - k_z V_{de}}{\sqrt{2}\,|k_z|\,v_{te}}\right) Z\left(\frac{\omega - k_z V_0}{\sqrt{2}\,|k_z|\,v_{te}}\right) + \frac{k_y}{k_z}\frac{dV_0/dx}{\mu\Omega_i}\left[1 + \left(\frac{\omega - k_z V_{0e}}{\sqrt{2}\,|k_z|\,v_{te}}\right) Z\left(\frac{\omega - k_z V_{0e}}{\sqrt{2}\,|k_z|\,v_{te}}\right)\right]$$

$$F_{ni} = \left(\frac{\omega}{\sqrt{2}\,|k_z|\,v_{te}}\right) Z\left(\frac{\omega - n\Omega_i}{\sqrt{2}\,|k_z|\,v_{ti}}\right) + \frac{k_y}{k_z}\frac{dV_0/dx}{\mu\Omega_i}\left[1 + \left(\frac{\omega - n\Omega_i}{\sqrt{2}\,|k_z|\,v_{ti}}\right) Z\left(\frac{\omega - n\Omega_i}{\sqrt{2}\,|k_z|\,v_{ti}}\right)\right]$$

Here, $\Gamma_n(b) = I_n(b)\exp(-b)$ where I_n are the modified Bessel functions, $b = (k_y\rho_i)^2$, $\tau = T_i/T_e$, λ_D is the Debye length, and $\mu = M_i/m_e$ is the ion/electron mass ratio. In the low frequency, long wavelength limit, Eq. (2) reduces to Eq. (1) and for no shear (i.e., $dV_d/dx = 0$), it reduces to the dispersion relation of *Kindel and Kennel* [1971]. Using this formalism, *Gavrishchaka et al.* [2000] showed that a spatial gradient in the parallel ion flow can give rise to multiple ion cyclotron harmonics that can overlap to provide a broadband spectrum if the Doppler shift arising from the perpendicular (transverse) electric field is also taken into account. Nonlinear development of this spectrum gave rise to coherent structures in the parallel electric field similar to observations [*Gavrishchaka et al.,* 2000].

While the formalism discussed above takes into account the important spatial inhomogeneities and accounts for small-scale structures in the ionosphere, it does not include temperature anisotropy. Temperature anisotropy can significantly alter the dispersive properties of the plasma medium [*Stix*, 1962]. Since it was not known whether and how temperature anisotropy would alter the results of *Gavrishchaka et al*. [2000], and because temperature anisotropy is often seen in the ionospheric and magnetospheric measurements [*André et al*., 1990; *Anderson et al*., 1994], we were motivated to generalize the formulation of *Ganguli et al.*, [1994] to include temperature anisotropy and examine its effects. In this work we present the calculations for the generalized theory and discuss their relevance to the analysis and interpretation of the FAST observations and laboratory experiments. In addition, we will propose controlled experiments in the LEIA device [*Scime et al.*, 2000] that have the potential to validate the theoretical model.

During the process of including temperature anisotropy in the theory, we have also developed experimentally relevant first-order perturbed-distribution-function calculations ($f_1(v_j)$'s, where j represents one Cartesian component). In combination with laser induced fluorescence (LIF) (a non-invasive way to measure particle distribution functions in a plasma [*Stern and Johnson*, 1975]) the perturbed distribution functions can be used to determine the amplitude and wavelength of electrostatic fluctuations from a single point measurement [*Sarfaty et al.*, 1996; *Kline et al.*, 1999]. The first order distributions are each a function of one velocity component and include temperature anisotropy, parallel flow, and a perpendicular gradient in the parallel flow. Specifically, we outline how the velocity dependence of measured perturbed distribution functions, in comparison with theoretical predictions, can serve as a method of non-invasive wave identification.

In section II, the general principles of the calculation are discussed. The dispersion relationship is calculated in section III and the perturbed distribution functions are reviewed in section IV. The theoretical results are compared to previous work for homogeneous flow and no anisotropy in section V. Numerical solutions to the calculations are reviewed in section VI and the results discussed in terms of the space and laboratory observations. The details of many of the calculations are completed in the appendices.

II. THEORY

The case of an inhomogeneous drift along a homogeneous magnetic field in a thermally anisotropic plasma of uniform density is considered. This represents a generalization of the formalism of *Ganguli* [1994]. Two separate calculations of the first order perturbed distribution, one as a function of the parallel (to the magnetic field) velocity and one as a function of the perpendicular velocity are described. The dispersion relation based on the perturbed distribution function is used to identify electrostatic instabilities that are driven by inhomogeneous parallel drift in the local limit is also presented.

We begin with the linearized Poisson's equation,

$$\begin{aligned} \vec{\nabla}\cdot\vec{E}_1 &= 4\pi\rho_1 \\ -\nabla^2\varphi_1 &= 4\pi e(n_{1i}-n_{1e}) \\ 4\pi e(n_{1i}-n_{1e}) - k^2\varphi_1 &= 0. \end{aligned} \tag{3}$$

Here $\vec{E}_1$ is the first order electric field, ρ_1 is the first order charge density, n_{1s} is the first order number density of the species (s) specified in the subscript, e is the elementary charge, φ_1 is the perturbed electrostatic potential, and k is the wavevector magnitude. Throughout this work, quantities with a "1" subscript refer to perturbed quantities. The dispersion relation is obtained by inserting expressions for the perturbed ion and electron densities into equation (3). In addition, φ_1, the wave electrostatic potential, can be eliminated if the perturbed densities are linear with the perturbed electrostatic potential.

To derive expressions for the perturbed densities, a kinetic theory is used. The velocity space dependent perturbed distribution function, $f_1(\vec{\mathrm{v}})$ (obtained by solving the linearized Vlasov equation) is integrated to provide the first-order, perturbed density. Since integration averages over velocity effects, the first order distribution as a function of velocity contains more information than the dispersion relation. The velocity dependent perturbed distribution function associated with a wave is also an experimentally measurable quantity [*Skiff et al.,* 1992; *Sarfaty et al.*, 1996; *Kline et al.,* 1999].

The total time derivative of the distribution function, $f(\vec{r},\vec{\mathrm{v}},t)$ is

$$\frac{df(\vec{r},\vec{\mathrm{v}},t)}{dt} = \left(\frac{\partial}{\partial t} + \frac{\partial\vec{r}}{\partial t}\cdot\vec{\nabla} + \frac{\partial\vec{v}}{\partial t}\cdot\vec{\nabla}_{\mathrm{v}}\right) f(\vec{r},\vec{\mathrm{v}},t), \tag{4}$$

where the conventions

$$\frac{\partial}{\partial \vec{r}} \equiv \vec{\nabla} \text{ and } \frac{\partial}{\partial \vec{\mathrm{v}}} \equiv \vec{\nabla}_{\mathrm{v}} \tag{5}$$

are used.

The time derivative of the velocity vector is the force (F) exerted on a particle divided by the mass (m). To separate the terms into more manageable time independent equilibrium and fluctuating parts, the distribution function, f, and force, F, are also linearized,

$$\begin{aligned} f &= f_o + f_1 + \ldots \\ \vec{F} &= \vec{F}_o + \vec{F}_1 + \ldots \end{aligned} \tag{6}$$

The zeroth order terms are assumed to be time independent. The first order terms are due to the perturbation resulting from a wave propagating in the plasma. Noting that the time derivative of the position vector is the velocity, the total time derivative of the linearized distribution function can now be separated into zeroth order and first order expressions. Without collisions, the total derivative (including all terms) is zero, i.e. the phase space density is conserved. This is known as the Vlasov equation [*Chen*, 1984]. The zeroth and first order equations are,

$$\frac{\partial f_0}{\partial t} + \vec{\mathrm{v}} \cdot \vec{\nabla} f_0 + \frac{\vec{F}_0}{M} \cdot \vec{\nabla}_{\mathrm{v}} f_0 = 0 \tag{7}$$

and

$$\left(\frac{\partial f_1}{\partial t} + \vec{\mathrm{v}} \cdot \vec{\nabla} f_1 + \frac{\vec{F}_0}{M} \cdot \vec{\nabla}_{\mathrm{v}} f_1\right) + \frac{\vec{F}_1}{M} \cdot \vec{\nabla}_{\mathrm{v}} f_0 = 0 \tag{8}$$

The sum of the terms in parenthesis in the first order equation is the total time derivative of the first order distribution function.

$$\left(\frac{\partial f_1}{\partial t} + \vec{\mathrm{v}} \cdot \vec{\nabla} f_1 + \frac{\vec{F}_0}{M} \cdot \vec{\nabla}_{\mathrm{v}} f_1\right) = \frac{df_1}{dt} \tag{9}$$

Letting the first order force be due to the interaction of the charge (q) with the first order perturbed electric field (E_1), the first order distribution function in velocity space is

$$f_1(\vec{\mathrm{v}},t) = -\frac{q}{M}\int_{-\infty}^{t} \vec{E}_1 \cdot \vec{\nabla}_{\mathrm{v}} f_0 dt' . \tag{10}$$

Equation (10) demonstrates that the state of the perturbation to the distribution function at some time *t* depends on the historical interaction of the particle with the perturbed electric field. Given an expression for f_0, $f_1(\vec{\mathrm{v}},t)$ can be determined explicitly if additional assumptions about the time history of the particle are made, e.g., contributions to $f_1(\vec{\mathrm{v}},t)$ at $t' = -\infty$ can be ignored due to some randomizing event like a collision in the particles' past.

III. CALCULATION OF THE DISPERSION RELATION AND $f_1(v_\parallel)$

The time derivative of any function of n independent variables can be expressed as a sum of products of partial derivatives. One way to insure that total time derivative of a function is zero, as must be the case for a function that does not depend explicitly on time, is to require that the function consist only of variables that constant in time, or "constants of the motion." Expanding the time derivative of some function $g(x_1, x_2, \ldots, x_n)$,

$$\frac{dg(x_1, x_2, \ldots, x_n)}{dt} = \sum_{m=1}^{n} \frac{\partial g}{\partial x_m} \frac{\partial x_m}{\partial t} = 0 \tag{11}$$

shows that $\partial x_m / \partial t = 0$ for all m forces the total time derivative to be zero. Thus, any f_0 that is a function of only constants of motion, i.e. time independent variables, is a solution to the zeroth order Vlasov equation. To determine $f_1(\vec{v}, t)$ from equation (10), a zeroth order distribution function must be constructed that both describes the physical situation and satisfies the Vlasov equation.

By constructing f_0 entirely of constants of the motion (see Appendix A), it automatically satisfies the zeroth order Vlasov equation. The constants of motion used in the treatment described here are:

$$\begin{aligned}
&\chi_g \equiv \frac{\dot{y}}{\Omega} + x \quad (x \text{ guiding center}),\\
&v_\parallel \equiv \text{parallel speed},\\
&v_\perp \equiv \text{perpendicular speed},\\
&m \equiv \text{mass of particle},\\
&T_\parallel \equiv m v_{th\parallel}^2 \equiv \text{parallel (to the magnetic field) kinetic energy},\\
&T_\perp \equiv m v_{th\perp}^2 \equiv \text{perpendicular kinetic energy, and}\\
&\text{the temperatures are defined such that } T_{total} = \left(T_\parallel + 2T_\perp\right)/3.
\end{aligned} \tag{12}$$

Here, Ω is a particle's gyrofrequency. It would be natural to describe inhomogeneity in the parallel flow as a function of a perpendicular direction in coordinate space. However, the associated f_0 would not satisfy the Vlasov equation (as a spatial coordinate is not a constant of the motion). A parallel velocity that depends on the particles' guiding center,

$V = V(\chi_g)$, does satisfy the Vlasov equation. In fact, the more "intuitive" x-dependent flow description is equivalent to the limit of the characteristic gradient length being much larger than a particle's gyroradius ($\rho \ll L, \chi_g \approx x$), which is the weak shear limit. An explanation and a comment on the validity of this approximation are discussed in both the section on experimental relevance and in the section highlighting the integration over perpendicular velocity. The zeroth order distribution function used in these calculations is,

$$f_0(H_\perp, H_\parallel, \chi_g) = Ce^{-2\beta_\parallel H_\parallel(\chi_g)} e^{-2\beta_\perp H_\perp} \; ; \tag{13}$$

where

$$H_\parallel(\chi_g) \equiv \frac{1}{2}(\mathrm{v}_\parallel - V_0(\chi_g))^2,$$

$$H_\perp \equiv \frac{1}{2}\mathrm{v}_\perp^2,$$

$$\beta_\parallel \equiv \frac{1}{2\mathrm{v}_{th\parallel}^2},$$

$$\beta_\perp \equiv \frac{1}{2\mathrm{v}_{th\perp}^2},$$

$$C \equiv \frac{n_0}{\pi^{3/2}} \beta_\parallel^{1/2} \beta_\perp,$$

$\mathrm{v}_{th\perp}$ is the thermal velocity in the perpendicular direction,

$\mathrm{v}_{th\parallel}$ is the thermal velocity in the parallel direction,

and n_o is the unperturbed, spatially uniform density. The geometry associated with this form of f_0 is illustrated in Figure 1.

At this point in the calculation, the next step in the derivation depends on what intermediate calculations are required, i.e., what form of the perturbed distribution function is desired before the final integration to obtain the perturbed density is performed. For the calculation of $f_1(\mathrm{v}_\parallel)$ and the dispersion relation, the perpendicular velocities, v_x and v_y, both serve as integration variables. Since we are to integrate over both perpendicular velocity coordinates, they need not be considered independently. In fact, the mathematics is greatly simplified by replacing the Cartesian description of the perpendicular velocity vector with a polar coordinate description, i.e. $(\mathrm{v}_x, \mathrm{v}_y) \rightarrow (\mathrm{v}_\perp, \varphi)$. The calculation of $f_1(\mathrm{v}_y)$, however, requires integration over only v_x. Therefore,

calculation of $f_1(\mathrm{v}_y)$ requires preserving the individual identity of each perpendicular velocity component

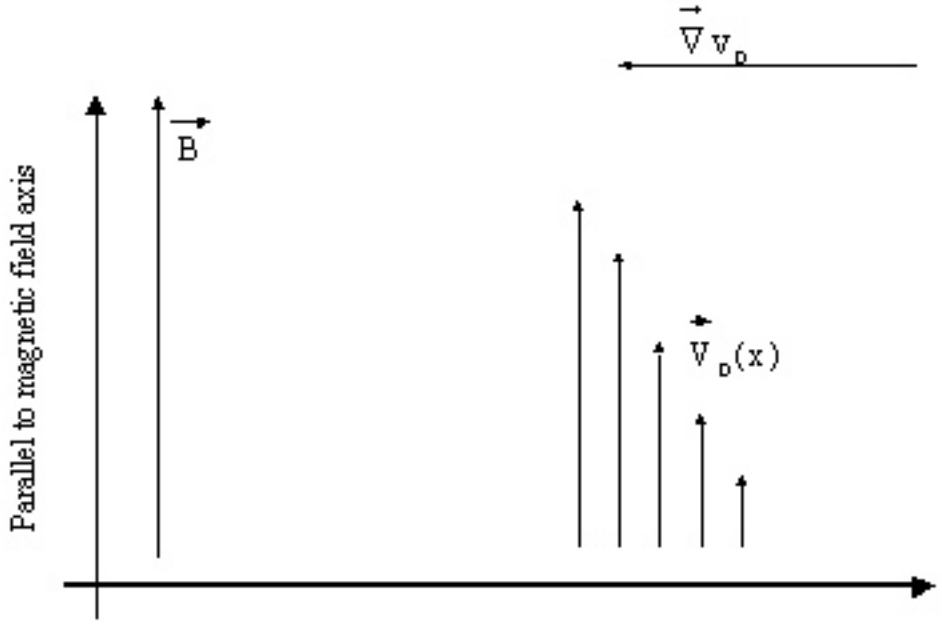

Figure 1. Geometry of flow shear. For $\rho \ll L, \chi_g \approx x$.

The calculation for $f_1(\mathbf{v}_{\|})$ is done first. For convenience, the velocity gradient in equation (10) is expanded in terms of the partial derivatives of polar velocity coordinates:

$$\vec{\nabla} f_0(H_\perp, H_{\|}, \chi_g) = \frac{\partial f_0}{\partial H_{\|}} \frac{\partial H_{\|}}{\partial \vec{\mathbf{v}}} + \frac{\partial f_0}{\partial H_\perp} \frac{\partial H_\perp}{\partial \vec{\mathbf{v}}} + \frac{\partial f_0}{\partial \chi_g} \frac{\partial \chi_g}{\partial \vec{\mathbf{v}}} \tag{14}$$

where:

$$\begin{aligned}
&\frac{\partial f_0}{\partial H_{\|}} = -2\beta_{\|} f_0, \\
&\frac{\partial H_{\|}}{\partial \vec{\mathrm{v}}} = (\mathrm{v}_{\|} - V_0(\chi_g))\hat{\|}, \\
&\frac{\partial f_0}{\partial H_\perp} = -2\beta_\perp f_0, \\
&\frac{\partial H_\perp}{\partial \vec{\mathrm{v}}} = \mathrm{v}_\perp \hat{\perp}, \\
&\frac{\partial f_0}{\partial \chi_g} = 2\beta_{\|}(\mathrm{v}_{\|} - V_0(\chi_g)) V_0'(\chi_g) f_0, \\
&\text{and } \frac{\partial \chi_g}{\partial \vec{\mathrm{v}}} = \frac{1}{\Omega}\hat{y} \ .
\end{aligned} \tag{15}$$

Note that $V_0'(\chi_g) \equiv \partial V_0(\chi_g)/\partial\chi_g$, and $\hat{\parallel}$ and $\hat{\perp}$ are the unit directional vectors in the parallel and perpendicular (that is, the direction along a particle gyro-orbit) directions, respectively.

The velocity gradient of the zeroth order distribution function is

$$\vec{\nabla}_v f_0(H_\parallel, H_\perp, \chi_g) = -2f_0\left[\beta_\parallel(v_\parallel - V_0(\chi_g))\hat{\parallel} + \beta_\perp v_\perp \hat{\perp} - \beta_\parallel(v_\parallel - V_0(\chi_g))\frac{V_0'(\chi_g)}{\Omega}\hat{y}\right]. \tag{16}$$

It is convenient to add and subtract $\beta_\perp v_\parallel \hat{\parallel}$ to the right side of Equation (16), so that

$$\vec{\nabla}_v f_0(H_\parallel, H_\perp, \chi_g) = -2f_0\left[\beta_\perp \vec{v} - \beta_\perp v_\parallel \hat{\parallel} + \beta_\parallel(v_\parallel - V_0(\chi_g))(\hat{\parallel} - \frac{V_0'(\chi_g)}{\Omega}\hat{y})\right]. \tag{17}$$

Since only electrostatic waves are being considered, the electric field can be written in terms of the scalar potential,

$$E_1 = -\vec{\nabla}\varphi_1 \ , \tag{18}$$

and the integrand of the dot product in equation (10) becomes,

$$\vec{\nabla}_v f_0(H_\parallel, H_\perp, \chi_g) = 2f_0\left[\beta_\perp \vec{v}\bullet\vec{\nabla}\varphi_1 - \vec{\nabla}\varphi_1\bullet\beta_\perp v_\parallel \hat{\parallel} + \vec{\nabla}\varphi_1\bullet\beta_\parallel(v_\parallel - V_0(\chi_g))(\hat{\parallel} - \frac{V_0'(\chi_g)}{\Omega}\hat{y})\right]. \tag{19}$$

The first term in equation (19) is rewritten using the identity,

$$\vec{v}\cdot\vec{\nabla}\varphi_1 = \frac{d\varphi_1}{dt} - \frac{\partial\varphi_1}{\partial t}. \tag{20}$$

Assuming all perturbed quantities (in particular, φ_1) vary as plane waves,

$$g_1 = \sum_k g_{1k} e^{i(\vec{k}\bullet\vec{r} - i\omega t)}, \tag{21}$$

equation (20) becomes,

$$\vec{v}\cdot\vec{\nabla}\varphi_1 = \frac{d\varphi_1}{dt} + i\omega\varphi_1 \ . \tag{22}$$

Using the plane wave assumption, the potential gradient can be written,

$$\vec{\nabla}\varphi_1 = i\vec{k}\varphi_1. \tag{23}$$

Combined with equations (23), (22), and (19), equation (10) becomes an integral expression for the amplitude of the first order perturbed distribution as a function of velocity and time.

$$\begin{aligned} f_1(\vec{\mathrm{v}},t) &= -\frac{q}{M}2f_0\left[\beta_\perp \int_{-\infty}^{t} dt' \frac{d\varphi_1(t')}{dt'} + \int_{-\infty}^{t}\left(i(\beta_\perp(\omega - k_{||}\mathrm{v}_{||}) + \beta_{||}(\mathrm{v}_{||} - V_0(\chi_g))(k_{||} - \frac{V_0'(\chi_g)k_y}{\Omega}))\varphi_1 \right)dt'\right] \\ &= -\frac{q}{M}2f_0\left[\beta_\perp\varphi_1(t')\,|_{-\infty}^{t} + \int_{-\infty}^{t}\left(i(\beta_\perp(\omega - k_{||}\mathrm{v}_{||}) + \beta_{||}(\mathrm{v}_{||} - V_0(\chi_g))(k_{||} - \frac{V_0'(\chi_g)k_y}{\Omega}))\varphi_1 \right)dt'\right], \end{aligned} \tag{24}$$

where the total perturbed distribution function is the sum of the perturbations due to all of the waves in the system,

$$f_1(\vec{\mathrm{v}},t) = \sum_k f_{1k}(\vec{\mathrm{v}})e^{i(\vec{k}\bullet\vec{r}-\omega t)}. \tag{25}$$

Upon expanding φ_1 in the same way,

$$f_{1k}(\vec{\mathrm{v}})e^{i(\vec{k}\bullet\vec{r}-\omega t)} = -\frac{q}{M}2f_0\left\{\begin{array}{l} \beta_\perp\varphi_{1k}e^{i(\vec{k}\bullet\vec{r}\,'-\omega t')}\,|_{-\infty}^{t} + \\ \int_{-\infty}^{t}\left(i(\beta_\perp(\omega - k_{||}\mathrm{v}_{||}) + \beta_{||}(\mathrm{v}_{||} - V_0(\chi_g))(k_{||} - \frac{V_0'(\chi_g)k_y}{\Omega}))\varphi_{1k}e^{i(\vec{k}\bullet\vec{r}\,'-\omega t')} \right)dt' \end{array}\right\}. \tag{26}$$

Rearranging the terms yields

$$f_{1k}(\vec{\mathrm{v}}) = -\frac{q}{M}2f_0\left\{\begin{array}{l} \beta_\perp\varphi_{1k}e^{i(\vec{k}\bullet(\vec{r}\,'-\vec{r})-\omega(t'-t))}\,|_{-\infty}^{t} + \\ \int_{-\infty}^{t}\left(i(\beta_\perp(\omega - k_{||}\mathrm{v}_{||}) + \beta_{||}(\mathrm{v}_{||} - V_0(\chi_g))(k_{||} - \frac{V_0'(\chi_g)k_y}{\Omega}))\varphi_{1k}e^{i(\vec{k}\bullet(\vec{r}\,'-\vec{r})-\omega(t'-t))} \right)dt' \end{array}\right\}. \tag{27}$$

The integral in equation (27) describes the effect of each particles' past experience on the perturbed distribution function at the present time, t. $f_{1k}(\vec{\mathrm{v}})$ is

completely determined by equation (27) and the assumed zeroth order distribution function (equation (13)). Since the expression is valid anywhere in velocity space, it is a complete description (to first order) of how the electric field of the wave modifies the velocity distribution of the particles. The argument of the exponential can be expressed in terms of the velocity components by using the unperturbed orbits (see Appendix B). Using a change of variables, $\Theta = t - t'$, in the solution to the unperturbed orbits yields,

$$\left\{ \begin{array}{c} x' - x = \frac{\mathrm{v}_\perp}{\Omega}\left[\sin(\bar{\varphi} - \Omega\Theta) - \sin(\bar{\varphi})\right] \\ y' - y = \frac{\mathrm{v}_\perp}{\Omega}\left[\cos(\bar{\varphi} - \Omega\Theta) - \cos(\bar{\varphi})\right] \\ z' - z = -\mathrm{v}_\parallel \Theta \end{array} \right\}, \tag{28}$$

where $\bar{\phi}$ is the particle's angular position at time *t*. These expressions are substituted into the argument of the exponential in equation (27) yielding,

$$\begin{aligned} i\vec{k}\cdot(\vec{r}' - \vec{r}) - i\omega(t' - t) &= i\left(k_x(x' - x) + k_y(y' - y) + k_z(z' - z)\right) - i\omega(t' - t) \\ &= i\frac{\mathrm{v}_\perp k_\perp}{\Omega}\left[\sin(\bar{\phi} - \Omega\Theta + \alpha) - \sin(\bar{\phi} + \alpha)\right] + i(\omega - k_\parallel \mathrm{v}_\parallel)\Theta . \end{aligned} \tag{29}$$

Here α is the wavevector's polar angular coordinate. That is,

$$\tan\alpha = \frac{k_y}{k_x} . \tag{30}$$

The details leading to Equation (29) are in Appendix B. Equation (27) then becomes,

$$\begin{aligned} f_{1k}(\vec{\mathrm{v}}) = -\frac{q}{M} 2 f_0 \Big[\beta_\perp \varphi_{1k} - i\Big(\beta_\perp(\omega - k_\parallel \mathrm{v}_\parallel) + \beta_\parallel(\mathrm{v}_\parallel - V_0(\chi_g))(k_\parallel - \frac{V_0'(\chi_g)k_y}{\Omega}) \Big) \\ \int_0^{2\pi} d\bar{\phi} \int_\infty^0 d\Theta e^{\,i\frac{\mathrm{v}_\perp k_\perp}{\Omega}\left[\sin(\bar{\phi} - \Omega\tau + \alpha) - \sin(\bar{\phi} + \alpha)\right] + i(w - k_\parallel \mathrm{v}_\parallel)\Theta} \Big] . \end{aligned} \tag{31}$$

The Θ and $\bar{\varphi}$ integrals are also completed in Appendix B. Having integrated over the particle's gyrophase angle, f_1 can now be expressed as a function of the parallel and perpendicular velocity components.

$$\begin{aligned} f_{1k}(\mathrm{v}_\parallel, \mathrm{v}_\perp) = -\frac{4\pi q f_0}{M} \beta_\perp \varphi_{1k} \\ \left[1 - \sum_{m=-\infty}^{\infty} \left[J_m(\frac{\mathrm{v}_\perp k_\perp}{\Omega}) \right]^2 \left(\frac{(\omega - k_\parallel \mathrm{v}_\parallel) + \frac{\beta_\parallel}{\beta_\perp}(\mathrm{v}_\parallel - V_0(\chi_g))(k_\parallel - \frac{V_0'(\chi_g)k_y}{\Omega})}{\omega - m\Omega - k_\parallel \mathrm{v}_\parallel} \right) \right] \end{aligned} \tag{32}$$

Note that the perpendicular velocity does not include any directional information because of the gyrophase integration. Integrating f_1 over $v_\perp$ and $v_\parallel$ yields n_1, which is then substituted into equation (3) to obtain the dispersion relationship.

The integrals over the perpendicular velocity component are shown in Appendix C.1. Upon their completion, the first order distribution function is a function of only the parallel velocity component,

$$f_{1k}(v_\parallel) = -\frac{2qn_o\,\varphi_{1k}}{M\sqrt{\pi}}\sqrt{\beta_\parallel}\,\beta_\perp e^{-2\beta_\parallel(v_\parallel - V_o(x))^2} \left[1 - \sum_{m=-\infty}^{\infty}\Gamma_m(b)\left(\frac{(\omega - k_\parallel v_\parallel) + \frac{T_\perp}{T_\parallel}(v_\parallel - V_0(\chi_g))(k_\parallel - \frac{V_0'(\chi_g)k_y}{\Omega})}{\omega - m\Omega - k_\parallel v_\parallel}\right)\right] \tag{33}$$

where,

$$b \equiv \frac{k_\perp^2}{2\Omega^2\beta_\perp} \text{ and } \Gamma_m(b) \equiv e^{-b}I_m(b)\,.$$

The two integrals over the parallel velocity component are,

$$I_{\parallel,1} = \int_{-\infty}^{\infty} dv_\parallel e^{-\beta_\parallel(v_\parallel - V_o(\chi_g))^2} = \sqrt{\frac{\pi}{\beta_\parallel}} \tag{34}$$

and

$$\begin{aligned} I_{\parallel,2} &= \int_{-\infty}^{\infty} dv_\parallel \frac{(\omega - k_\parallel v_\parallel) + \frac{\beta_\parallel}{\beta_\perp}(v_\parallel - V_0(\chi_g))(k_\parallel - \frac{V_0'(\chi_g)k_y}{\Omega})}{\omega - m\Omega - k_\parallel v_\parallel} e^{-\beta_\parallel(v_\parallel - V_0(\chi_g))^2} \\ &= -\sqrt{\frac{\pi}{\beta_\parallel}}\left(\frac{\beta_\parallel}{\beta_\perp} - 1 + \sqrt{\beta_\parallel}(\frac{m\Omega}{k_\parallel})Z(\zeta_m) + \frac{\beta_\parallel}{\beta_\perp}\zeta_m Z(\zeta_m) - \frac{\beta_\parallel}{\beta_\perp}\frac{V_0'(x)}{\Omega u}(1 + \zeta_m Z(\zeta_m))\right), \end{aligned} \tag{35}$$

where,

$$\begin{aligned} Z(\zeta_m) &\equiv \frac{1}{\sqrt{\pi}}\int ds \frac{e^{-s^2}}{s - \zeta}; \\ \zeta_m &= \frac{\omega - m\Omega - k_\parallel V_0(x)}{\sqrt{2}k_\parallel v_{th\parallel}}; \\ \text{and } u &= \frac{k_\parallel}{k_y}\,. \end{aligned} \tag{36}$$

The details of the $I_{\|,2}$ integration are presented in Appendix C.2.

With both integrals evaluated, the first order, perturbed density is

$$n_{1k} = \frac{-2\varphi_{1k} n_o \beta_\perp}{M}\left[\frac{T_\perp}{T_\|} + \sum_{n=-\infty}^{\infty} \Gamma_n(b)\left(\left(\frac{n\Omega}{\sqrt{2}k_\| \mathrm{v}_{th\|}}(1-\frac{T_\perp}{T_\|}) + \frac{T_\perp}{T_\|}\varsigma_o\right) Z(\varsigma_n) - \frac{T_\perp V_o'(x)}{T_\| u\Omega}(1+\varsigma_n Z(\varsigma_n))\right)\right]. \quad (37)$$

Substituting the appropriate expressions into Poisson's equation, transforming to the ion frame, keeping only the $n = 0$ term for electrons (as the series converges rapidly for particles with large gyrofrequency), and assuming the parallel flow shears are the same for electrons and ions, the dispersion relation becomes,

$$k^2 \lambda_{Di\perp}^2 + \frac{T_{\perp i}}{T_{\|i}} + \sum_{n=-\infty}^{\infty} \Gamma_n(b) F_{ni} + \tau \frac{T_{\perp e}}{T_{\|e}}(1 + F_{0e}) = 0 \ , \quad (38)$$

where,

$$F_{n,i} = (\frac{1}{\sqrt{2}k_\| \mathrm{v}_{th\|i}})\left(n\Omega(1-\frac{T_{\perp i}}{T_{\|i}}) + \frac{T_{\perp i}}{T_{\|i}}\omega\right) Z(\frac{\omega - n\Omega}{\sqrt{2}k_\| \mathrm{v}_{th\|i}}) -$$
$$\frac{T_{\perp i} V_o'(x)}{T_{\|i}\Omega u}\left(1 + (\frac{\omega - n\Omega}{\sqrt{2}k_\| \mathrm{v}_{th\|i}}) Z(\frac{\omega - n\Omega}{\sqrt{2}k_\| \mathrm{v}_{th\|i}})\right),$$

$$F_{0e} = (\frac{1}{\sqrt{2}k_\| \mathrm{v}_{th\|e}})\left(\omega - k_\| V_0(x)\right) Z(\frac{\omega - k_\| V_0(x)}{\sqrt{2}k_\| \mathrm{v}_{th\|e}}) + \frac{V_0'(x)}{u\mu\Omega}\left(1 + (\frac{\omega - k_\| V_0(x)}{\sqrt{2}k_\| \mathrm{v}_{th\|e}}) Z(\frac{\omega - k_\| V_0(x)}{\sqrt{2}k_\| \mathrm{v}_{th\|e}})\right),$$

$$\tau = \frac{T_{\perp i}}{T_{\perp e}},$$

and

$$\lambda_{Di\perp}^2 = \frac{M \mathrm{v}_{th\perp i}^2}{4\pi e^2 n_0}$$

is the ion "perpendicular" Debye length.

Equation (38) is the dispersion relation of *Gavrishchaka et al.* [1998] generalized to include the effects of temperature anisotropy. The effects of temperature anisotropy on the ion acoustic and ion cyclotron modes studied previously [*Gavrishtchaka et al.*, 1996, 1999, 2000] is provided in the Computational Results section of this work. The parameters used are those of *Gavrishtchaka et al.* [1999, 2000] with varying values of

anisotropy. The isotropic case is included for comparison to the previously published results.

IV. Interpretation and application of the perturbed distribution functions

The typical application of a dispersion relation is to predict which mode or modes are most likely to grow in a particular plasma environment. The dispersion relation is solved for modes with complex frequencies and for a given set of plasma parameters. Then the wavevector and real (oscillatory) frequency associated with the largest growth rate is determined. In the previous section, during the calculation of the dispersion function, the perturbed distribution as a function of $v_{||}$ was calculated for an electrostatic wave in a thermally anisotropic medium. Such an expression can be directly compared to plasma observations by measuring the component of the Doppler shifted absorption profile of metastable ions that oscillate at the wave frequency. That is to say, directly measurable quantities are involved. The first order perturbed distribution function is a one dimensional (in velocity space) description of an ensemble of particles. It contains information of the particles' entire past interaction with the wave fields. Therefore, wave properties can be extracted from measurements of $f_1(\mathbf{v}_{||})$. Experiments performed in laboratory plasmas have demonstrated that electrostatic wave amplitudes and wavelengths (assuming a particular dispersion relationship to eliminate either $k_\perp$ or $k_{||}$) can be non-invasively measured using this technique [*Stern and Johnson*, 1975; *Sarfaty*, 1996; *Skiff and Anderegg*. 1987; *Kline et al.*, 1999].

For those experiments, the data were compared with theoretical expressions that included the effects of thermal anisotropy and parallel flow, but not shear in the parallel flow. Because this work has focused on the development of a more general theory for use in experiments with both parallel flow shear and thermal anisotropy, it is instructive to investigate what changes in the perturbed distribution functions will occur due to the inclusion of parallel flow shear. For comparison of the generalized theory with the previous zero-shear work, the plasma parameters chosen are those used in *DeSouza-Machado's* dissertation [*DeSouza-Machado*, 1996]. These are,

$$V_{zo}/\mathrm{v}_{thi||} = .2952$$
$$k_{\perp}\rho = .0220,$$
$$\Omega/k_{||}\mathrm{v}_{th||} = 4.95 - .285i,$$
$$\omega/\Omega = 1.3116,$$
$$T_{i||}/T_{i\perp} = .7133 \text{ and}$$
$$\theta = .71\ rad$$

Here θ represents the propagation angle with respect to the magnetic field axis. The real part of $f_1(\mathrm{v}_{||})$ versus the normalized parallel velocity (normalized to the ion thermal velocity) is shown for three different normalized shear values in Figure 2. The multiplicative constant in front of Equation (33) is the same for all three calculations.

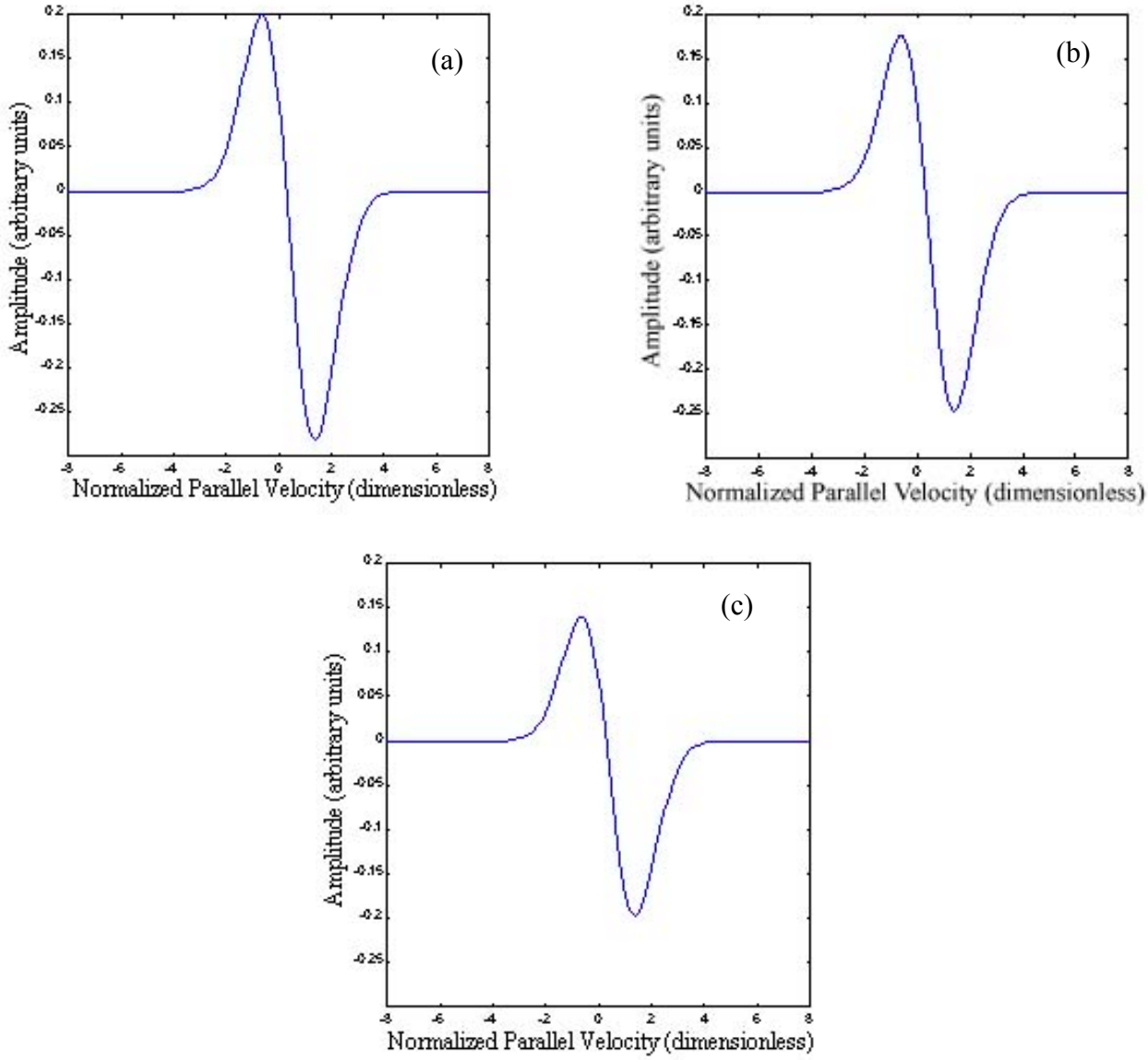

Figure 2. $f_1(\mathrm{v}_{\|})$ versus $\mathrm{v}_{\|}/\mathrm{v}_{ith\|}$ for (a) $V'/\Omega = 0$, (b) $V'/\Omega = 2$, and (c) $V'/\Omega = 5$.

Increasing the parallel shear appears to modestly reduce the overall amplitude of the perturbation to the parallel distribution function. As the shear is increased, there are fewer particles at any given velocity. With fewer particles at a velocity, the resonance with a wave of that velocity will be less robust. Thus, the perturbation amplitude is attenuated in comparison to a case with less shear.

In the zero shear limit, $f_1(\mathrm{v}_{\|})$ depends only on $k_{\perp}$ (not k_x or k_y). Without the shear in the parallel flow to break the cylindrical symmetry, there is nothing special about any direction perpendicular to the field and the perpendicular wavevector information vanishes during the angular integration [*DeSouza-Machado*, 1996]. With shear in the

parallel flow, a unique shear direction is defined and both components of the wavevector appear in $f_1(\mathrm{v}_{\|})$. In the local limit, the shear is defined to be along one axis (the *x*-axis), but not the other (the *y*-axis). One effect of velocity shear may be to provide a means of determining both $k_{\|}$ and $k_{\perp}$ from measurements of $f_1(\mathrm{v}_{\|})$. The normalized shear term in Equation (33) is multiplied by the quantity $k_y/k_{\|}$. If the wave amplitude and shear are directly measured (perhaps with a single probe and a parallel LIF measurement), comparison of an experimentally measured $f_1(\mathrm{v}_{\|})$ with numerically generated curves could be used to determine $k_{\|}$ and $k_y/k_{\|}$.

With a conceptually similar analysis, an expression for the first order distribution as a function of the *y*-component of velocity can be also obtained. Such an expression is required to compare the theory to experimental data as LIF measurements made perpendicular to the background magnetic field will yeild the distribution function along a single line-of-sight. This calculation differs from the preceeding one in that the perpendicular components of velocity must be considered in the Cartesian coordinate system. The approach used in this portion of this work was chosen for two reasons: a desire for an expression that is relatively straightforward to interpret and a desire to keep the solution in a form that can be easily compared to previous, less general results [*Sarfaty et al*, 1996].

For the $f_1(\mathrm{v}_y)$ calculation, it is most convenient to expand the velocity gradient of the zeroth order distribution function in such a way as to keep the Cartesian components of the perpendicular velocities separate.

$$\vec{\nabla}_{\vec{\mathrm{v}}} f_0(H_{\perp}, H_{\|}, \chi_g) = \frac{\partial f_0}{\partial H_{\perp}} \frac{\partial H_{\perp}}{\partial \mathrm{v}_x} \hat{i} + \frac{\partial f_0}{\partial H_{\perp}} \frac{\partial H_{\perp}}{\partial \mathrm{v}_y} \hat{j} + \frac{\partial f_0}{\partial H_{\|}} \frac{\partial H_{\|}}{\partial \mathrm{v}_{\|}} \hat{k} + \frac{\partial f_0}{\partial \chi_g} \frac{\partial \chi_g}{\partial \mathrm{v}_y} \hat{j} \tag{39}$$

The variables $H_{\perp}, H_{\|}$ are as defined in equation (13). The individual terms are,

$$\begin{aligned} &\frac{\partial f_0}{\partial H_{\|}} = -2\beta_{\|} f_0; \quad \frac{\partial H_{\|}}{\partial v_{\|}} = (\mathrm{v}_{\|} - V_0(\chi_g)); \quad \frac{\partial f_0}{\partial H_{\perp}} = -2\beta_{\perp} f_0; \; \frac{\partial H_{\perp}}{\partial \mathrm{v}_{x,y}} = \mathrm{v}_{x,y}; \\ &\frac{\partial f_0}{\partial \chi_g} = 2\beta_{\|}(\mathrm{v}_{\|} - V_0(\chi_g)) V_0'(\chi_g) f_0; \quad \text{and} \quad \frac{\partial \chi_g}{\partial \mathrm{v}_y} = \frac{1}{\Omega} \hat{y} \; . \end{aligned} \tag{40}$$

As before,

$$\vec{E}_1 = -\vec{\nabla} \varphi_1 = -i\vec{k} \varphi_1, \tag{41}$$

and equation (10) is written as,

$$f_1(\vec{\mathrm{v}},t)=\frac{iq}{M}\int_{-\infty}^{t}\varphi_1\vec{k}\cdot\vec{\nabla}_v f_0\,dt'. \tag{42}$$

Combining Equations (39), (40), and (42), and recalling the plane wave space-time dependence of φ_1,

$$\begin{aligned}
f_1(\vec{\mathrm{v}})&=\frac{iq\varphi_1}{M}\left[k_x\frac{\partial f_0}{\partial H_\perp}\mathrm{v}_x+k_y\left(\frac{\partial f_0}{\partial H_\perp}\mathrm{v}_y+\frac{\partial f_0}{\partial\chi_g}\frac{1}{\Omega}\right)+k_z\frac{\partial f_0}{\partial \mathrm{v}_{||}}\right]\int_{-\infty}^{t}e^{j(\vec{k}\bullet\vec{r}'-\omega t')}dt'\\
f_1(\vec{\mathrm{v}})&=\frac{iq\varphi_1 f_0}{M}\left[k_x(-2\beta_\perp)\mathrm{v}_x+k_y\left((-2\beta_\perp)\mathrm{v}_y+(2\beta_{||}V_o')(\mathrm{v}_{||}-V_o)\frac{1}{\Omega}\right)-k_z(2\beta_{||})(\mathrm{v}_{||}-V_o)\right]\int_{-\infty\ 0}^{t}e^{j(\vec{k}\bullet\vec{r}'-\omega t')}dt'\\
f_1(\vec{\mathrm{v}})&=\frac{iq\varphi_1 f_0}{M}\left[-2\beta_\perp k_x\mathrm{v}_x-2\beta_\perp k_y\mathrm{v}_y-2\beta_{||}\left(k_z-\frac{k_yV_o'}{\Omega}\right)(\mathrm{v}_{||}-V_o)\right]\int_{-\infty\ 0}^{t}e^{j(\vec{k}\bullet\vec{r}'-\omega t')}dt'
\end{aligned} \tag{43}$$

The unperturbed orbit calculation is used again [*Swanson,* 1989] to simplify the time integration (see Appendix B). However, it is important to use an expression for the unperturbed orbits in Cartesian coordinates, as we are not free to average over the gyrophase and still obtain a meaningful expression. The wavevectors in the unperturbed orbit calculation are changed to a polar coordinate representation (this is acceptable, as there is no wavevector integration to erase a component of wavevector information). Also, the integration in time is again simplified by using the change of variables, $\Theta=t-t'$. Inserting these substitutions, the perturbed distribution function in velocity space is

$$\begin{aligned}
f_{1k}(\vec{\mathrm{v}})=\frac{-2q\varphi_{1k}}{M}f_0(\vec{\mathrm{v}})e^{\frac{i}{\Omega}(\mathrm{v}_yk_x-\mathrm{v}_xk_y)}\sum_{m,n=-\infty}^{\infty}&\left[\beta_\perp(m+n)\Omega+\beta_{||}\left(k_z-\frac{k_yv_o}{\Omega}\right)(\mathrm{v}_{||}-V_o)\right]\\
e^{i(m+n)\theta}e^{-im\frac{\pi}{2}}J_m\left(\frac{\mathrm{v}_yk_\perp}{\Omega}\right)&J_n\left(\frac{\mathrm{v}_xk_\perp}{\Omega}\right)\left(\frac{1}{\Omega(m+n)+k_{||}\mathrm{v}_{||}-\omega}\right).
\end{aligned} \tag{44}$$

The steps leading up to equation (44) and an additional step detailing the appearance of the *m* and *n* indices in the brackets are outlined in Appendix D.

$f_1(v_y)$ is obtained by integrating over the parallel and *x*-components of velocity. Inserting f_0 from equation (13), the integral form of the first order distribution as a function of v_x and v_y is

$$f_{1k}(\mathrm{v}_x,\mathrm{v}_y)=\frac{-2qn_o\varphi_{1k}}{\pi^{3/2}M}\beta_\perp\sqrt{\beta_\parallel}e^{-\beta_\perp(\mathrm{v}_x^2+\mathrm{v}_y^2)}e^{\frac{i}{\Omega}(\mathrm{v}_y k_x-\mathrm{v}_x k_y)}\sum_{m,n=-\infty}^{\infty}e^{i(m+n)\theta}e^{-im\frac{\pi}{2}}J_m(\frac{\mathrm{v}_y k_\perp}{\Omega})J_n(\frac{\mathrm{v}_x k_\perp}{\Omega})$$
$$\int_{-\infty}^{\infty}\mathrm{dv}_\parallel e^{-\beta_\parallel(\mathrm{v}_\parallel-V_o)^2}\left(\frac{\beta_\perp(m+n)+\beta_\parallel\left(k_\parallel-\frac{k_y V_o'}{\Omega}\right)(\mathrm{v}_\parallel-V_o)}{\Omega(m+n)+k_\parallel\mathrm{v}_\parallel-\omega}\right). \tag{45}$$

The integral in equation (45), $I_{m,n}$, is evaluated in Appendix E, resulting in,

$$I_{m,n}=\sqrt{\pi}\left[\frac{\beta_\perp}{\sqrt{\beta_\parallel}}(\xi_0-\xi_{m+n})Z(\xi_{m+n})+\sqrt{\beta_\parallel}\left(1+\xi_{m+n}Z(\xi_{m+n})\right)-\frac{k_y V_o'}{\Omega}\frac{\sqrt{\beta_\parallel}}{k_\parallel}\left(1+\xi_{m+n}Z(\xi_{m+n})\right)\right]. \tag{46}$$

Equation (45) becomes,

$$f_{1k}(\mathrm{v}_x,\mathrm{v}_y)=\frac{-2qn_o\varphi_{1k}}{\pi^{3/2}M}\beta_\perp\sqrt{\beta_\parallel}e^{-\beta_\perp(\mathrm{v}_x^2+\mathrm{v}_y^2)}e^{\frac{i}{\Omega}(\mathrm{v}_y k_x-\mathrm{v}_x k_y)}$$
$$\sum_{m,n=-\infty}^{\infty}I_{m,n}e^{i(m+n)\theta}e^{-im\frac{\pi}{2}}J_m(\frac{\mathrm{v}_y k_\perp}{\Omega})J_n(\frac{\mathrm{v}_x k_\perp}{\Omega}). \tag{47}$$

Thus,

$$f_{1k}(\mathrm{v}_y)=\frac{-2qn_o\varphi_{1k}}{\pi^{3/2}M}\beta_\perp\sqrt{\beta_\parallel}e^{-\beta_\perp(\mathrm{v}_x^2+\mathrm{v}_y^2)}e^{\frac{i}{\Omega}(\mathrm{v}_y k_x)}\sum_{m,n=-\infty}^{\infty}I_{m,n}e^{i(m+n)\theta}e^{-im\frac{\pi}{2}}J_m(\frac{\mathrm{v}_y k_\perp}{\Omega})\int_{-\infty}^{\infty}d\mathrm{v}_x e^{\frac{i\mathrm{v}_x k_y}{\Omega}}e^{-\beta_\perp\mathrm{v}_x^2}J_n(\frac{\mathrm{v}_x k_\perp}{\Omega}). \tag{48}$$

The integral over v_x, $I_{n,j}$, is completed in Appendix F and,

$$I_{n,j}=e^{-\frac{c^2}{4}}e^{-\frac{a^2}{8}}e^{-ij\frac{\pi}{2}}\sqrt{\frac{\pi}{\beta_\perp}}\sum_{j=-\infty}^{\infty}I_j(\frac{ac}{2})I_{\frac{n-j}{2}}(\frac{a^2}{8}). \tag{49}$$

$f_1(\mathrm{v}_y)$ is then given by

$$f_{1k}(\mathrm{v}_y)=\frac{-2qn_o\varphi_{1k}}{\pi^{3/2}M}\beta_\perp\sqrt{\beta_\parallel}\sqrt{\frac{\pi}{\beta_\perp}}e^{-\frac{c^2}{4}}e^{-\frac{a^2}{8}}e^{-\beta_\perp(\mathrm{v}_x^2+\mathrm{v}_y^2)}$$
$$e^{\frac{i}{\Omega}(\mathrm{v}_y k_x)}\sum_{m,n=-\infty}^{\infty}I_{m,n}e^{i(m+n)\theta}e^{-im\frac{\pi}{2}}J_m(\frac{\mathrm{v}_y k_\perp}{\Omega})\sum_{k=-\infty}^{\infty}e^{-ij\frac{\pi}{2}}I_j(\frac{ac}{2})I_{\frac{n-j}{2}}(\frac{a^2}{8}). \tag{50}$$

Inserting the definition of $I_{m,n}$ (equation (46)),

$$f_{1k}(\mathrm{v}_y)=\frac{-2qn_o\varphi_{1k}}{\pi^{1/2}M}\beta_{\|}\sqrt{\beta_\perp}e^{-\frac{c^2}{4}}e^{-\frac{a^2}{8}}e^{-\beta_\perp(\mathrm{v}_y^2)}e^{\frac{i}{\Omega}(\mathrm{v}_y k_x)}$$
$$\sum_{m,n=-\infty}^{\infty}\left(\frac{\beta_\perp}{\beta_{\|}}(\xi_0-\xi_{m+n})Z(\xi_{m+n})+(1+\xi_{m+n}Z(\xi_{m+n}))\left(1-\frac{k_y V_o'}{k_{\|}\Omega}\right)\right) \tag{51}$$
$$e^{j(m+n)\theta}e^{-im\frac{\pi}{2}}J_m\left(\frac{\mathrm{v}_y k_\perp}{\Omega}\right)\sum_{j=-\infty}^{\infty}e^{-ij\frac{\pi}{2}}I_j\left(\frac{ac}{2}\right)I_{\frac{n-j}{2}}\left(\frac{a^2}{8}\right).$$

Letting $j\to -j$ (to preserve the notation of *Sarfaty et al.* [1996]) and using the definitions of $\beta_{\|}$ and $\beta_\perp$ given in Equation (13),

$$f_{1k}(\mathrm{v}_y)=\frac{-qn_o\varphi_{1k}}{M}\frac{1}{\mathrm{v}_{th\|}^2}\sqrt{\frac{1}{2\pi\mathrm{v}_{th\perp}^2}}e^{-(\mathrm{v}_y^2/2\mathrm{v}_{th\perp}^2)}e^{-\frac{c^2}{4}}e^{-\frac{a^2}{8}}e^{\frac{i}{\Omega}(\mathrm{v}_y k_x)}$$
$$\sum_{m,n=-\infty}^{\infty}\left(\frac{T_{\|}}{T_\perp}(\xi_0-\xi_{m+n})Z(\xi_{m+n})+(1+\xi_{m+n}Z(\xi_{m+n}))\left(1-\frac{k_y V_o'}{k_{\|}\Omega}\right)\right) \tag{52}$$
$$e^{j(m+n)\theta}e^{-im\frac{\pi}{2}}J_m\left(\frac{\mathrm{v}_y k_\perp}{\Omega}\right)\sum_{j=-\infty}^{\infty}e^{-ij\frac{\pi}{2}}I_j\left(\frac{ac}{2}\right)I_{\frac{n-j}{2}}\left(\frac{a^2}{8}\right).$$

Inserting the normalized $f_o(\mathrm{v}_y)$, i.e.,

$$f_o(\mathrm{v}_y)=\sqrt{\frac{1}{2\pi\mathrm{v}_{th\perp}^2}}e^{-(\mathrm{v}_y^2/2\mathrm{v}_{th\perp}^2)}\quad, \tag{53}$$

yields,

$$f_{1k}(v_y)=\frac{-qn_o\varphi_{1k}}{M}\frac{1}{\mathrm{v}_{th\|}^2}f_o(\mathrm{v}_y)e^{-\frac{c^2}{4}}e^{-\frac{a^2}{8}}e^{\frac{i}{\Omega}(\mathrm{v}_y k_x)}$$
$$\sum_{m,n=-\infty}^{\infty}\left(\frac{T_{\|}}{T_\perp}(\xi_0-\xi_{m+n})Z(\xi_{m+n})+(1+\xi_{m+n}Z(\xi_{m+n}))\left(1-\frac{k_y V_o'}{k_{\|}\Omega}\right)\right) \tag{54}$$
$$e^{j(m+n)\theta}e^{-im\frac{\pi}{2}}J_m\left(\frac{\mathrm{v}_y k_\perp}{\Omega}\right)\sum_{j=-\infty}^{\infty}e^{-ij\frac{\pi}{2}}I_j\left(\frac{ac}{2}\right)I_{\frac{n-j}{2}}\left(\frac{a^2}{8}\right).$$

Equation (54) is the first order perturbed distribution as a function of v_y. Letting $v_d' = 0$ and normalizing the unperturbed density, n_o, to unity results in

$$f_{1k}(v_y) = \frac{-q\varphi_{1k}}{M v_{th\|}^2} f_o(v_y) e^{-\frac{c^2}{4}} e^{-\frac{a^2}{8}} e^{\frac{i}{\Omega}(v_y k_x)}$$
$$\sum_{m,n=-\infty}^{\infty} \left(\frac{T_\|}{T_\perp}(\xi_0 - \xi_{m+n}) Z(\xi_{m+n}) + (1 + \xi_{m+n} Z(\xi_{m+n})) \right) \tag{55}$$
$$e^{j(m+n)\theta} e^{-im\frac{\pi}{2}} J_m\left(\frac{v_y k_\perp}{\Omega}\right) \sum_{k=-\infty}^{\infty} e^{-ik\frac{\pi}{2}} I_k\left(\frac{ac}{2}\right) I_{\frac{n-k}{2}}\left(\frac{a^2}{8}\right).$$

Apart from a factor of $1/\pi$ in the amplitude, this is equivalent to the expression obtained in *Sarfaty et al.* [1996].

The effects of anisotropy and velocity shear on $f_1(v_y)$ are examined in Figure 3 through Figure 6. The graphs are of amplitude (arbitrary units) versus velocity (normalized to the perpendicular thermal velocity). For each plot $V_o = 0$, $k_\perp \rho = 1.1$, $\omega/\Omega = 1.3116$, $\Omega/k_\| v_{th\|} = 7.62$, and θ=.71 *rad* to match the parameters of *Sarfaty et al.* [1996]. The values for the anisotropy and normalized shear strength are listed in the captions for each figure.

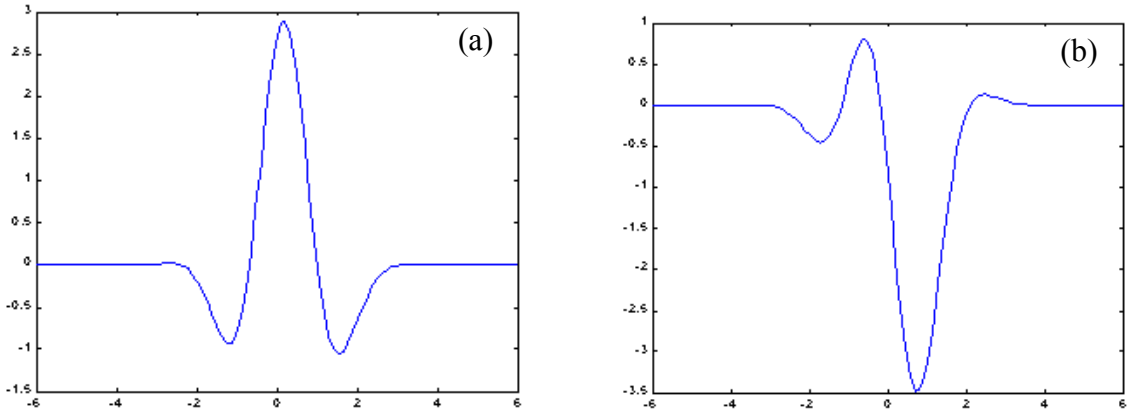

Figure 3. For $T_\|/T_\perp = 1$ and $V'/\Omega = 0$, the (a) imaginary and (b) real parts of $f_1(v_y)$.

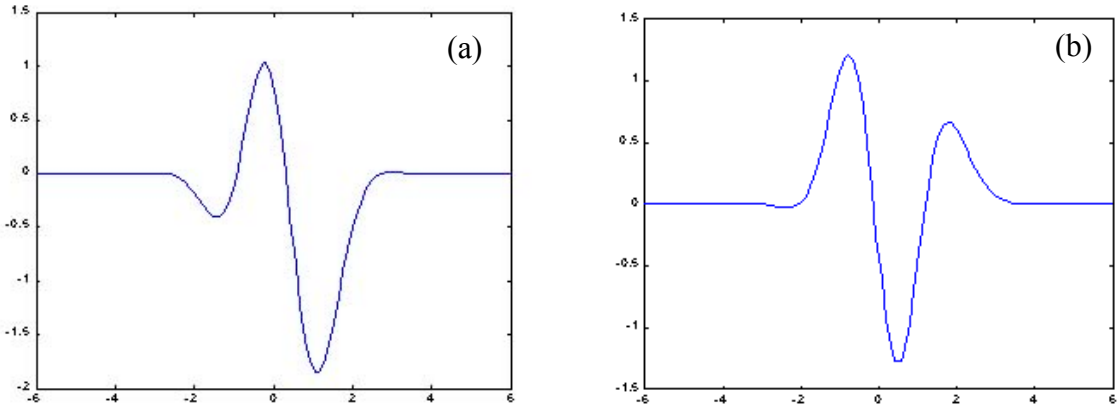

Figure 4. For $T_{\|}/T_{\perp}=1$ and $V'/\Omega=2$, the (a) imaginary and (b) real parts of $f_1(\mathrm{v}_y)$.

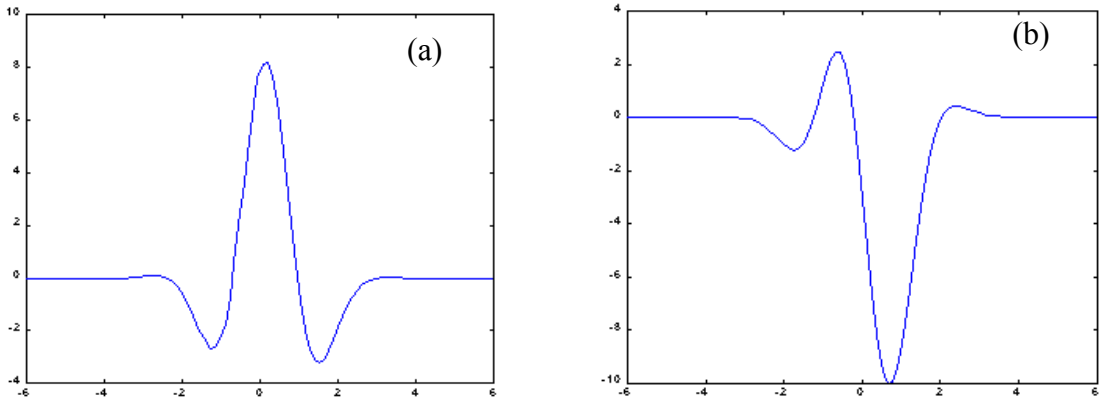

Figure 5. For $T_{\|}/T_{\perp}=3$ and $V'/\Omega=0$, the (a) imaginary and (b) real parts of $f_1(\mathrm{v}_y)$.

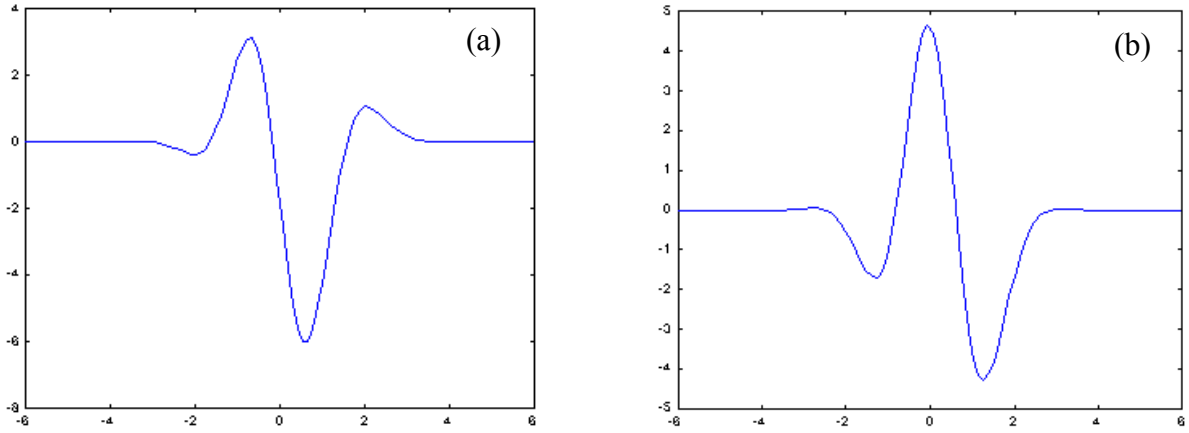

Figure 6. For $T_{\|}/T_{\perp}=3$ and $V'/\Omega=2$, the (a) imaginary and (b) real parts of $f_1(\mathrm{v}_y)$.

Figures 3 through 6 suggest that velocity shear has a significant effect on both the out of phase (imaginary) and in phase (real) parts of $f_1(\mathrm{v}_y)$. Without shear, the out of phase (imaginary) part of the perturbation looks nearly symmetric about $v = 0$ (Figure 3 and Figure 5). Adding shear assigns an unambiguous coordinate system in the plane perpendicular to the magnetic field and results in an imaginary part of the perturbation that is vaguely representative of a sinc function about $v = 0$ (Figure 4). The amplitude of the out of phase perturbation also decreases with increasing shear. The amplitude of the perturbed distribution functions, which is proportional to the inverse of the parallel ion temperature, was left constant while the temperature ratios were varied. The most noticeable effect of shear on the in phase (real) part of the perturbation is a tendency towards equal positive and negative oscillations in the magnitude of $f_1(\mathrm{v}_y)$. Shear seems to affect both the real and imaginary parts regardless of anisotropy. That is, $f_1(\mathrm{v}_y)$ is altered by shear to the same extent in an isotropic plasma as in an anisotropic plasma. Although the form of the perturbed distribution function changes, accurate measuring capabilities may enable a rough estimate of shear in a plasma by noting the attenuation of the overall amplitude.

V. Comparison of Calculations with Zero-shear and Isotropic Cases

The validity of the dispersion relation is verified in two limits. The first is the isotropic limit, $T_\perp = T_\parallel$. [*Gavrishchaka et al.*, 1999], and the second is the zero-shear limit [*Stix*, 1962].

V. A. Isotropic Limit

If the ratio of the perpendicular and parallel ion temperatures in equation (38) is set to unity, the dispersion relation becomes,

$$k^2\lambda_{Di}^2 + 1 + \sum_{n=-\infty}^{\infty} \Gamma_n(b) F_{\substack{ni \\ isotropic}} + \tau\left(1 + F_{\substack{0e \\ isotropic}}\right) = 0 \tag{56}$$

where

$$F_{\substack{ni \\ isotropic}} = \left(\frac{\omega}{\sqrt{2}k_{\|}\mathrm{v}_{th\|i}}\right) Z\left(\frac{\omega - n\Omega}{\sqrt{2}k_{\|}\mathrm{v}_{th\|i}}\right) - \frac{V_o'(x)}{\Omega u}\left(1 + \left(\frac{\omega - n\Omega}{\sqrt{2}k_{\|}\mathrm{v}_{th\|i}}\right) Z\left(\frac{\omega - n\Omega}{\sqrt{2}k_{\|}\mathrm{v}_{th\|i}}\right)\right)$$

and

$$F_{\substack{0e \\ isotropic}} = \left(\frac{\omega - k_{\|}V_0(x)}{\sqrt{2}k_{\|}\mathrm{v}_{th\|e}}\right) Z\left(\frac{\omega - k_{\|}V_0(x)}{\sqrt{2}k_{\|}\mathrm{v}_{th\|e}}\right) + \frac{V_0'(x)}{u\mu\Omega}\left(1 + \left(\frac{\omega - k_{\|}V_0(x)}{\sqrt{2}k_{\|}\mathrm{v}_{th\|e}}\right) Z\left(\frac{\omega - k_{\|}V_0(x)}{\sqrt{2}k_{\|}\mathrm{v}_{th\|e}}\right)\right)$$

Equation (57) is identical to the isotropic calculation described in *Gavrishchaka et al.* [1998].

V. B. Zero-shear Limit:

The other limiting case is that of a thermally anisotropic plasma with zero shear. In demonstrating agreement in this limit, the generalized dispersion relation and Stix's [*Stix,* 1962] expression for this limit will both be modified to show that they are equivalent. Modification of both expressions is needed to avoid a complicated discussion of the steps leading to the generalized dispersion relation. First, the shear terms in the generalized dispersion relation are set to zero. Then, Stix's version of this limiting case is written for a two species plasma and treated under the same constraints as used for the

work here, i.e. transformed to the ion frame, retention of only $n = 0$ term for electrons, etc.

In the zero-shear limit, $V_o^{'}(x) = 0$, the generalized dispersion relation becomes,

$$k^2\lambda_{Di}^2 + \frac{T_{\perp i}}{T_{\|i}} + \sum_{n=-\infty}^{\infty} \Gamma_n(b) F_{\substack{ni \\ no\,shear}} + \tau \frac{T_{\perp e}}{T_{\|e}}(1 + F_{\substack{0e \\ no\,shear}}) = 0$$

where

$$F_{\substack{0e \\ no\,shear}} = (\frac{\omega - k_{\|}V_0}{\sqrt{2}k_{\|}\mathrm{v}_{th\|e}})Z(\frac{\omega - k_{\|}V_0}{\sqrt{2}k_{\|}\mathrm{v}_{th\|e}}) \tag{57}$$

and,

$$F_{\substack{ni \\ no\,shear}} = (\frac{1}{\sqrt{2}k_{\|}\mathrm{v}_{th\|i}})\left(n\Omega(1 - \frac{T_{\perp i}}{T_{\|i}}) + \frac{T_{\perp i}}{T_{\|i}}\omega \right) Z(\frac{\omega - n\Omega}{\sqrt{2}k_{\|}\mathrm{v}_{th\|i}}).$$

The linear dispersion relation for electrostatic waves in a current-carrying plasma with anisotropic Maxwellian velocity distributions is [*Stix*, 1962],

$$-k^2 = \sum_{j=species} \sum_{n=-\infty}^{n=\infty} \frac{\Gamma_n(\mu_i)}{\lambda_{Di}^2}\left[\frac{T_{\perp i}}{T_{\|i}} + \left(\frac{(\omega - k_{\|}V_{oj} + n\Omega_i)T_{\perp i} - n\Omega_i T_{\|i}}{k_{\|}T_{\|i}A_{\|i}} \right) Z(\frac{\omega - k_{\|}V_{dj} + n\Omega_i}{k_{\|}A_{\|j}}) \right] ,$$

where,

$$A_{\|j} = \left(\frac{2T_{\|j}}{m_j} \right)^{\frac{1}{2}} = \sqrt{2}\mathrm{v}_{th\|} \quad . \tag{58}$$

Summing over species, keeping only the $n = 0$ term for electrons, and transforming to the ion frame yields

$$-k^2 = \sum_{n=-\infty}^{n=\infty} \frac{\Gamma_n(\mu_i)}{\lambda_{Di}^2}\left[\frac{T_{\perp i}}{T_{\|i}} + \left(\frac{(\omega + n\Omega_i)T_{\perp i} - n\Omega_i T_{\|i}}{k_{\|}T_{\|i}A_{\|i}} \right) Z(\frac{\omega + n\Omega_i}{k_{\|}A_{\|j}}) \right] + \frac{\Gamma_0(\mu_j)}{\lambda_{De}^2}\left[\frac{T_{\perp e}}{T_{\|e}} + \left(\frac{(\omega - k_{\|}V_o)T_{\perp e}}{k_{\|}T_{\|e}A_{\|e}} \right) Z(\frac{\omega - k_{\|}v_D}{k_{\|}A_{\|e}}) \right] \tag{59}$$

Inserting the expressions for $A_{\|}$,

$$0 = k^2\lambda_{Di}^2 + \sum_{n=-\infty}^{n=\infty} \Gamma_n(\mu_i)\left[\frac{T_{\perp i}}{T_{\|i}} + \left(\frac{(\omega + n\Omega_i)T_{\perp i} - n\Omega_i T_{\|i}}{k_{\|}T_{\|i}\sqrt{2}v_{th\|i}} \right) Z(\frac{\omega + n\Omega_i}{k_{\|}\sqrt{2}v_{th\|i}}) \right] + \frac{\lambda_{Di}^2}{\lambda_{De}^2}\left[\frac{T_{\perp e}}{T_{\|e}} + \left(\frac{(\omega - k_{\|}V_o)T_{\perp e}}{k_{\|}T_{\|e}\sqrt{2}\mathrm{v}_{th\|e}} \right) Z(\frac{\omega - k_{\|}V_o}{k_{\|}\sqrt{2}\mathrm{v}_{th\|e}}) \right] \tag{60}$$

and recalling the definition

$$\tau = \frac{T_{\perp i}}{T_{\perp e}} = \frac{\lambda_{Di}^2}{\lambda_{De}^2},$$

equation (59) becomes

$$0 = k^2\lambda_{Di}^2 + \frac{T_{\perp i}}{T_{\|i}} + \sum_{n=-\infty}^{n=\infty} \Gamma_n(\mu_i) \underbrace{\left[\left(n\Omega_i \left(\frac{T_{\perp i}}{T_{\|i}} - 1 \right) + \frac{T_{\perp i}}{T_{\|i}} \omega \right) \left(\frac{1}{\sqrt{2} k_{\|} \mathrm{v}_{th\|i}} \right) Z\left(\frac{\omega - n\Omega_i}{k_{\|}\sqrt{2}\mathrm{v}_{th\|i}} \right) \right]}_{F_{ni}} +$$

$$\tau \left(\frac{T_{\perp e}}{T_{\|e}} \right) \left[1 + \underbrace{\left(\frac{(\omega - k_{\|} V_o)}{\sqrt{2} k_{\|} \mathrm{v}_{th\|e}} \right) Z\left(\frac{\omega - k_{\|} V_o}{\sqrt{2} k_{\|} \mathrm{v}_{th\|e}} \right)}_{F_{0e}} \right]. \tag{61}$$

Noting that

$$\mu_i = \frac{k_{\perp}^2 A_{\perp i}^2}{2\Omega_i^2} = \frac{k_{\perp}^2}{2\Omega_i^2} * \frac{2T_{\perp}}{M} = \frac{k_{\perp}^2 v_{th\perp i}^2}{\Omega_i^2} = \frac{k_{\perp}^2}{2\Omega_i^2 \beta_{\perp}} = b \quad ,$$

equation (61) reduces to

$$0 = k^2\lambda_{Di}^2 + \frac{T_{\perp i}}{T_{\|i}} + \sum_{n=-\infty}^{\infty} \Gamma_n(\mu_i) F_{ni}\underset{zeroshear}{} + \tau \left(\frac{T_{\perp e}}{T_{\|e}} \right) \left[1 + F_{oe}\underset{zeroshear}{} \right] \tag{62}$$

and is identical to the zero shear limit of the generalized dispersion relationship (Equation (57)).

V.C. Zero-shear, isotropic limit

In a discussion of critical currents in the upper ionosphere, *Kindel and Kennel* [1971] used the isotropic limit of the dispersion relation given by *Stix* [1962]. It was shown in the previous section that, for a two-species plasma, the zero shear limit of the generalized dispersion relation derived in this work is equivalent to *Stix's* [1962] result (Equation (62)). Taking the isotropic limit of Equation (62) yields

$$0 = k^2\lambda_{Di}^2 + 1 + \sum_{n=-\infty}^{\infty} \Gamma_n(\mu_i) F_{ni}\underset{zeroshear}{} + \tau \left[1 + F_{oe}\underset{zeroshear}{} \right] \tag{63}$$

where

$$F_{\substack{ni \\ zeroshear \\ isotropic}} = \left(\frac{\omega}{\sqrt{2} k_{||} \mathrm{v}_{th||i}} \right) Z\left(\frac{\omega - n\Omega_i}{k_{||} \sqrt{2} \mathrm{v}_{th||i}} \right)$$

and

$$F_{\substack{0e \\ zeroshear \\ isotropic}} = \left(\frac{(\omega - k_{||} V_o)}{\sqrt{2} k_{||} \mathrm{v}_{th||e}} \right) Z\left(\frac{\omega - k_{||} V_o}{\sqrt{2} k_{||} \mathrm{v}_{th||e}} \right) \quad .$$

Using essentially the same dispersion relationship, *Kindel and Kennel* [1971] investigated plasma waves in the auroral zone for a range of T_i / T_e. Although both electrostatic ion cyclotron waves and ion acoustic waves can be driven by field-aligned currents in the ionosphere, *Kindel and Kennel* [1971] showed that the ion cyclotron mode is unstable to smaller values of the field-aligned current. Therefore, their work suggested that observed auroral zone electrostatic waves result from the ion cyclotron instability and should appear at frequencies around the ion cyclotron frequency [*Gavrishchaka*, 1996]. Observations of low frequency ion-acoustic like waves in ionospheric plasmas where $T_i \sim T_e$ [*Knudsen and Wahlund,* 1998; *Wahlund et al.*, 1994a; 1994b; 1998] motivated the work of *Gavrishachaka et al.* [1998; 1999], which demonstrated that a gradient in the parallel flow lowers the threshold current for the ion-acoustic mode below that of the threshold current of the ion-cyclotron mode and allows propagation even when the ion temperature (T_i) exceeds the electron temperature (T_e).

VI. Computational results

An existing FORTRAN code (to treat velocity shear in a thermally isotropic plasma) was modified to include the effects of thermal anisotropy [*Gavrishtchaka*, 1996]. Because equation (38), the dispersion relationship, can be expressed solely as a function of $k_y\rho$, $k_{||}/k_y$, $T_{i\perp}/T_{i||}$, $T_{e\perp}/T_{e||}$, $T_{i\perp}/T_{e\perp}$, and $V_o/v_{ith\perp}$ (see Appendix G) the numerical results are independent of the absolute temperature of either species. Therefore, the effects of temperature components (e.g. $T_{i\perp}$) need not be considered individually. Solutions to equation (38), written in the dimensionless form derived in Appendix G, are obtained with a root finding algorithm that returns both the real and imaginary components of the wave frequency.

The effects of ion temperature anisotropy on two different plasma instabilities, the ion-acoustic mode and the ion cyclotron mode, were investigated. Of these two modes, most of the analysis focused on the ion acoustic mode and only a preliminary study of the ion cyclotron mode was completed. The two modes are distinguished by the values of $k_y\rho$ at which they occur. The ion acoustic mode occurs at small values of $k_y\rho << 1$, while the ion cyclotron mode grows for values of $k_y\rho$ much greater than unity.

VI.A Ion Acoustic mode

Ion-acoustic mode growth rates, γ, as a function of real frequency for varying values of ion temperature anisotropy are shown in Figure 7. The mode described by Figure 7 is identified as the ion-acoustic mode since it has a small (but non-zero) real frequency in an isotropic plasma. The isotropic case shown in Figure 7 is identical to the ion acoustic mode growth rate plot in *Gavrishchaka et al.* [1999]. The parameters used for Figure 7 are

$$T_{i\perp}/T_{e\perp} = .3,$$
$$M_i/M_e = 29392 \text{ (O+ plasma)},$$
$$V_o/v_{ith\perp} = 60,$$
$$|V_o'|/\Omega = .5$$

The growth rate curves were produced by fixing $B = (k_y\rho)^2$ at the value used by *Gavrishchaka et al.* [1999], $(k_y\rho)^2 = .0675$, and varying u, where $u = k_z/k_y$, until the

peak growth rate was obtained for each value of real frequency. For the isotropic case, u is varied such that $0.004 \le u \le .64$. For these parameters, the dispersion relationship solutions obtained from the FORTRAN code were inserted into a MATLAB™ representation of Equation (G.1). In all cases, the FORTRAN results were found to be roots of Equation (G.1).

Maximization over both wavevector parameters is necessary in order to find the peak growth rate. In this analysis, however, B was fixed to the same value for all ion acoustic graphs. The effect of maximizing over B is small, and the result, if any, is an additional upshift in real frequency. In a sense, a more profound result was traded for simplicity. Numerical cases are presented in Appendix H to justify fixing the value of B.

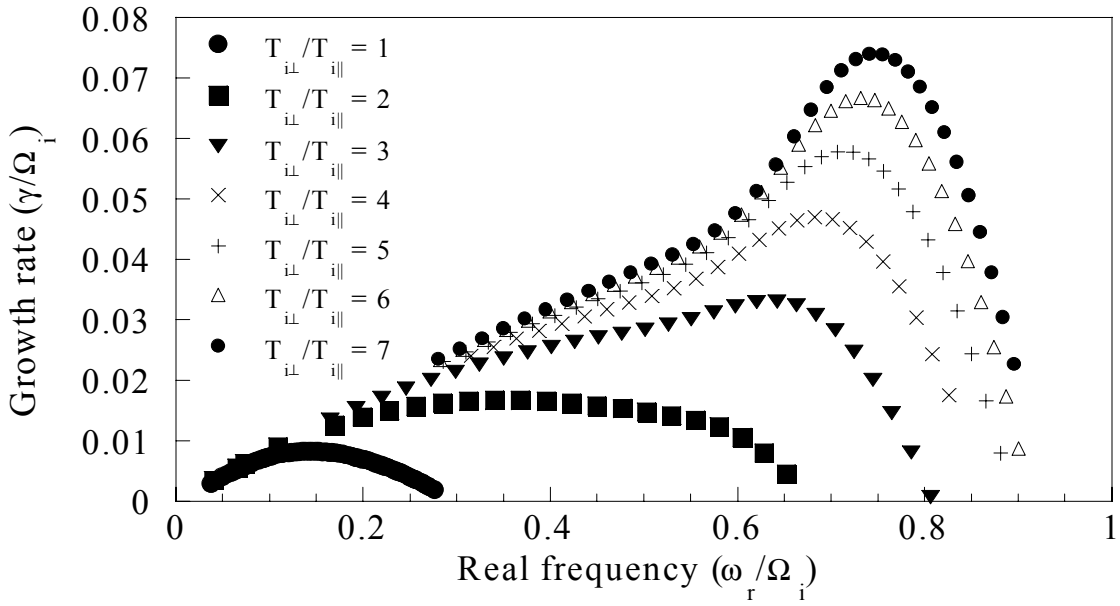

Figure 7. Growth rate versus real frequency for the ion acoustic mode in plasmas for values of ion temperature anisotropy from $T_{i\perp}/T_{i||} = 1$ to $T_{i\perp}/T_{i||} = 7$. Here, $T_{i\perp}/T_{e\perp} = .3, M_i/M_e = 29392, V_o/v_{ith\perp} = 60, |V_o'|/\Omega = .5$.

Increasing $T_{i\perp}/T_{i||}$ not only increases the growth rate, but also leads to a substantial upshift in the real frequency of the mode with maximum growth rate. Since only the ion temperature ratio appears in Equation (G.1), the frequency upshift would not occur if the overall temperature of the ions and electrons were increased isotropically. It is the change in the ion temperature anisotropy that causes the frequency upshift observed in the computational results. Dependence of the real frequency on the ion temperature

anisotropy was not observed in studies of the effects of ion temperature anisotropy in plasmas with a perpendicular gradient in the transverse flow. In those studies, the dispersion relationship was found to depend explicitly on the individual temperature components [*Gavrishchaka*, 1996]. For the plasma parameters investigated in Figure 7, the real frequency of the ion-acoustic mode shifts upwards by more than 700%. Depending on the effect of thermal anisotropy on the ion-cyclotron mode (to discussed later), both ion-acoustic and ion-cyclotron modes could appear in the same frequency range for plasmas with large thermal anisotropies.

A zeroth order calculation of the real and imaginary parts of the ion acoustic mode frequency is provided in Appendix H. In the analysis of Appendix H, zeroth order means that none of the ion cyclotron harmonic effects are included in the calculation. The real part of the frequency is given by

$$\omega \approx \left(k_{||}\right)\sqrt{\frac{T_{||e}}{M}\left(1-\frac{V_o^{'}(x)}{\Omega u}\right)}. \tag{64}$$

Equation (64) is equivalent to the zeroth order expression reported in *Gavrishchaka et al.* [1998], except that the relevant electron temperature is the *parallel* electron temperature. Clearly, there is no ion temperature anisotropy dependence in Equation (64). Rewriting Equation (64) in terms of the dimensionless ratios used in Appendix G, Equation (64) becomes

$$\hat{\omega} \approx u\left(k_y \rho\right)\sqrt{\left(\frac{1}{\tau \hat{T}_e}\right)\left(1-\frac{V_o^{'}(x)}{\Omega u}\right)}, \tag{65}$$

where

$$\hat{\omega} \equiv \frac{\omega}{\Omega}, \hat{T}_e \equiv \frac{T_{e\perp}}{T_{e||}}, \tau \equiv \frac{T_{i\perp}}{T_{e\perp}}.$$

For the analysis of Figure 7, $\hat{T}_e, \tau, k_y\rho$ and $V_o^{'}$, are all held constant. Therefore, to zeroth order, the dependence of the real frequency on the ion temperature anisotropy in Figure 7 arises from a dependence of the wavevector ratio, u, at peak growth rate on ion temperature anisotropy. This increase in u at which the maximum growth rate occurs, according to the FORTRAN code, is shown in Figure 8. As a check, values of u were extracted from Figure 8, then the real frequency corresponding to the that value of u was

calculated using Equation (65). The results are identical to the values indicated in Figure 9 (note that Figure 9 contains information from Figure 7). Figure 7 also shows that the frequency spectrum initially becomes broader as $T_{i\perp}/T_{i||}$ is increased from the isotropic case. At larger values of ion temperature anisotropy, the frequency spectrum of strongly growing modes becomes narrower and the dependence of the real frequency on ion temperature anisotropy vanishes.

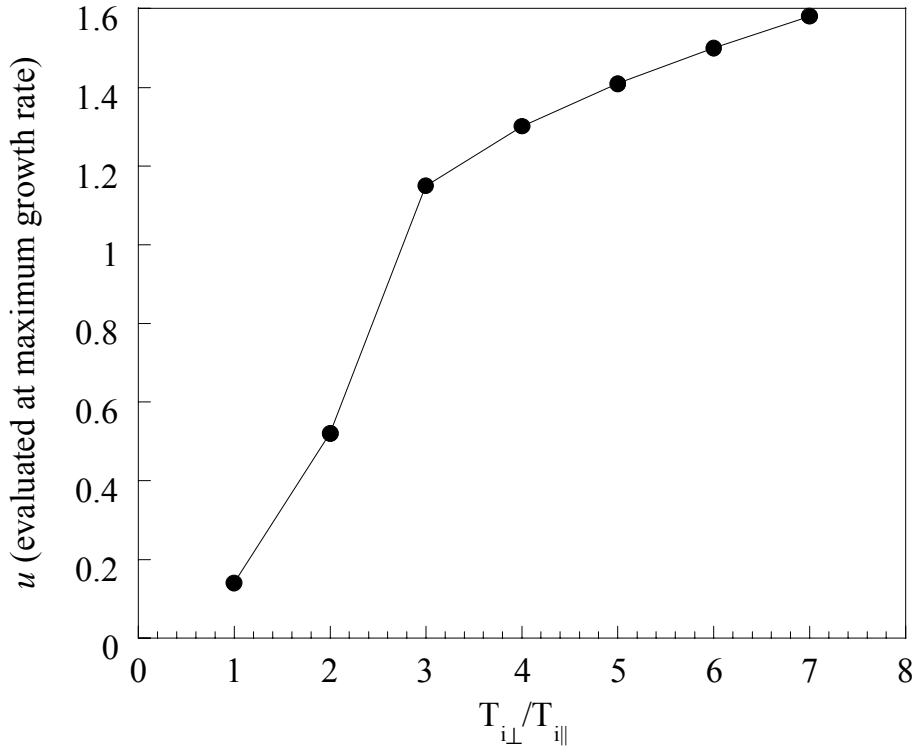

Figure 8. $u = k_{||}/k_y$ versus ion thermal anisotropy. The propagation angle used corresponds to the mode with the largest growth rate. Here, $T_{i\perp}/T_{e\perp} = .3, M_i/M_e = 29392, V_o/v_{ith\perp} = 60, |V_o'|/\Omega = .5$.

The real frequency corresponding to the largest growth rate (maximized over u) as a function of the ion thermal anisotropy for the ion-acoustic mode is shown in Figure 9. Essentially Figure 9 is a summary of Figure 7. The saturation in the value of the real frequency for ion temperature anisotropies greater than 3 is clearly evident. That the real frequency of the ion-acoustic mode should depend so strongly on the ion temperature

anisotropy is a new result. It is worth noting that the real frequency corresponding to $T_{i\perp}/T_{i\|}=1$ is the same as reported in *Gavrishchaka et al.* [1998].

Experiments could be performed in a thermally anisotropic background plasma with inhomogeneous parallel flow to test this predicted frequency upshift of the ion-acoustic mode. Evidence suggesting that strong parallel flows are associated with low frequency wave activity and the conversion of parallel ion energy into perpendicular ion energy has been reported from the LEIA experiment [*Scime et al.*, 2000]. If those parallel flows are also inhomogeneous, the mechanism described in this work could be responsible for the low frequency wave activity.

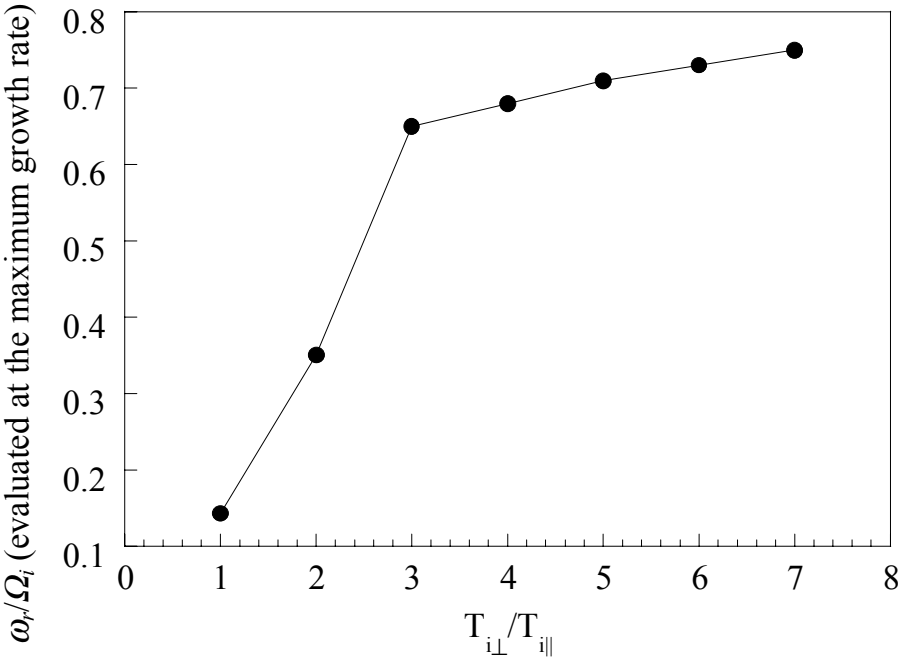

Figure 9. Real frequency corresponding to the ion acoustic wave with the largest growth rate versus ion thermal anisotropy. Here, $T_{i\perp}/T_{e\perp}=.3, M_i/M_e=29392, V_o/v_{ith\perp}=60, |V_o'|/\Omega=.5$.

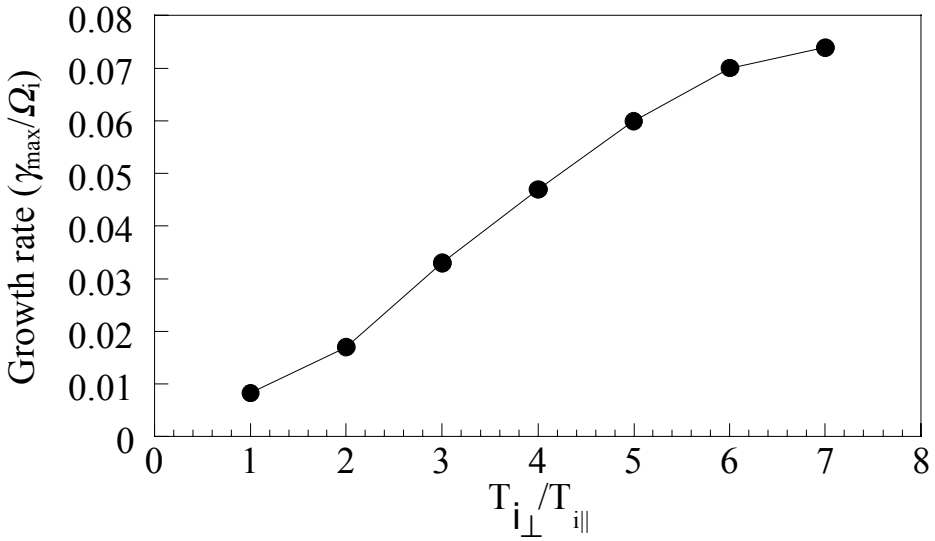

Figure 10. Growth rate of the ion-acoustic mode (maximized over the wavenumber spectrum) versus ion temperature anisotropy. Here, $T_{i\perp}/T_{e\perp} = .3, M_i/M_e = 29392, V_o/v_{ith\perp} = 60, |V_o'|/\Omega = .5$.

As shown in Figure 7, the growth rate of the ion-acoustic mode is also affected by thermal anisotropy. Figure 10 shows the growth rate of the ion-acoustic mode as a function of ion thermal anisotropy. The growth rate used is the largest found in scanning over the parameter *u*. The same parameters used to generate Figure 7 were used. The growth rate for $T_{i\perp}/T_{i||} = 1$ is the same value reported by *Gavrishchaka et al.* [1998]. According to the data shown in Figure 10, the growth rate of the ion acoustic mode increases approximately linearly with increasing $T_{i\perp}/T_{i||}$.

The angle of propagation, $u = k_{||}/k_y$, at peak growth rate as a function of thermal anisotropy has already been shown in Figure 8. An acoustic wave typically propagates along the magnetic field, corresponding to a large value for *u*. However, Figure 8 shows that the propagation direction of the ion-acoustic mode changes as a function of ion temperature anisotropy. In the presence of an inhomogeneous parallel flow, an ion acoustic wave in an isotropic plasma propagates obliquely. As $T_{i\perp}/T_{i||}$ increases, the wave propagation becomes more parallel to the magnetic field. The isotropic case yields a propagation angle of *u* =.14 for maximum growth rate, the same value reported in *Gavrishchaka et al.* [1998].

To zeroth order, the increase in u with anisotropy is responsible for the upshift in the real frequency seen in Figure 7 and Figure 9. By keeping only the zeroth order terms in the dispersion relationship used in the FORTRAN code, the zeroth order dependence of the real frequency on ion temperature anisotropy was investigated. The real frequency was found to depend on the propagation angle, u, as described by Equation (66). Since the value of u at which the maximum growth rate occurs increases with anisotropy, the real frequency also increases with anisotropy.

Figures 11, 12, and 13 are plots of the real frequency versus normalized shear, the growth rate versus normalized shear, and the selected (by maximum growth rate) wavevector ratio, u, versus shear, respectively. Each curve was generated keeping all quantities except for shear constant. These plots are provided to illustrate the effects of ion thermal anisotropy at different values of normalized shear. Each plot has a curve describing a plasma with ion temperature anisotropies of $T_{i\perp}/T_{i||} = 1, 2, 4, \text{and } 6$. The value of B was held constant, and the growth rate was maximized over the quantity u. See Appendix H for a discussion of how not maximizing over B (in addition to u) may affect the analysis.

Figure 11 not only demonstrates the frequency shift that accompanies a change in anisotropy (as in Figures 7 and 9), but also shows how the frequency shift changes with normalized shear. As the shear is increased, the shift in real frequency becomes less dramatic (although still significant). Thus, the real frequency upshifts with increasing anisotropy or increasing shear. A shift due to an increase in either parameter tends to saturate at a real frequency slightly below the ion cyclotron frequency.

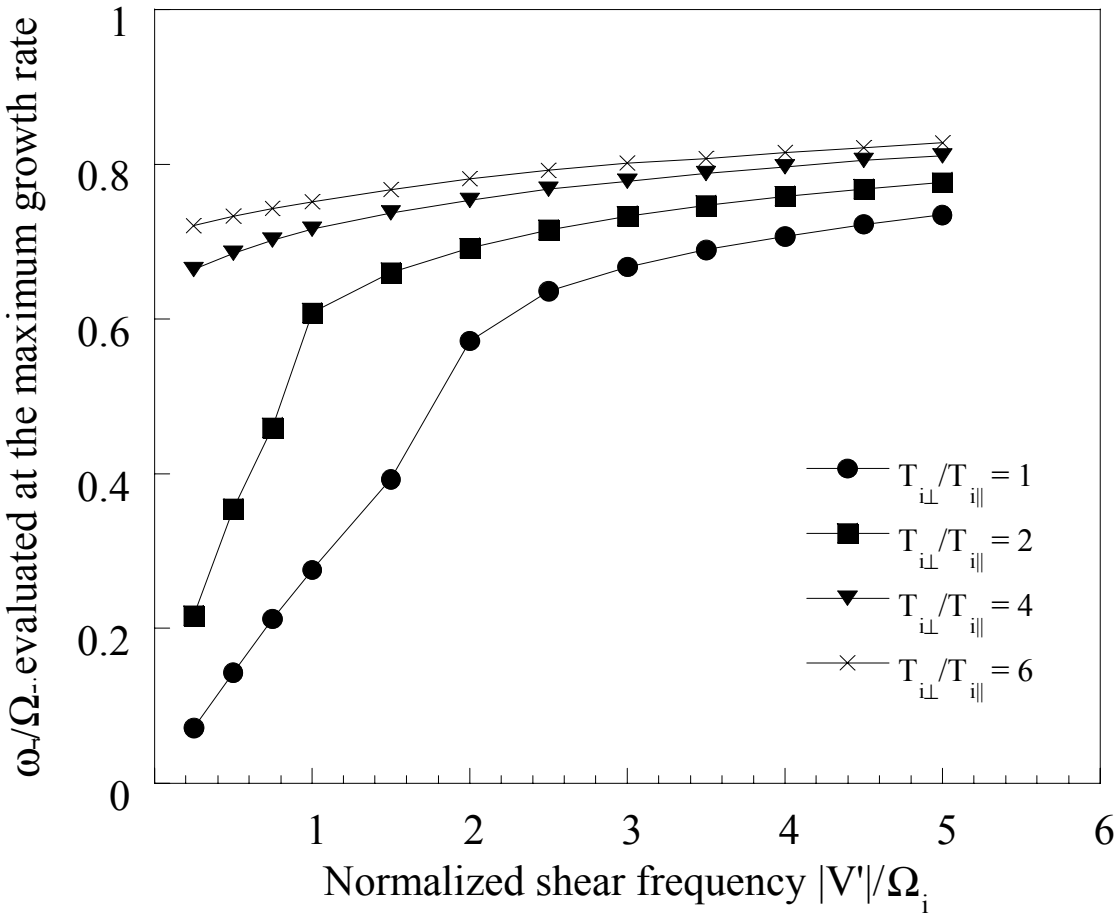

Figure 11. Real frequency versus normalized shear for $T_{i\perp}/T_{i||}=1$, $T_{i\perp}/T_{i||}=2$, $T_{i\perp}/T_{i||}=4$, and $T_{i\perp}/T_{i||}=6$. The real frequencies shown correspond to the modes with the largest growth rates. Here, $T_{i\perp}/T_{e\perp}=.3, M_i/M_e=29392, V_o/v_{ith\perp}=60$.

Figure 12 shows that the growth rate of an ion acoustic plasma wave increases both with $T_{i\perp}/T_{i||}$ and with normalized shear. In the isotropic case, the growth rate becomes extremely small in the absence of shear, thereby confirming that a perpendicular gradient in the parallel flow is required to excite this instability. However, the anisotropic cases still have a substantial growth rate at small values of normalized shear. This suggests that the equilibrium flow (i.e., current) is sufficient to excite low frequency, ion-acoustic modes in such thermally anisotropic plasmas. However, the growth rate increases significantly with the shear parameter, σ. No saturation in growth rate is apparent.

Figure 13 reiterates the tendency of the wavevector ratio, *u*, to increase with anisotropy. The change in *u*, however, is less dramatic as the shear increases. This is the same trend exhibited by the real frequency in Figure 11. At large values of normalized shear, the trend is for *u*'s of all anisotropies to approach each other. As shear is increased the effects of anisotropy become less apparent for the propagation angle and the real frequency, but the effect of anisotropy on the growth rate seems unaffected.

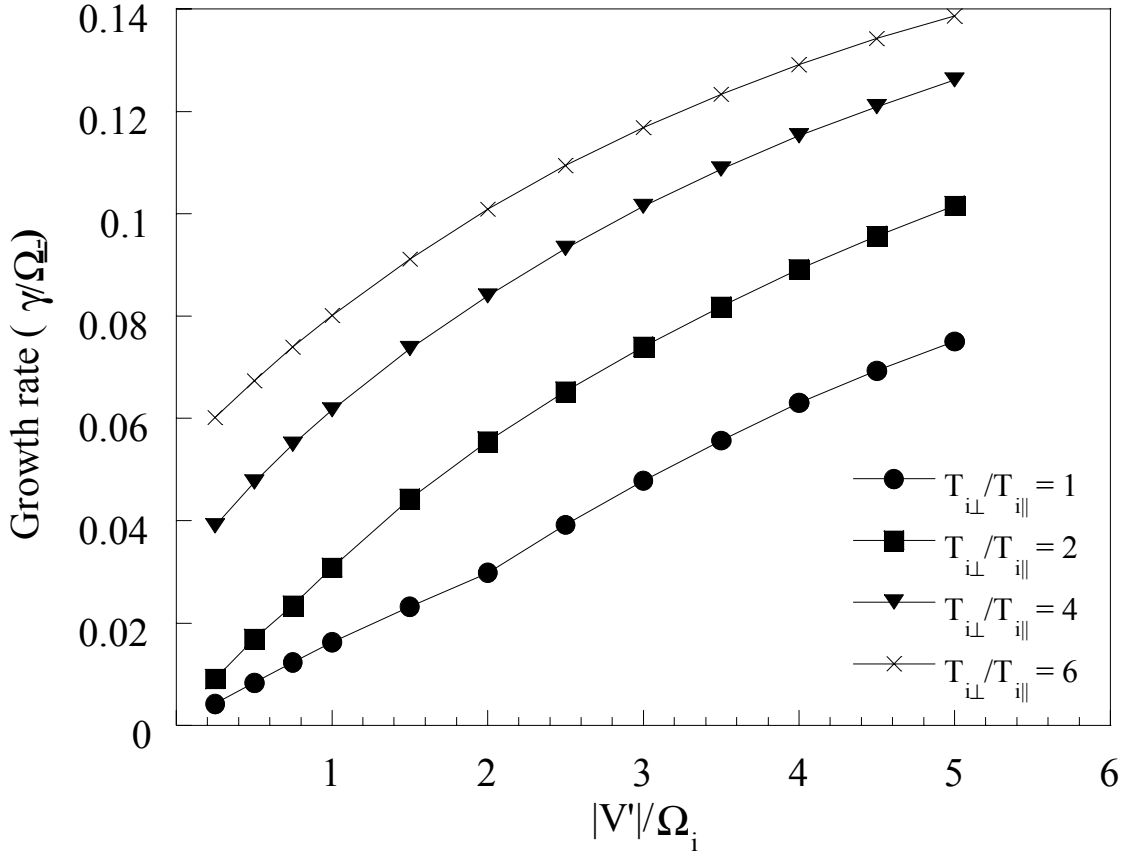

Figure 12. Growth rate versus normalized shear for $T_{i\perp}/T_{i\|}=1$, $T_{i\perp}/T_{i\|}=2$, $T_{i\perp}/T_{i\|}=4$, and $T_{i\perp}/T_{i\|}=6$.. Here, $T_{i\perp}/T_{e\perp}=.3, M_i/M_e=29392, V_o/v_{ith\perp}=60.$

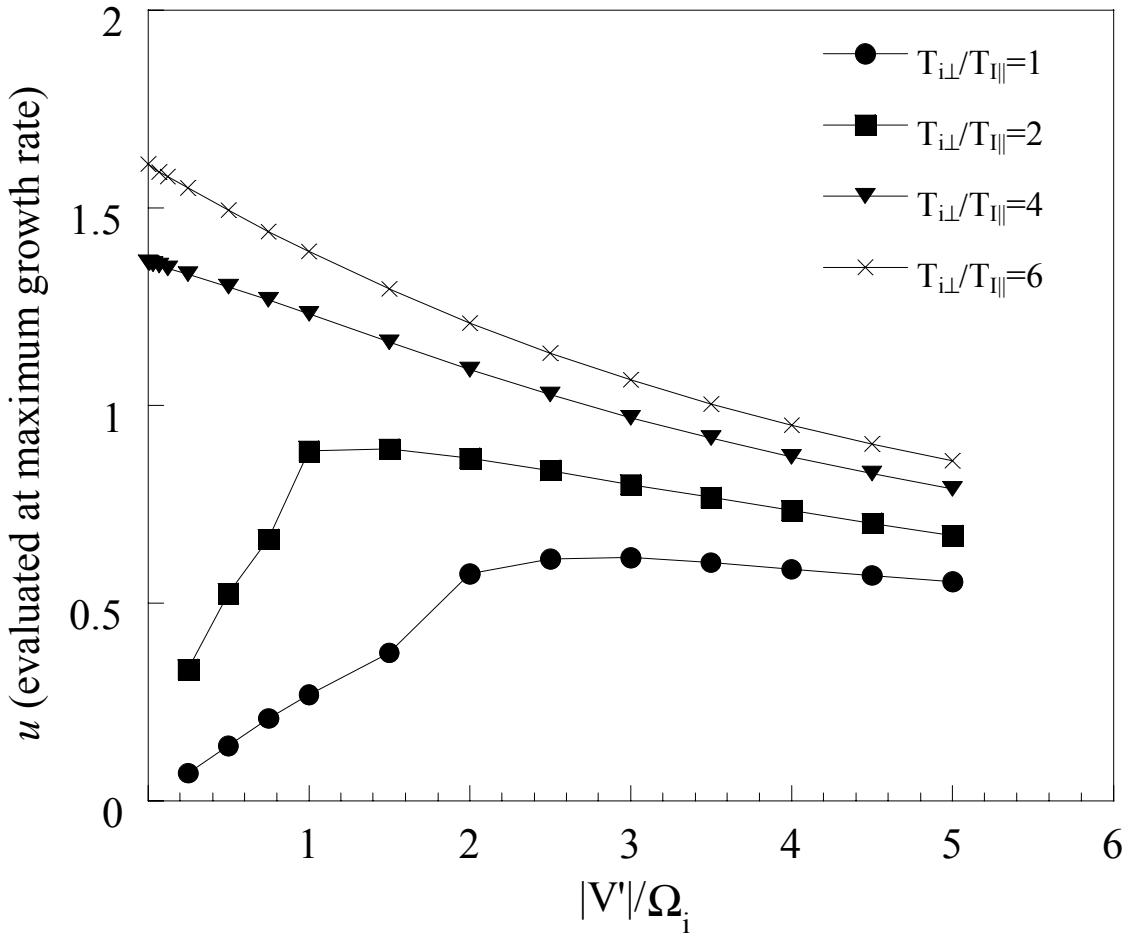

Figure 13. u versus normalized shear for $T_{i\perp}/T_{i||}=1$, $T_{i\perp}/T_{i||}=2$, $T_{i\perp}/T_{i||}=4$, and $T_{i\perp}/T_{i||}=6$. u is evaluated at the maximum growth rate for each case. Here, $T_{i\perp}/T_{e\perp}=.3, M_i/M_e=29392, V_o/v_{ith\perp}=60.$

VI.B Ion Cyclotron Mode

The effects of ion temperature anisotropy on the ion cyclotron mode were also briefly investigated for comparison with the ion acoustic mode. The analysis presented here does not include all the effects observed on the characteristics of the ion cyclotron mode. Figure 14 shows the effect of thermal anisotropy on the growth rate of the ion-cyclotron mode. These modes are identified as ion-cyclotron modes as their real frequencies are peaked at integer multiples of the ion cyclotron frequency. Also, these modes propagate nearly perpendicularly to the background magnetic field. The growth rate as a function of real frequency is shown for plasma parameters given by

$$
\begin{aligned}
&(k_y\rho)^2 = 100\ , \\
&\omega_{ce}/\omega_{pe} = 8.2, \\
&T_{i\perp}/T_{e\perp} = 1, \\
&M_i/M_e = 1837, \\
&V_o = 0, \\
&B_{xeff} = 4, \\
&\text{and } V_o'/\Omega = 2 \quad .
\end{aligned}
$$

The quantity u was varied such that only positive growth rates were considered. For the isotropic case, u was varied such that $4\times10^{-4} \le u \le 2.71\times10^{-2}$.

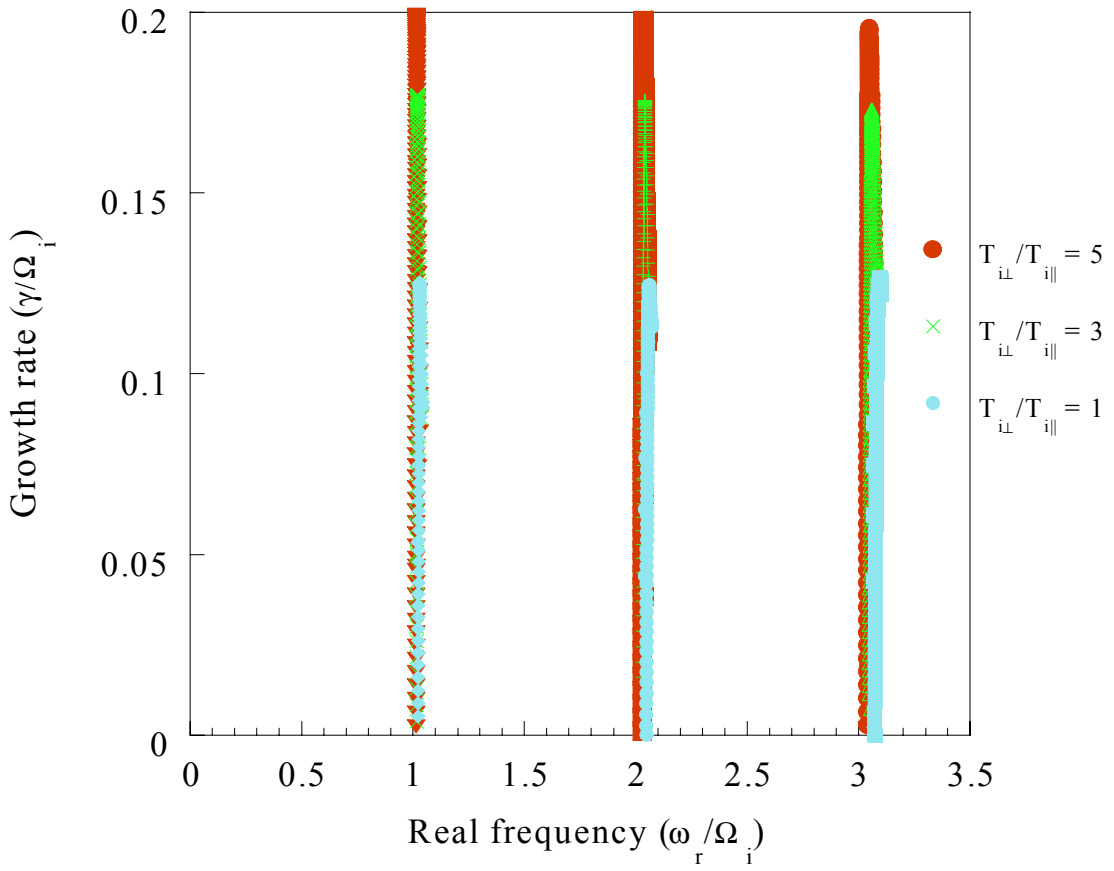

Figure 14 Growth rate versus real frequency for the ion-cyclotron mode in plasmas of varying thermal anisotropies.

For the ion-cyclotron mode in the presence of inhomogeneous field-aligned flow, increasing the value of $T_{i\perp}/T_{i\|}$ increases the growth rate. However, the real frequency of the mode is unaltered. For each value of $T_{i\perp}/T_{i\|}$ examined in Figure 14, the value of $T_{e\perp}/T_{e\|}$ was not changed. The increase in growth rate with $T_{i\perp}/T_{i\|}$ seems to be in sharp contrast to the theoretical prediction of *Lee* [1972], who showed that the growth rate should decrease with $T_{i\perp}/T_{i\|}$. This discrepancy is resolved by noting that the theoretical treatment of *Lee* [1972] modeled a current driven ion cyclotron wave and not a velocity shear driven instability. Figure 15 shows the dependence of growth rate on ion thermal anisotropy for the shearless, current driven case.

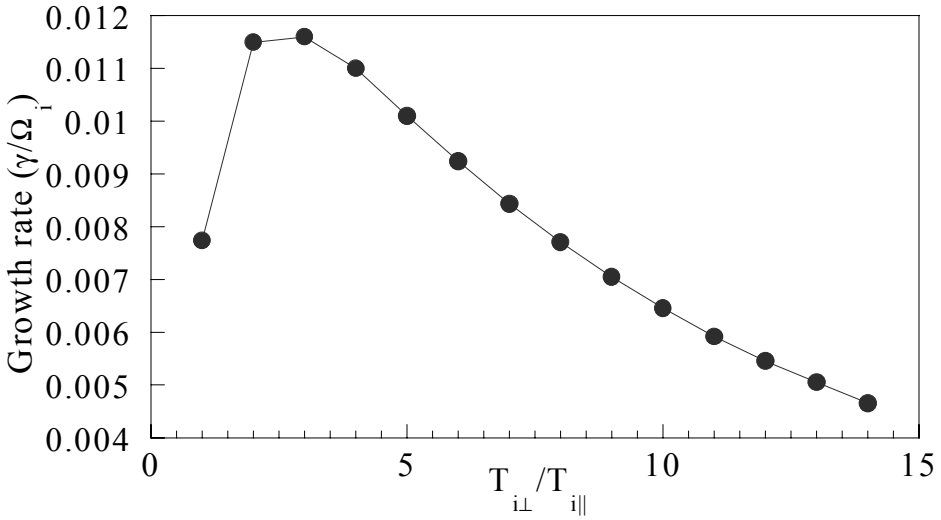

Figure 15. Growth rate versus ion thermal anisotropy for the ion-cyclotron mode in shearless plasmas of varying thermal anisotropies. The same parameters used in Figure 14 are used except that $v_o / v_{ith\perp} = 100$ and $V_o^{'} = 0$.

Consequently, the dependence of the growth rate on $T_{i\perp}/T_{i||}$ is consistent with the zero-shear limit investigated by *Lee* [1972]. In that work, it was shown that the growth rate for the two-stream ion cyclotron mode increases with $T_{e||}/T_{i\perp} = \left(T_{e||}/T_{i||}\right)\left(T_{i||}/T_{i\perp}\right)$. Thus, with $T_{e||}/T_{i||}$ held constant, the growth rate of a shearless ion cyclotron mode decreases with $T_{i\perp}/T_{i||}$. The currentless, shear driven ion cyclotron mode, however, exhibits a different growth rate dependence on ion thermal anisotropy. This is a new result.

The ion cyclotron mode remains sharply peaked at the cyclotron frequency and its harmonics. Changing the anisotropy has a significant effect on the growth rate, but not on the real frequency or the perpendicular wavenumber at which the wave propagates.

VII. DISCUSSION

The dispersion relation derived in this work is a generalization of *Ganguli et al.* [1994] to include thermal anisotropy. It is clear that ion thermal anisotropy can play an important role in changing the frequency, growth rate, and propagation angle of plasma instabilities in the presence of a perpendicular gradient in the field-aligned flow. According to Figure 7, the real frequency corresponding to the largest growth rate upshifts significantly for ion-acoustic waves as $T_{i\perp}/T_{i||}$ increases. The upshift saturates at a real frequency of approximately $\omega_r \approx .8\Omega_i$, corresponding to an increase of almost 700%. Since there is no appreciable shift in real frequency due to a change in $T_{i\perp}/T_{i||}$ for the ion cyclotron mode (see Figure 14), ion acoustic and ion cyclotron modes should be found in close, but not overlapping, regions of frequency space in plasmas with inhomogeneous parallel flow and ion thermal anisotropy.

The frequency upshift in an ion acoustic wave is actually a two-step process. In the analysis, the mode with the largest growth rate was selected by scanning through the parameter *u*. As the anisotropy is increased, the value of *u* corresponding to the maximum growth rate also increases (see Figure 8). The zeroth order expression for real frequency in the presence of inhomogeneous parallel flow shear is (Equation (66))

$$\hat{\omega} \approx u\left(k_y \rho\right)\sqrt{\left(\frac{1}{\tau \hat{T}_e}\right)\left(1-\frac{V_o^{'}(x)}{\Omega u}\right)}.$$

In this analysis, the quantity $k_y \rho$ is held constant as $u = k_{||}/k_y$ is varied. Such a scan is equivalent to varying $\rho k_{||}$. A higher value of *u* is equivalent to a higher value of $\rho k_{||}$, so it is no surprise that the real frequency is upshifted. Additionally, the broadbanded nature of the ion acoustic mode for intermediate anisotropy can be interpreted a weak dependence of *u* (at which the maximum growth rate occurs) on $T_{i\perp}/T_{i||}$.

An interesting characteristic of the upshift is that it tends to saturate at high values of shear. As the shear is increased, the same upshifts in real frequency and *u* occur, and both saturate at the same values of shear and anisotropy. Increasing anisotropy in the parameter regime of high shear has a much less dramatic effect on frequency, since saturation has already occurred. For instance, increasing the value of $T_{i\perp}/T_{i||}$ from unity to 6 results in a frequency upshift of approximately 800% for the lowest normalized shear

value shown in Figure 11, while the frequency upshifts only 10% for the highest shear value shown in Figure 11. Growth rate, on the other hand, shows only a slight saturation at the highest anisotropy (Figure 12). The relative spacing of the curves for varying anisotropy seems unaffected by the magnitude of the shear.

When investigating the effects of anisotropy τ and $T_{e\perp}/T_{e||}$ were fixed, and only the value of $T_{i\perp}/T_{i||}$ was changed. This can be interpreted either as changing $T_{i\perp}$ or $T_{i||}$. If the latter is changed, no other implications exist in the dispersion relation as treated computationally (see Appendix G). If $T_{i\perp}$ is changed, however, τ must be changed in order to keep the electron temperature constant. Also, the normalized wavevectors will have to be interpreted differently. If $T_{i\perp}$ is changed, the ion gyroradius (ρ) changes. Thus, for a particular value of $B=(k_y\rho)^2$ and $u=k_{||}/k_y$, the values of k_y and $k_{||}$ are different. Since the value of $k_{||}$ affects Landau damping, a change in growth rate is expected. In this work, however, the value of *u* was varied to maximize the growth rate, essentially finding the $k_{||}$ associated with the maximum growth rate. Appendix J shows the effects of varying τ to compensate for a change in electron temperature.

The perturbed distribution functions presented in this work are a generalization of the work of *Sarfaty et al.* [1996] to include velocity shear. Since the perturbed distribution function is a measurable plasma quantity, the profound effect of shear in the parallel flow (see Figures 2 through 6) is of significant experimental interest. In fact, one may even be able to determine the orientation of the wavevector in the plane perpendicular to the magnetic axis by measuring $f_1(v_{||})$ alone. Without the effects of shear inhomogeneous parallel flow included, $f_1(v_{||})$ only depends on the parallel wavenumber of the perturbation [*DeSouza-Machado*, 1996]. There is nothing to distinguish one Cartesian direction in the plane perpendicular to the magnetic field from another. Including inhomogeneous parallel flow, however, includes the parameter $u=k_y/k_{||}$. The shear direction establishes a reference axis. Given the complete (including the inhomogeneous flow) expression for $f_1(v_{||})$, one could vary the value of the parameter $V_o' k_y/\Omega k_{||}$ in a computer-generated $f_1(v_{||})$ plot until it matches an experimentally obtained $f_1(v_{||})$. If the value of the normalized velocity shear is known, the wavevector ratio $k_y/k_{||}$ is then indirectly determined.

VIII. REFERENCES

Agrimson, Erick, Nicola D'Angelo, Robert L. Merlino, Excitation of ion-acoustic-like waves by sub-critical currents in a plasma having equal electron and ion temperatures, *PRL*, **86**, 5282 (2001).

Alport, M.J., S.L. Cartier, and R.L. Merlino, Laboratory observations of ion cyclotron waves associated with a double layer in an inhomogeneous magnetic field, J. Geophys. Res., **91**, 1599, (1986).

Amatucci, William, Experimental observation of ion-cyclotron turbulence in the presence of transverse-velocity shear, Ph.D. Dissertation, (1994).

Amatucci, W.E., D.N. Walker, G. Ganguli, J.A. Antoniades, D. Duncan, J.H. Bowles, V. Gavrichtchaka, and M.E. Koepke, Plasma response to strongly sheared flows, Phys. Rev. Lett., **77**, 1978 (1996).

Amatucci, W.E., M.E. Koepke, J.J. Carroll III, and T.E. Sheridan, Geophys. Res. Lett., Observation of ion-cyclotron turbulence at small values of field-aligned current, **21**, 1595 (1994).

Amatucci, W.E., Inhomogeneous plasma flows: A review of in situ observations and laboratory experiments, J. Geophys. Res., **104**, 14481, 1999

Anderson, B. J., S. A. Fuselier, S. P. Gary, and R. E. Denton, Magnetic spectral signatures in the Earth's magnetosheath and plasma depletion layer, J. Geophys. Res., **99**, 5877 (1994).

André, M., G.B. Crew, W.K. Peterson, A.M. Persoon, C.J. Pollock, and M.J. Engebretson, Ion heating by broadband low-frequency waves in the cusp/cleft, J. Geophys. Res., **95**, 20809 (1990).

André, M., P., P. Norqvist, L. Anderson, L. Eliasson, A. Eriksson, L. Blomberg, R. Erlandson, and J. Waldemark, Ion energization mechanism at 1700 km in the auroral region, J. Geophys. Res., **103**, 4199 (1998).

Carroll, Jim, Experimental Investigation of the IEDD Instability, Ph.D. Dissertation, (1997).

Chen, F. , *Introduction to Plasma Physics and Controlled Fusion* , (Plennum Press, New York, 1984).

D'Angelo, N., and R.W. Motley, Electrostatic oscillations near the ion cyclotron frequency, *Phys. Fluids*, **5**, pp. 633-6XX, (1962); R.W. Motley and N.D'Angelo, *Phys. Fluids*, **6**, 296, (1963).

D'Angelo, N., Kelvin-Helmholtz instability in a fully ionized plasma in a magnetic field, Phys. Fluids, **8**, 1748 (1965).

De Souza-Machado, Sergio, First Order Perturbed Distribution Functions in a Gas Discharge Plasma in the Presence of Electrostatic Ion Cyclotron Waves, Ph.D. Dissertation, (1996).

Drummond, W.E., and M.N. Rosenbluth, Anomolous diffusion arising from microinstabilities in a plasma, *Phys. Fluids*, **5**, 1507, (1962).

Ergun, R.E., C.W. Carlson, J.P. McFadden, F.S. Mozer, G.T. Delory, W. Peria, C.C. Chaston, M. Temerin, R. Elphic, R. Strangeway, R. Pfaff, C.A. Cattell, D. Klumpar, E. Shelly, W. Peterson, E. Moebius, and L. Kistler, FAST satellite observations of electric field structures in the auroral zone, Geophys. Res. Lett., **25**, 2025 (1998).

Ganguli, G., Y.C. Lee, and P. Palmadesso, Electrostatic ion-cyclotron instability due to a nonuniform electric field perpendicular to the external magnetic field, *Phys. Fluids* **28**, pp. 761, (1985); G. Ganguli, P.J. Palmadesso, and Y.C. Lee, *Geophys. Res. Lett.*, **12**, (1985).

Ganguli, G., Y.C. Lee, P. Palmadesso, Kinetic Theory for electrostatic waves due to transverse velocity shears, *Phys. Fluids* **31**, 823, (1988).

Ganguli, G., M.J. Keskinen, H. Romero, R. Heelis, T. Moore, C. Pollock, Coupling of microprocesses and macroprocesses due to velocity shear: An application to the low-altitude ionosphere, *J. Geophys. Res.* , **99**, 8873, (1994).

Ganguli, G., "Stability of an inhomogeneous transverse plasma flow", Phys. Plasmas, **5**, 1544 (1997).

Gavrichtchaka, Valeriy, Collective phenomena in a magnetized plasma with a field-aligned drift and inhomogeneous transverse flow, Ph.D. Dissertation, (1996).

Gavrishchaka, V., M. Koepke, and G. Ganguli, Dispersive properties of a plasma with a field-aligned drift and an inhomogeneous transverse flow, Phys Plasmas, Phys. Plasmas, **3**, 3091 (1996).

Gavrishchaka, V.V., M.E. Koepke, and G.I. Ganguli, "Ion-cyclotron modes in a multi-component plasma with transverse-velocity shear", J. Geophys. Res., **102**, 11653 (1997).

Gavrishchaka, Valeriy V., Gurudas I. Ganguli, Supriya B. Ganguli, Origin of Low-Frequency Oscillations in the Ionosphere, *PRL*, **80**, 728 , (1998).

Gavrishchaka, Valeriy V., Supriya B. Ganguli, Guruda I. Ganguli, Electrostatic oscillations due to filamentary structures in the magnetic-field-aligned flow: The ion-acoustic branch, *J. Geophys. Res*., **104**, 12,683, (1999).

Heelis, R.A., J.D. Winningham, M. Sugiura, and N.C. Maynard, Particle acceleration parallel and perpendicular to the magnetic field observed by DE 2, J. Geophys. Res., **89**, 3893 (1984).

Ivchenko, N., G. Marklund, K. Lynch, D. Pietrowski, R. Torbert, F. Primdahl, and A. Ranta, Quasiperiodic oscillations observed at the edge of an auroral arc by Auroral Turbulence 2, Geophys. Res. Lett, (submitted) (1999).

Kindel, J.M. and C.F. Kennel, Topside current instabilities, J. Geophys. Res., **76**, 3055 (1971).

Kintner, P.M., Observation of velocity shear driven plasma turbulence, J. Geophys. Res., **81**, 5114 (1976).

Kline, J. L., E. E. Scime, P.A. Keiter, M. M. Balkey, and R. F. Boivin, Resonant Ion Heating in the HELIX Helicon Plasma Source, *Phys. Plasmas* **6**, 4767 (1999).

Knudsen, D. J., J. H. Clemmons, and J. -E. Wahlund, Correlation between core ion energization, suprathermal electron bursts, and ELF plasma waves, J. Geophys. Res., **103**, 4171 (1998).

Knudsen, D. J. and J.E. Wahlund, Core ion flux bursts within solitary kinetic Alfven waves, J. Geophys. Res., **103**, 4157 (1998).

Koepke, M.E. and W.E. Amatucci, IEEE Trans. Plasma Sci. 20, 631 (1992); M.E. Koepke, W.E. Amatucci, J.J. Carroll III, M. Alport, and T.E. Sheridan, in Auroral Plasma Dynamics, Geophysical Monograph Series, vol. 80, Lysak, ed. (AGU, Washington, D.C., 1993), 287.

Koepke, M.E., W.E. Amatucci, J.J. Carroll III, and T.E. Sheriden, Experimental verification of inhomogeneous energy density driven instability, Phys. Rev. Lett., **72**, 3355 (1994).

Koepke, M.E., J.J. Carroll III, and M. W. Zintl, Excitation and propagation of electrostatic ion-cyclotron waves in plasma with structured flow, Phys. Plasmas, **5**, 1671 (1998).

Koepke, M.E.; Carroll, J.J.III; Zintl, M.W., Laboratory simulation of broadband ELF waves in the auroral ionosphere, Journal-of-Geophysical-Research. **104**, no.A7, 14397 (1999).

Lee, Kai Fong, Ion cyclotron instability in current-carrying plasmas with anisotropic temperatures, *J. Plasma Physics*, **8**, Part 3, 379, (1972).

Lynch, K.A., R.L. Arnoldy, P.M. Kinter, and J. Bonnell, The AMICIST auroral sounding rocket: A comparison of transverse ion acceleration mechanisms, Geophys. Res. Lett., **23**, 3293 (1996).

Marklund, G., L. Blomberg, C. Falthammar, and P. Lindqvist, On intense diverging electric fields associated with black aurora, Geophys. Res. Lett., **21**, 1859 (1994).

McFadden, J.P., et. al., Spatial structure and gradients of ion beams observed by FAST, *Geophys. Res. Lett*., **25**, 2021, (1998).

McFadden, J.P., C.W. Carlson, R.E. Ergun, C.C. Chaston, F.S. Mozer, M. Temerin, D.M. Klumpar, E.G. Shelley, W.K. Peterson, E. Moebius, L. Kistler, R. ElphicR. Strangeway, C. Cattell, and R. Pfaff, Electron modulation and ion cyclotron waves observed by FAST, Geophys. Res. Lett., **25**, 2045, (1998).

Mishin, E.V. and M. Forster, Alfvenic shocks and low-altitude auroral acceleration, Geophys. Res. Lett., **22**, 1745 (1995).

Mozer, F.S., R. Ergun, M. Temerin, C. Cattell, J. Dombeck and J. Wygant, New features of time domain electric-field structures in the auroral acceleration region, Phys. Rev. Lett., **79**, 292 (1997).

Mozer, F.S., ISEE-1 observations of electrostatic shocks on auroral zone field lines between 2.5 and 7 Earth radii, Geophysical-Research-Letters. **8**, no.7, 823 (1981).

Mozer, F.S., C.W. Carlson, M.K. Hudson, R.B. Torbert, B. Parady, J. Yatteau, and M.C. Kelley, Observation of paired electrostatic shocks in the polar magnetosphere, Phys. Rev. Lett., **38**, 292 (1977).

Norqvist, P., M. Andre, and M. Tyrland, A statistical study of ion energization mechanisms in the auroral region, J. Geophys. Res., **103**, 23459 (1998).

Potemra, T.A., J.P. Doering, W.K. Peterson, C.O. Bostrom, R.A. Hoffman, and L.H. Brace, AE-C observations of low-energy particles and ionospheric temperatures in the turbulent polar cusp: evidence for Kelvin-Helmholtz instability, J. Geophys. Res., **83**, 3877 (1978).

Pfaff, R., et. al., Initial FAST observations of acceleration processes in the cusp, *Geophys. Res. Lett*., **25**, 2037, (1998).

Sarfaty, M., S. DeSouza Machado, F. Skiff, Direct determination of ion wave fields in a hot magnetized and weakly collisional plasma, *Phys. Plasmas*, **3**, 4316, (1996).

Sato, N., M. Nakamura, and R. Hatakeyama, Three-dimensional double layers inducing ion-cyclotron oscillations in a collisionless plasma, Phys. Rev. Lett., **57**, 1227 (1986).

Scime, E. Earl, Paul A. Keiter, Matthew M. Balkey, Robert F. Boivin, John L. Kline, Melanie Blackburn, S. Peter Gary, Ion temperature anisotropy limitation in high beta plasmas, Phys. Plasmas, **7**, 2157, (2000).

Skiff, F., Determination of Wave Fields from Perturbed Particle Orbits, *IEEE Transactions of Plasma Science*, **20**, 701 (1992).

Skiff, F., F. Anderegg, Direct Observation of Plasma Dielectric Motion, *Phys. Plasmas*, **59**, 896 (1987).

Stern, R. A. and J. A. Johnson, Plasma ion diagnostics using resonant fluorescence, *Phys. Rev. Lett*., **34**, 1548, (1975).

Stix, T.H., *The Theory of Plasma Waves* (American Institute New York, 1962).

Swanson, D.G., *Plasma Waves* (Academic, San Diego, 1989).

Teodorescu, C., E.W. Reynolds, M.E. Koepke, Experimental Verification of the Shear-Modified Ion-Acoustic Instability, Phys. Rev. Lett., submitted, (2001).

Wahlund, J.-E., P. Louran, T. Chust, H. de Feraudy, R. Roux, B. Holback, P.-O. Dovner, and G. Holmgren, On ion acoustic turbulence and nonlinear evolution of kinetic Alfven waves in the aurora, Geophys. Res. Lett., **21**, 1831 (1994a).

Wahlund, J.-E., P. Louran, T. Chust, H. de Feraudy, R. Roux, B. Holback, B. Cabrit, A.I. Ericksson, P.M. Kintner, M.C. Kelley, J. Bonnell, and C. Chesney, Observations of ion acoustic fluctuations in the auroral topside ionosphere by the FREJA S/C, Geophys. Res. Lett., **21**, 1835 (1994b).

Wahlund, J.-E., A.I. Eriksson, B. Holback, M.H. Boehm, J. Bonnell, P.M. Kintner, C.E. Seyler, J.H. Clemmons, L. Eliasson, D.J. Knudsen, P. Norqvist, and L.J. Zanetti,

Broadband ELF plasma emission during auroral energization. 1. Slow ion acoustic waves, J. Geophys. Res., **103**, 4343 (1998).

Appendix A Derivation of the Constants of Motion

It is necessary that f_0 satisfy the Vlasov equation. If f_0 is a function of only constants of the motion, the Vlasov equation is automatically satisfied. The necessary constants are derived in this appendix. Beginning with the equations of motion for a charged particle in a magnetic field along the z axis:

$$\vec{F} = \frac{q}{c}\vec{v}\times\vec{B} \Rightarrow \vec{F} = \frac{q}{c}\begin{vmatrix} \hat{x} & \hat{y} & \hat{z} \\ v_x & v_y & v_{\|} \\ 0 & 0 & B_z \end{vmatrix} \Rightarrow \begin{Bmatrix} \ddot{x} = \Omega v_y \\ \ddot{y} = -\Omega v_x \\ \ddot{z} = 0 \end{Bmatrix} \quad \text{A.1}$$

and combining terms, some natural constants of the motions appear.

$$\begin{Bmatrix} \frac{d}{dt}(\dot{\frac{x}{\Omega}} - y) = 0 \\ \frac{d}{dt}(\dot{\frac{y}{\Omega}} + x) = 0 \\ \frac{d}{dt}(v_{\|}) = 0 \end{Bmatrix}. \quad \text{A.2}$$

$\Omega \equiv \frac{qB}{Mc}$ is the "cyclotron frequency". By combining the x and y expressions in Equations A.2, an additional constant of the motion is obtained. Namely,

$$\begin{Bmatrix} \dot{v}_x v_x = \Omega v_y v_x \\ \dot{v}_y v_y = -\Omega v_y v_x \end{Bmatrix} \Rightarrow \dot{\vec{v}}_{\perp}\cdot\vec{v}_{\perp} = 0 \Rightarrow \frac{d}{dt}(\frac{1}{2}\vec{v}_{\perp}\cdot\vec{v}_{\perp}) = 0 \Rightarrow \frac{d}{dt}v_{\perp}^2 = 0 \quad . \quad \text{A.3}$$

Physically, these quantities are

$$\begin{Bmatrix} Y_g \equiv \dot{\frac{x}{\Omega}} - y \equiv y \ \text{ guidingcenter} \\ \chi_g \equiv \dot{\frac{y}{\Omega}} + x \equiv x \ \text{ guidingcenter} \\ v_{\|}^2 \ \textit{and} \ T_{\|} \equiv \text{parallel(to the magnetic field) kinetic energy} \\ v_{\perp}^2 \ \textit{and} \ T_{\perp} \equiv \text{perpendicular kinetic energy} \end{Bmatrix} \quad \text{A.4}$$

Appendix B Derivation of unperturbed orbits

In Appendix A, it was shown that

$$\left\{\begin{array}{c} \ddot{v}_x = -\Omega^2 v_x \\ \ddot{v}_y = -\Omega^2 v_y \\ \dot{v}_z = v_{||} \end{array}\right\}. \qquad \text{B.1}$$

Thus,

$$\left\{\begin{array}{c} v_x = A\cos(\Omega t + \varphi) \\ v_y = -A\sin(\Omega t + \varphi) \\ v_z = const \equiv v_{||} \end{array}\right\}, \qquad \text{B.2}$$

where 'A' is an arbitrary constant. 'A' can be determined from the definition of the perpendicular speed, namely,

$$v_\perp^2 = v_x^2 + v_y^2 \Rightarrow A = v_\perp \qquad \text{B.3}$$

so, the complete set of velocity components is

$$\left\{\begin{array}{c} v_x = v_\perp \cos(\Omega t + \varphi) \\ v_y = -v_\perp \sin(\Omega t + \varphi) \\ v_z = const \equiv v_{||} \end{array}\right\}. \qquad \text{B.4}$$

To obtain the change in position from the time t to the present, t', the equations of B.4 are integrated.

$$\left\{\begin{array}{c} x' - x = \frac{v_\perp}{\Omega}\left[\sin(\Omega t' + \varphi) - \sin(\Omega t + \varphi)\right] \\ y' - y = \frac{v_\perp}{\Omega}\left[\cos(\Omega t' + \varphi) - \cos(\Omega t + \varphi)\right] \\ z' - z = v_{||} t' - v_{||} t \end{array}\right\}. \qquad \text{B.5}$$

Changing variables from $t - t'$ to Θ,

$$\left\{\begin{array}{c} x'-x=\frac{\mathrm{v}_\perp}{\Omega}\left[\sin(\Omega(t-\Theta)+\varphi)-\sin(\Omega t+\varphi)\right] \\ y'-y=\frac{\mathrm{v}_\perp}{\Omega}\left[\cos(\Omega(t-\Theta)+\varphi)-\cos(\Omega t+\varphi)\right] \\ z'-z=-\mathrm{v}_{\|}\Theta \end{array}\right\}. \qquad \text{B.6}$$

It is convenient to replace the particle's original polar angle with the polar angle at time t. That is,

$$\bar{\phi}=\Omega t+\varphi\,, \qquad \text{B.7}$$

and the displacements become

$$\left\{\begin{array}{c} x'-x=\frac{\mathrm{v}_\perp}{\Omega}\left[\sin(\bar{\phi}-\Omega\Theta)-\sin(\bar{\phi})\right] \\ y'-y=\frac{\mathrm{v}_\perp}{\Omega}\left[\cos(\bar{\phi}-\Omega\Theta)-\cos(\bar{\phi})\right] \\ z'-z=-\mathrm{v}_{\|}\Theta \end{array}\right\}. \qquad \text{B.8}$$

Therefore,

$$i\vec{k}\cdot(\vec{r}'-\vec{r})=i\frac{\mathrm{v}_\perp}{\Omega}\left[k_x\left(\sin(\bar{\phi}-\Omega\Theta)-\sin(\bar{\phi})\right)+k_y\left(\cos(\bar{\phi}-\Omega\Theta)-\cos(\bar{\phi})\right)\right]-ik_{\|}\mathrm{v}_{\|}\Theta\,. \qquad \text{B.9}$$

The Cartesian wavevector components are expressed in terms of the wavevector gyrophase, α,

$$\left\{\begin{array}{l} k_x=k_\perp\cos\alpha \\ k_y=k_\perp\sin\alpha \end{array}\right\}. \qquad \text{B.10}$$

Equation B.9 becomes,

$$\begin{aligned} i\vec{k}\cdot(\vec{r}'-\vec{r}) &= i\frac{\mathrm{v}_\perp k_\perp}{\Omega}\left[(\cos\alpha)\left(\sin(\bar{\phi}-\Omega\Theta)-\sin(\bar{\phi})\right)+(\sin\alpha)\left(\cos(\bar{\phi}-\Omega\Theta)-\cos(\bar{\phi})\right)\right]-ik_{\|}\mathrm{v}_{\|}\Theta \\ &= i\frac{\mathrm{v}_\perp k_\perp}{\Omega}\left[(\cos\alpha)\sin(\bar{\phi}-\Omega\Theta)-(\cos\alpha)\sin(\bar{\phi})+(\sin\alpha)\cos(\bar{\phi}-\Omega\Theta)-(\sin\alpha)\cos(\bar{\phi})\right]-ik_{\|}\mathrm{v}_{\|}\Theta \\ &= i\frac{\mathrm{v}_\perp k_\perp}{\Omega}\left[\sin(\bar{\phi}-\Omega\Theta+\alpha)-\sin(\bar{\phi}+\alpha)\right]-ik_{\|}\mathrm{v}_{\|}\Theta, \end{aligned}$$

and

$$i\vec{k}\cdot(\vec{r}'-\vec{r})-i\omega(t'-t)=i\frac{\mathrm{v}_\perp k_\perp}{\Omega}\left[\sin(\bar{\phi}-\Omega\Theta+\alpha)-\sin(\bar{\phi}+\alpha)\right]+i(\omega-k_{\|}\mathrm{v}_{\|})\Theta. \qquad \text{B.11}$$

This result is consistent with the treatment by Swanson [*Swanson*, 1989]. Starting with Swanson's result,

$$i\vec{k}'\bullet\vec{r}' - i\omega t' = i\vec{k}\bullet\vec{r} - i\omega t + \frac{i\mathrm{v}_x}{\Omega}\cos\bar{\varphi}\left[-k_x\sin\Omega\Theta - \varepsilon k_y\sin\alpha\left(1-\cos\Omega\Theta\right)\right] + \qquad \text{B.12}$$

$$\frac{i\mathrm{v}_y}{\Omega}\sin\bar{\varphi}\left[-k_y\sin\Omega\Theta + \varepsilon k_x\left(1-\cos\Omega\Theta\right)\right] + i\left(\omega - k_{\|}\mathrm{v}_{\|}\right)\Theta,$$

using,

$$\begin{array}{ccc} k_x = k_\perp\cos\alpha & & \mathrm{v}_x = \mathrm{v}_\perp\cos\bar{\varphi} \\ k_y = k_\perp\sin\alpha & \text{and} & \mathrm{v}_y = -\mathrm{v}_\perp\sin\bar{\varphi} \end{array}, \qquad \text{B.13}$$

and letting the charge specification, ε, be unity, the unperturbed orbits become,

$$\begin{aligned} i\vec{k}'\bullet\vec{r}' - i\omega t' &= i\vec{k}\bullet\vec{r} - i\omega t + \frac{i\mathrm{v}_\perp}{\Omega}\cos\bar{\varphi}\left[-k_\perp\cos\alpha\sin\Omega\Theta - k_\perp\sin\alpha\left(1-\cos\Omega\Theta\right)\right] + \\ &\quad \frac{i\mathrm{v}_\perp}{\Omega}\sin\bar{\varphi}\left[k_\perp\sin\alpha\sin\Omega\Theta - k_\perp\cos\alpha\left(1-\cos\Omega\Theta\right)\right] + i\left(\omega - k_{\|}\mathrm{v}_{\|}\right)\Theta \\ &= \frac{i\mathrm{v}_\perp k_\perp}{\Omega}\left[-\cos\bar{\varphi}\cos\alpha\sin\Omega\Theta - \cos\bar{\varphi}\sin\alpha + \cos\bar{\varphi}\sin\alpha\cos\Omega\Theta + \sin\bar{\varphi}\sin\alpha\sin\Omega\Theta - \sin\bar{\varphi}\cos\alpha + \sin\bar{\varphi}\cos\alpha\cos\Omega\Theta\right] + \\ &\quad + \left(\omega - k_{\|}\mathrm{v}_{\|}\right)\Theta \\ i\vec{k}'\bullet\vec{r}' - i\omega t' &= \frac{i\mathrm{v}_\perp k_\perp}{\Omega}\left[-\sin(\bar{\varphi}+\alpha) + \sin\Omega\Theta\left(\sin\bar{\varphi}\sin\alpha - \cos\bar{\varphi}\cos\alpha\right) + \cos\Omega\Theta\left(\sin\bar{\varphi}\cos\alpha + \cos\bar{\varphi}\sin\alpha\right)\right] + \left(\omega - k_{\|}\mathrm{v}_{\|}\right)\Theta \\ &= \frac{i\mathrm{v}_\perp k_\perp}{\Omega}\left[-\sin(\bar{\varphi}+\alpha) + \sin\Omega\Theta\left(-\cos(\bar{\varphi}+\alpha)\right) + \cos\Omega\Theta\left(\sin(\bar{\varphi}+\alpha)\right)\right] + \left(\omega - k_{\|}\mathrm{v}_{\|}\right)\Theta \\ &= \frac{i\mathrm{v}_\perp k_\perp}{\Omega}\left[\sin(\bar{\varphi}+\alpha-\Omega\Theta) - \sin(\bar{\varphi}+\alpha)\right] + \left(\omega - k_{\|}\mathrm{v}_{\|}\right)\Theta \end{aligned} \qquad \text{B. 14}$$

Equation B. 14 is identical to Equation B.11.

Appendix C1 Integration over perpendicular velocity needed for the dispersion relation calculation

The integrals

$$I_{\perp,1} \equiv \int_0^\infty d\mathrm{v}_\perp \mathrm{v}_\perp e^{-\beta_\perp \mathrm{v}_\perp^2} \qquad \text{C. 1}$$

and

$$I_{\perp,2} \equiv \int_0^\infty d\mathrm{v}_\perp \mathrm{v}_\perp \left[J_m\left(\frac{\mathrm{v}_\perp k_\perp}{\Omega}\right)\right]^2 e^{-\beta_\perp \mathrm{v}_\perp^2} \qquad \text{C. 2}$$

are quite complicated if an approximation is not made. This is because the drift velocity is a function of the *x*-guiding center, which is in turn a function of v_y. To keep the v_y dependence would render the integration impossible by analytical methods. The following argument allows these integrals to be written in the simplified form above. The drift velocity can be expanded in a Taylor series,

$$V_0(\chi_g) = V_0(\chi_g - x + x) = V_0(\rho + x) \Rightarrow V_0(\chi_g) \approx V_0(x) + O\left(\frac{\rho}{L}\right) + \ldots . \qquad \text{C.3}$$

In many plasmas of interest, the characteristic length of the shear is much longer than a gyroradius. The drift can then be considered an approximate function of the *x*-coordinate, rather than exactly a function of the *x*-coordinate and the *y*-velocity component. The approximation described here is commonly referred to as the *local approximation*. This approximation is valid in the region a few thousand kilometers above the earth where the ratio of the ion gyroradius to the characteristic shear length (ρ/L) is small. According to FAST data [*Pfaff*, 1998; *McFadden*, 1998], the ratio of the ion gyroradius to the shear scale length is on the order of 10^{-2}. The ratio of ρ/L in laboratory devices is not as small. For instance, a typical ion gyroradius in the Large Experiment on Instabilities and Anisotropies is a few centimeters. The shear scale length has not been measured, but it is believed that the length over which the shear is about the same distance as an ion gyroradius. Thus ρ/L is of the order of unity and the local

approximation is not valid. A calculation of the non-local version of the dispersion relation is planned for the future.

The integrals over $v_\perp$ become

$$I_{\perp,1} \equiv \int_0^\infty d\mathrm{v}_\perp \mathrm{v}_\perp e^{-\beta_\perp \mathrm{v}_\perp^2} = \frac{1}{2\beta_\perp} \qquad \text{C.4}$$

and

$$I_{\perp,2} \equiv \int_0^\infty d\mathrm{v}_\perp \mathrm{v}_\perp \left[J_m\left(\frac{\mathrm{v}_\perp k_\perp}{\Omega}\right) \right]^2 e^{-\beta_\perp \mathrm{v}_\perp^2} = \frac{1}{2\beta_\perp} \Gamma_m(b), \qquad \text{C.5}$$

where,

$$b \equiv \frac{k_\perp^2}{2\Omega^2 \beta_\perp}; \text{ and } \Gamma_m(b) \equiv e^{-b} I_m(b) \qquad \text{C.6}$$

The solution to the integral in Equation C.5 is taken from a standard integral table [private communication, G. Ganguli].

Appendix C2 Integration over parallel velocity needed for the dispersion relation calculation

The integral considered here is,

$$I_{\|,2} = \int_{-\infty}^{\infty} d\mathrm{v}_{\|} \frac{(\omega - k_{\|}\mathrm{v}_{\|}) + \frac{\beta_{\|}}{\beta_{\perp}}(\mathrm{v}_{\|} - V_0(\chi_g))(k_{\|} - \frac{V_0'(\chi_g)k_y}{\Omega})}{\omega - m\Omega - k_{\|}\mathrm{v}_{\|}} e^{-\beta_{\|}(\mathrm{v}_{\|} - V_0(\chi_g))^2}. \quad \text{C.7}$$

Let,

$$s \equiv \sqrt{\beta_{\|}}\left(\mathrm{v}_{\|} - V_0(\chi_g)\right) \Rightarrow \left\{ \begin{array}{c} d\mathrm{v}_{\|} = \frac{ds}{\sqrt{\beta_{\|}}} \\ \mathrm{v}_{\|} = \frac{s}{\sqrt{\beta_{\|}}} + V_0(\chi_g) \end{array} \right\} \quad \text{C.8}$$

so that the integral can be written as,

$$\begin{aligned} I_{\|,2} &= \int_{-\infty}^{\infty} \frac{ds}{\sqrt{\beta_{\|}}} \frac{\omega - k_{\|}(\frac{s}{\sqrt{\beta_{\|}}} + V_o(\chi_g)) + \frac{\beta_{\|}}{\beta_{\perp}}(\frac{s}{\sqrt{\beta_{\|}}} + V_o(\chi_g) - V_0(\chi_g))(k_{\|} - \frac{V_0'(\chi_g)k_y}{\Omega})}{\omega - m\Omega - k_{\|}\left(\frac{s}{\sqrt{\beta_{\|}}} + V_o(\chi_g)\right)} e^{-s^2} \\ &= \int_{-\infty}^{\infty} \frac{ds}{\sqrt{\beta_{\|}}} \frac{\omega - k_{\|}\frac{s}{\sqrt{\beta_{\|}}} - k_{\|}V_o(\chi_g) + \frac{\beta_{\|}}{\beta_{\perp}}(\frac{s}{\sqrt{\beta_{\|}}})(k_{\|} - \frac{V_0'(\chi_g)k_y}{\Omega})}{(\omega - m\Omega - k_{\|}V_o(\chi_g)) - \frac{sk_{\|}}{\sqrt{\beta_{\|}}}} e^{-s^2} \\ &= -\int_{-\infty}^{\infty} \frac{ds}{\sqrt{\beta_{\|}}} \frac{\omega - k_{\|}V_o(\chi_g) + (\frac{s}{\sqrt{\beta_{\|}}})\left(\frac{\beta_{\|}}{\beta_{\perp}}(k_{\|} - \frac{V_0'(\chi_g)k_y}{\Omega}) - k_{\|}\right)}{\frac{sk_{\|}}{\sqrt{\beta_{\|}}} - (\omega - m\Omega - k_{\|}V_o(\chi_g))} e^{-s^2} \\ &= -\int_{-\infty}^{\infty} \frac{ds}{\sqrt{\beta_{\|}}} \frac{\frac{\sqrt{\beta_{\|}}}{k_{\|}}\left(\omega - k_{\|}V_o(\chi_g)\right) + (s)\left(\frac{\beta_{\|}}{\beta_{\perp}}(1 - \frac{V_0'(\chi_g)k_y}{\Omega k_{\|}}) - 1\right)}{s - (\omega - m\Omega - k_{\|}V_o(\chi_g))\frac{\sqrt{\beta_{\|}}}{k_{\|}}} e^{-s^2} \end{aligned} \quad \text{C.9}$$

With the definition of ζ_m given in Equation (36), C.7 can be written as,

$$I_{||,2} = -\frac{1}{\sqrt{\beta_{||}}}\left[\zeta_0 \underbrace{\int_{-\infty}^{\infty} ds \frac{e^{-s^2}}{s-\zeta_m}}_{I_1} + \left(\frac{\beta_{||}}{\beta_\perp}\left(1-\frac{V_0'(\chi_g)}{\Omega u}\right)-1\right)\underbrace{\int_{-\infty}^{\infty} ds \frac{se^{-s^2}}{s-\zeta_m}}_{I_2}\right] \qquad \text{C.10}$$

The first integral is in the form of the plasma dispersion function definition [*Fried and Conte*, 1962]. Specifically,

$$I_1 = \sqrt{\pi} Z(\zeta_m)$$

Given this, evaluating the second integral is a matter of adding and subtracting ζ_m in the numerator,

$$\begin{aligned} I_2 &= \int_{-\infty}^{\infty} ds \frac{se^{-s^2}}{s-\zeta_m} \\ &= \int_{-\infty}^{\infty} ds \frac{(s-\zeta_m+\zeta_m)e^{-s^2}}{s-\zeta_m} \\ &= \int_{-\infty}^{\infty} ds e^{-s^2} + \zeta_m \int_{-\infty}^{\infty} ds \frac{e^{-s^2}}{s-\zeta_m} \\ &= \sqrt{\pi}\left(1+\zeta_m Z(\zeta_m)\right) \end{aligned} \qquad \text{C.11}$$

and therefore $I_{||,2}$ can be written as

$$\begin{aligned} I_{||,2} &= -\sqrt{\frac{\pi}{\beta_{||}}}\left[\zeta_0 Z(\zeta_m) + \left(\frac{\beta_{||}}{\beta_\perp}\left(1-\frac{V_0'(\chi_g)}{\Omega u}\right)-1\right)\left(1+\zeta_m Z(\zeta_m)\right)\right] \\ &= -\sqrt{\frac{\pi}{\beta_{||}}}\left[\zeta_0 Z(\zeta_m) + \left(\frac{\beta_{||}}{\beta_\perp}-1-\frac{\beta_{||}}{\beta_\perp}\left(\frac{V_0'(\chi_g)}{\Omega u}\right)\right)\left(1+\zeta_m Z(\zeta_m)\right)\right] \\ &= -\sqrt{\frac{\pi}{\beta_{||}}}\left[\zeta_0 Z(\zeta_m) + \left(\frac{\beta_{||}}{\beta_\perp}-1-\frac{\beta_{||}}{\beta_\perp}\left(\frac{V_0'(\chi_g)}{\Omega u}\right)\right)\left(\zeta_m Z(\zeta_m)\right) + \left(\frac{\beta_{||}}{\beta_\perp}-1-\frac{\beta_{||}}{\beta_\perp}\left(\frac{V_0'(\chi_g)}{\Omega u}\right)\right)\right] \\ &= -\sqrt{\frac{\pi}{\beta_{||}}}\left[\frac{\beta_{||}}{\beta_\perp}-1+\zeta_0 Z(\zeta_m) - \zeta_m Z(\zeta_m) + \left(\frac{\beta_{||}}{\beta_\perp}\right)\zeta_m Z(\zeta_m) + \left(-\frac{\beta_{||}}{\beta_\perp}\left(\frac{V_0'(\chi_g)}{\Omega u}\right)\right)\zeta_m Z(\zeta_m) + \left(-\frac{\beta_{||}}{\beta_\perp}\left(\frac{V_0'(\chi_g)}{\Omega u}\right)\right)\right] \\ I_{||,2} &= -\sqrt{\frac{\pi}{\beta_{||}}}\left(\frac{\beta_{||}}{\beta_\perp}-1+\sqrt{\beta_{||}}\left(\frac{m\Omega}{k_{||}}\right)Z(\zeta_m) + \frac{\beta_{||}}{\beta_\perp}\zeta_m Z(\zeta_m) - \frac{\beta_{||}}{\beta_\perp}\frac{V_0'(x)}{\Omega u}\left(1+\zeta_m Z(\zeta_m)\right)\right). \end{aligned} \qquad \text{C.12}$$

Thus

$$f_{1k}(v_\perp) = -\frac{4q\varphi_{1k}n_0\beta_\perp^2}{M}e^{-2\beta_\perp v_\perp^2} *$$
$$\left[1+\sum_{n=-\infty}^{\infty}\left(J_n(\frac{v_\perp k_\perp}{\Omega}\right)^2\left(Z(\zeta_n)\left(\zeta_n(\frac{T_\perp}{T_\parallel}-1+\frac{T_\perp V_0^{'}(\chi_g)}{T_\parallel\Omega u})+\zeta_0\right)+\frac{T_\perp}{T_\parallel}-1-\frac{T_\perp V_0^{'}(\chi_g)}{T_\parallel\Omega u}\right)\right], \qquad \text{C.13}$$

where the integral over $v_\parallel$ has been completed.

Appendix D Integration over unpertubed orbits needed for the calculation of $f_1(\mathrm{v}_y)$

For use in Equation B.12, it is useful to define a wavevector angle, θ, such that

$$\left\{\begin{matrix} k_x = k_\perp \cos\theta \\ k_y = k_\perp \sin\theta \end{matrix}\right\}. \tag{D.1}$$

The integral in Equation (43) is then,

$$\int_0^\infty d\Theta e^{i\frac{\mathrm{v}_x}{\Omega}\left(-k_x \sin\Omega\Theta - k_y(1-\cos\Omega\Theta)\right)+i\frac{\mathrm{v}_y}{\Omega}\left(-k_y \sin\Omega\Theta + k_x(1-\cos\Omega\Theta)\right)+i(\omega-k_\parallel \mathrm{v}_\parallel)\Theta} =$$
$$e^{\frac{i}{\Omega}(\mathrm{v}_y k_x - \mathrm{v}_x k_y)}\int_0^\infty d\Theta e^{i\frac{\mathrm{v}_x k_\perp}{\Omega}\left(-\sin\Omega\Theta\cos\theta+\cos\Omega\Theta\sin\theta\right)+i\frac{\mathrm{v}_y k_\perp}{\Omega}\left(-\sin\Omega\Theta\sin\theta+-\cos\Omega\Theta\cos\theta\right)+i(\omega-k_\parallel \mathrm{v}_\parallel)\Theta}. \tag{D.2}$$

With the use of the trigonometric identities

$$\begin{aligned} &\cos A\sin B - \sin A\cos B = \sin(B-A) \\ &\sin A\sin B + \cos A\cos B = \sin(A-B+\frac{\pi}{2}), \end{aligned} \tag{D.3}$$

Equation D.2 becomes

$$\int_0^\infty d\Theta e^{i\frac{\mathrm{v}_x k_\perp}{\Omega}\left(-\sin\Omega\Theta\cos\theta+\cos\Omega\Theta\sin\theta\right)+i\frac{\mathrm{v}_y k_\perp}{\Omega}\left(-\sin\Omega\Theta\sin\theta+-\cos\Omega\Theta\cos\theta\right)+i(\omega-k_\parallel \mathrm{v}_\parallel)\Theta} =$$
$$\int_0^\infty d\Theta e^{i\frac{\mathrm{v}_x k_\perp}{\Omega}\left(\sin(\theta-\Omega\Theta)\right)} e^{i\frac{\mathrm{v}_y k_\perp}{\Omega}\left(\sin(\theta-\Omega\Theta-\frac{\pi}{2})\right)} e^{i(\omega-k_\parallel \mathrm{v}_\parallel)\Theta}. \tag{D.4}$$

With the use of the Bessel identity,

$$e^{iax\sin\theta} = \sum_{n=-\infty}^{\infty} J_n(ax)e^{in\theta} \tag{D.5}$$

Equation D.4 is,

$$e^{\frac{i}{\Omega}(\mathrm{v}_y k_x - \mathrm{v}_x k_y)} \sum_{m,n=-\infty}^{\infty} e^{i(m+n)\theta} e^{-im\frac{\pi}{2}} J_m(\frac{\mathrm{v}_y k_\perp}{\Omega}) J_n(\frac{\mathrm{v}_x k_\perp}{\Omega}) \int_0^\infty d\Theta e^{-i\Omega(m+n)\Theta} e^{i(\omega-k_\parallel \mathrm{v}_\parallel)\Theta} =$$
$$e^{\frac{i}{\Omega}(\mathrm{v}_y k_x - \mathrm{v}_x k_y)} \sum_{m,n=-\infty}^{\infty} e^{i(m+n)\theta} e^{-im\frac{\pi}{2}} J_m(\frac{\mathrm{v}_y k_\perp}{\Omega}) J_n(\frac{\mathrm{v}_x k_\perp}{\Omega}) \left(\frac{-i}{\Omega(m+n)+k_\parallel \mathrm{v}_\parallel - \omega}\right). \tag{D.6}$$

With the integral evaluated as such, Equation (43) becomes,

$$f_{1k}(\vec{v}) = \frac{2q\varphi_1}{M}\left[\beta_\perp(k_x v_x + k_y v_y) + \beta_{||}\left(k_z - \frac{k_y V_o'}{\Omega}\right)(v_{||} - V_o)\right] f_0 * \qquad \text{D.7}$$
$$e^{\frac{i}{\Omega}(v_y k_x - v_x k_y)} \sum_{m,n=-\infty}^{\infty} e^{i(m+n)\theta} e^{-im\frac{\pi}{2}} J_m\left(\frac{v_y k_\perp}{\Omega}\right) J_n\left(\frac{v_x k_\perp}{\Omega}\right)\left(\frac{1}{\Omega(m+n) + k_{||}v_{||} - \omega}\right)$$

To replace the explicit dependence on $v_x k_x$ with a dependence on an index number times the cyclotron frequency ($n\Omega$), the perpendicular wavevector velocity products are eliminated from the first term in the brackets of Equation D.7. Each product is replaced by the product of a summation index and the particles' gyrofrequency. This is accomplished by considering each term with the Bessel function that contains the same velocity component. First, consider,

$$\begin{aligned}
\sum_n v_x k_x J_n\left(\frac{v_x k_\perp}{\Omega}\right) e^{in\theta} &= \sum_n v_x k_\perp (\cos\theta) J_n\left(\frac{v_x k_\perp}{\Omega}\right) e^{in\theta} \\
&= \sum_n v_x k_\perp \left(\frac{e^{i\theta} + e^{-i\theta}}{2}\right) J_n\left(\frac{v_x k_\perp}{\Omega}\right) e^{in\theta} \\
&= \sum_n v_x k_\perp \left(\frac{e^{i(n+1)\theta} + e^{-i(n-1)\theta}}{2}\right) J_n\left(\frac{v_x k_\perp}{\Omega}\right) \\
&= \sum_n v_x k_\perp \left(\frac{1}{2}\right)\left(J_{n+1}\left(\frac{v_x k_\perp}{\Omega}\right) + J_{n-1}\left(\frac{v_x k_\perp}{\Omega}\right)\right) e^{in\theta}.
\end{aligned} \qquad \text{D.8}$$

The recursive property of Bessel functions,

$$J_{n+1}(X) + J_{n-1}(X) = \frac{2n}{X} J_n(X), \qquad \text{D.9}$$

is used to simplify the expression in parenthesis, and Equation D.8 becomes

$$\begin{aligned}
\sum_n v_x k_x J_n\left(\frac{v_x k_\perp}{\Omega}\right) e^{in\theta} &= \sum_n v_x k_\perp \left(\frac{1}{2}\right)\left(\frac{2n\Omega}{v_x k_\perp}\right) J_n\left(\frac{v_x k_\perp}{\Omega}\right) e^{in\theta} \\
&= \sum_n n\Omega J_n\left(\frac{v_x k_\perp}{\Omega}\right) e^{in\theta}.
\end{aligned} \qquad \text{D.10}$$

A similar method eliminates the y-components of the velocity and the wavevector.

$$\begin{aligned}
\sum_n \mathrm{v}_y k_y J_m\left(\frac{\mathrm{v}_y k_\perp}{\Omega}\right) e^{jm\theta} e^{-im\frac{\pi}{2}} &= \sum_m \mathrm{v}_y k_\perp (\sin\theta) J_m\left(\frac{\mathrm{v}_y k_\perp}{\Omega}\right) e^{jm\theta} e^{-im\frac{\pi}{2}} \\
&= \sum_m \mathrm{v}_y k_\perp \left(\frac{e^{j\theta} - e^{-i\theta}}{2i}\right) J_m\left(\frac{\mathrm{v}_y k_\perp}{\Omega}\right) e^{jm\theta} e^{-im\frac{\pi}{2}} \\
&= \sum_n \mathrm{v}_y k_\perp \left(\frac{e^{j(m+1)\theta} - e^{-i(m-1)\theta}}{2i}\right) J_m\left(\frac{\mathrm{v}_y k_\perp}{\Omega}\right) e^{-im\frac{\pi}{2}} \\
&= \sum_m \mathrm{v}_y k_\perp \left(\frac{1}{2i}\right)\left(J_{m-1}\left(\frac{\mathrm{v}_y k_\perp}{\Omega}\right) e^{-i(m-1)} - J_{m+1}\left(\frac{\mathrm{v}_y k_\perp}{\Omega}\right) e^{-i(m+1)}\right) e^{jm\theta} \\
&= \sum_m \mathrm{v}_y k_\perp \left(\frac{1}{2}\right)\left(J_{m-1}\left(\frac{\mathrm{v}_y k_\perp}{\Omega}\right) - J_{m+1}\left(\frac{\mathrm{v}_y k_\perp}{\Omega}\right)\right) e^{jm\theta} e^{-im\frac{\pi}{2}} \qquad \text{D.11}
\end{aligned}$$

$$\sum_n v_y k_y J_m\left(\frac{v_y k_\perp}{\Omega}\right) e^{jm\theta} e^{-im\frac{\pi}{2}} = \sum_m m\Omega J_m\left(\frac{\mathrm{v}_y k_\perp}{\Omega}\right) e^{jm\theta} e^{-im\frac{\pi}{2}}.$$

Appendix E **Integration over $v_{\|}$ needed for $f_1(v_y)$**

The equation evaluated in this appendix is,

$$I_{m,n} = \int_{-\infty}^{\infty} d\mathrm{v}_z e^{-\beta_{\|}(\mathrm{v}_{\|}-V_o)^2} \left(\frac{\beta_{\perp}(m+n)\Omega + \beta_{\|}\left(k_z - \frac{k_y V_o'}{\Omega}\right)(\mathrm{v}_{\|}-V_o)}{\Omega(m+n)+k_{\|}\mathrm{v}_{\|}-\omega} \right) . \quad \text{E.1}$$

Using the definitions

$$s \equiv \sqrt{\beta_{\|}}(\mathrm{v}_{\|}-V_o) \Rightarrow \left\{ \begin{array}{c} \mathrm{v}_{\|} = \frac{s}{\sqrt{\beta_{\|}}} + V_o \\ d\mathrm{v}_{\|} = \frac{ds}{\sqrt{\beta_{\|}}} \end{array} \right\} \text{ and } \xi_l \equiv \frac{\sqrt{\beta_{\|}}}{k_{\|}}\left(\omega - l\Omega - k_{\|}V_o\right), \quad \text{E.2}$$

the integral is written,

$$I_{m,n} = \int_{-\infty}^{\infty} \frac{ds}{\sqrt{\beta_{\|}}} e^{-s^2} \left(\frac{\beta_{\perp}(m+n)\Omega + \beta_{\|}\left(k_z - \frac{k_y V_o'}{\Omega}\right)\left(\frac{s}{\sqrt{\beta_{\|}}} + V_0 - V_0\right)}{\Omega(m+n)+k_{\|}\left(\frac{s}{\sqrt{\beta_{\|}}} + V_0\right)-\omega} \right)$$

$$= \int_{-\infty}^{\infty} \frac{ds}{\sqrt{\beta_{\|}}} \left(\frac{\sqrt{\beta_{\|}}}{k_{\|}} \right) e^{-s^2} \left(\frac{\beta_{\perp}(m+n)\Omega + \beta_{\|}\left(k_{\|} - \frac{k_y V_d'}{\Omega}\right)\left(\frac{s}{\sqrt{\beta_{\|}}}\right)}{s - \xi_{m+n}} \right) . \quad \text{E.3}$$

Writing Equation E.3 as the sum of two integrals,

$$I_{m,n} = \frac{\beta_{\perp}(m+n)\Omega}{k_{\|}} \int_{-\infty}^{\infty} ds \left(\frac{e^{-s^2}}{s-\xi_{m+n}} \right) + \frac{\sqrt{\beta_{\|}}}{k_{\|}} \left(k_{\|} - \frac{k_y V_o'}{\Omega} \right) \int_{-\infty}^{\infty} ds \left(\frac{s e^{-s^2}}{s-\xi_{m+n}} \right)$$

$$= \frac{\beta_{\perp}(m+n)\Omega}{k_{\|}} \sqrt{\pi} Z(\xi_{m+n}) + \frac{\sqrt{\beta_{\|}}}{k_{\|}} \left(k_{\|} - \frac{k_y V_o'}{\Omega} \right) \sqrt{\pi} \left(1 + \xi_{m+n} Z(\xi_{m+n})\right) \quad \text{E.4}$$

where $$a = \frac{\sqrt{2} k_{\perp} \mathrm{v}_{th\perp}}{\Omega} \text{ and } c = \frac{\sqrt{2} k_y \mathrm{v}_{th\perp}}{\Omega}.$$

Then the first term in Equation E.4 is rewritten by recalling the definition,

$$
\begin{aligned}
\xi_{m+n} &\equiv \frac{\sqrt{\beta_{\|}}}{k_{\|}}\left(\omega-(m+n)\Omega-k_{\|}V_o\right) \\
&= \beta_{\perp}\frac{\sqrt{\beta_{\|}}}{\sqrt{\beta_{\|}}}\frac{\sqrt{\pi}}{k_{\|}}(m+n)\Omega \\
&= \beta_{\perp}\frac{\sqrt{\pi}}{\sqrt{\beta_{\|}}}\left(\frac{\sqrt{\beta_{\|}}}{k_{\|}}\left(\omega-k_{\|}V_o\right)-\xi_{m+n}\right) \\
&= \beta_{\perp}\frac{\sqrt{\pi}}{\sqrt{\beta_{\|}}}\frac{\sqrt{\beta_{\|}}}{k_{\|}}(m+n)\Omega \\
\xi_{m+n} &= \beta_{\perp}\frac{\sqrt{\pi}}{\sqrt{\beta_{\|}}}(\xi_0-\xi_{m+n}).
\end{aligned}
\qquad \text{E.5}
$$

Thus, Equation E.4 becomes,

$$
I_{m,n}=\frac{\sqrt{\pi}\beta_{\perp}}{\sqrt{\beta_{\|}}}(\xi_0-\xi_{m+n})Z(\xi_{m+n})+\frac{\sqrt{\beta_{\|}}}{k_{\|}}\left(k_{\|}-\frac{k_yV_o^{'}}{\Omega}\right)\sqrt{\pi}\left(1+\xi_{m+n}Z(\xi_{m+n})\right)
$$

$$
I_{m,n}=\frac{\sqrt{\pi}\beta_{\perp}}{\sqrt{\beta_{\|}}}(\xi_0-\xi_{m+n})Z(\xi_{m+n})+\sqrt{\beta_{\|}}\sqrt{\pi}\left(1+\xi_{m+n}Z(\xi_{m+n})\right)-\frac{k_yV_o^{'}}{\Omega}\frac{\sqrt{\beta_{\|}}}{k_{\|}}\sqrt{\pi}\left(1+\xi_{m+n}Z(\xi_{m+n})\right) \quad . \qquad \text{E.6}
$$

Appendix F Integration over v_x needed for derivation of $f_1(v_y)$

The integral to be evaluated in this Appendix is,

$$I = \int_{-\infty}^{\infty} d\mathrm{v}_x e^{-\frac{i\mathrm{v}_x k_y}{\Omega}} e^{-\beta_\perp \mathrm{v}_x^2} J_n\left(\frac{\mathrm{v}_x k_\perp}{\Omega}\right). \qquad \text{F.1}$$

First, the Bessel function is replaced with an integral representation. Using

$$J_n(ax) = \frac{1}{2\pi}\int_0^{2\pi} d\omega e^{iax\sin\omega - in\omega} \quad ,$$

Equation F.1 is written,

$$I = \frac{1}{2\pi}\int_{-\infty}^{\infty} d\mathrm{v}_x e^{-\frac{i\mathrm{v}_x k_y}{\Omega}} e^{-\beta_\perp \mathrm{v}_x^2} \int_0^{2\pi} d\omega e^{i\frac{\mathrm{v}_x k_\perp}{\Omega}\sin\omega - in\omega}. \qquad \text{F. 2}$$

Since the integral converges absolutely, the order of integration may be changed without affecting the outcome.

$$\begin{aligned} I &= \frac{1}{2\pi}\int_0^{2\pi} d\omega \int_{-\infty}^{\infty} d\mathrm{v}_x e^{-\frac{i\mathrm{v}_x k_y}{\Omega}} e^{-\beta_\perp \mathrm{v}_x^2} e^{i\frac{\mathrm{v}_x k_\perp}{\Omega}\sin\omega - in\omega} \\ &= \frac{1}{2\pi}\int_0^{2\pi} d\omega e^{-in\omega} \int_{-\infty}^{\infty} d\mathrm{v}_x e^{-\left(\beta_\perp \mathrm{v}_x^2 + \frac{i\mathrm{v}_x}{\Omega}\left(k_y - k_\perp \sin\omega\right)\right)}. \end{aligned} \qquad \text{F.3}$$

The *x*-velocity integral is done in Appendix F1. With the result

$$\int_{-\infty}^{\infty} d\mathrm{v}_x e^{-\left(\beta_\perp \mathrm{v}_x^2 + \frac{i\mathrm{v}_x}{\Omega}\left(k_y - k_\perp \sin\omega\right)\right)} = \sqrt{\frac{\pi}{\beta_\perp}} e^{-\frac{c^2}{4}} e^{-\frac{a^2}{8}} \sum_{k,l=-\infty}^{\infty} I_k\left(\frac{ac}{2}\right) e^{ik\left(\omega - \frac{\pi}{2}\right)} I_l\left(\frac{a^2}{8}\right) e^{il2\omega}. \qquad \text{F.4}$$

Therefore, equation F.3 can be written as

$$\begin{aligned} I &= \frac{e^{-\frac{c^2}{4}} e^{-\frac{a^2}{8}} e^{-ik\frac{\pi}{2}}}{2\pi}\sqrt{\frac{\pi}{\beta_\perp}} \sum_{k,l=-\infty}^{\infty} I_k\left(\frac{ac}{2}\right) I_l\left(\frac{a^2}{8}\right) \int_0^{2\pi} d\omega e^{-in\omega} e^{ik\omega} e^{il2\omega} \\ &= \frac{e^{-\frac{c^2}{4}} e^{-\frac{a^2}{8}} e^{-ik\frac{\pi}{2}}}{2\pi}\sqrt{\frac{\pi}{\beta_\perp}} \sum_{k,l=-\infty}^{\infty} I_k\left(\frac{ac}{2}\right) I_l\left(\frac{a^2}{8}\right) 2\pi\delta_{l,\frac{n-k}{2}} \\ I &= e^{-\frac{c^2}{4}} e^{-\frac{a^2}{8}} e^{-ik\frac{\pi}{2}}\sqrt{\frac{\pi}{\beta_\perp}} \sum_{k=-\infty}^{\infty} I_k\left(\frac{ac}{2}\right) I_{\frac{n-k}{2}}\left(\frac{a^2}{8}\right) \equiv I_{n,k}. \end{aligned} \qquad \text{F.5}$$

Appendix F1

The integral evaluated in this Appendix is,

$$I(\mathrm{v}_x) = \int_{-\infty}^{\infty} d\mathrm{v}_x e^{-\left(\beta_\perp \mathrm{v}_x^2 + \frac{i\mathrm{v}_x}{\Omega}\left(k_y - k_\perp \sin\omega\right)\right)}. \qquad \text{F1.1}$$

Consider,

$$\begin{aligned} u &\equiv A\mathrm{v}_x + B \\ u^2 &= A^2\mathrm{v}_x^2 + 2AB\mathrm{v}_x + B^2 \\ e^{-A^2\mathrm{v}_x^2 - 2AB\mathrm{v}_x} &= e^{u^2} e^{B^2} \end{aligned} \qquad \text{F1.2}$$

.

Note also that,

$$d\mathrm{v}_x = \frac{du}{A}$$

With these definitions, it is natural to assign,

$$A = \sqrt{\beta_\perp} \qquad \text{F1.3}$$

and,

$$\begin{aligned} 2AB &\equiv \frac{i}{\Omega}\left(k_y - k_\perp \sin\omega\right) \\ B &= \frac{\frac{i}{\Omega}\left(k_y - k_\perp \sin\omega\right)}{2\sqrt{\beta_\perp}} \\ B^2 &= \frac{-\left(k_y{}^2 - 2k_\perp k_y \sin\omega + k_\perp{}^2 \sin^2\omega\right)}{4\Omega^2\beta_\perp} \end{aligned} \qquad \text{F1.4}$$

Since the sine functions are not multiplied by *i* and are in the argument of an exponential function, it is convenient to change them into cosine functions so that they are in the form of the modified Bessel function. Using

$$\sin\omega = \cos(\omega - \frac{\pi}{2}) \qquad \text{F1.5}$$

and

$$\sin^2\omega = \frac{1}{2}(1 - \cos 2\omega), \qquad \text{F1.6}$$

Equation F1.4 becomes

$$B^2 = \frac{-{k_y}^2 + 2k_\perp k_y \sin\omega - {k_\perp}^2 \sin^2\omega}{4\Omega^2\beta_\perp} = -\frac{{k_y}^2}{4\Omega^2\beta_\perp} + \frac{2k_\perp k_y \cos(\omega - \frac{\pi}{2})}{4\Omega^2\beta_\perp} - \frac{{k_\perp}^2}{4\Omega^2\beta_\perp}\left(\frac{1}{2}(1-\cos 2\omega)\right) \qquad \text{F1.7}$$

$$B^2 = -\frac{{k_y}^2}{4\Omega^2\beta_\perp} + \frac{2k_\perp k_y \cos(\omega - \frac{\pi}{2})}{4\Omega^2\beta_\perp} - \frac{{k_\perp}^2}{8\Omega^2\beta_\perp} + \frac{{k_\perp}^2}{8\Omega^2\beta_\perp}\cos 2\omega.$$

Defining,

$$a^2 \equiv \frac{k_\perp^2}{\beta_\perp\Omega^2} = \frac{2k_\perp^2 \mathrm{v}_{th\perp}^2}{\Omega^2} \text{ and } c^2 \equiv \frac{k_y^2}{\beta_\perp\Omega^2} = \frac{2k_y^2 \mathrm{v}_{th\perp}^2}{\Omega^2}\ , \qquad \text{F1.8}$$

Equation F1.7 becomes,

$$B^2 = -\frac{c^2}{4} + \frac{ac}{2}\cos(\omega - \frac{\pi}{2}) - \frac{c^2}{8} + \frac{c^2}{8}\cos 2\omega\ . \qquad \text{F1.9}$$

Substituting into Equation F1.1,

$$I = e^{-\frac{c^2}{4}} e^{-\frac{a^2}{8}} e^{\frac{ac}{2}\cos(\omega-\frac{\pi}{2})} e^{\frac{a^2}{8}\cos 2\omega} \int_{-\infty}^{\infty} \frac{du}{\sqrt{\beta_\perp}} e^{-u^2}$$

$$I = e^{-\frac{c^2}{4}} e^{-\frac{a^2}{8}} e^{\frac{ac}{2}\cos(\omega-\frac{\pi}{2})} e^{\frac{a^2}{8}\cos 2\omega} \sqrt{\frac{\pi}{\beta_\perp}}\ . \qquad \text{F1.10}$$

With the modified Bessel identity,

$$e^{ax\cos\theta} = \sum_{-\infty}^{\infty} I_n(ax) e^{in\theta}\ , \qquad \text{F1.11}$$

Equation F1.10 becomes

$$I = \sqrt{\frac{\pi}{\beta_\perp}} e^{-\frac{c^2}{4}} e^{-\frac{a^2}{8}} \sum_{j,l=-\infty}^{\infty} I_j(\frac{ac}{2}) e^{ij(\omega-\frac{\pi}{2})} I_l(\frac{a^2}{8}) e^{il2\omega}\ . \qquad \text{F1.12}$$

APPENDIX G Equation (38) expressed in terms of computational variables

The dispersion relation can be expressed as,

$$Q(\hat{B},\hat{\omega},\hat{T}_i,\hat{T}_e,\tau,\hat{V}_o',\hat{V}_o,u,\mu)=0, \tag{G.1}$$

with

$$Q = O(k^2\lambda_{Di\perp}^2)+\hat{T}_i+\sum_{n=-\infty}^{\infty}\Gamma_n(b)F_{ni}+\tau\hat{T}_e(1+F_{0e}),$$

where,

$$F_{ni}=\hat{T}_i^{1/2}\left[\frac{n(1-\hat{T}_i)+\hat{\omega}\hat{T}_i}{u\sqrt{2\hat{B}}}\right]Z\left(\frac{(\hat{\omega}-n)\hat{T}_i^{1/2}}{u\sqrt{2\hat{B}}}\right)-\frac{\hat{T}_i\hat{V}_o'}{u}\left[1+\left(\frac{(\hat{\omega}-n)}{u\sqrt{2\hat{B}}}\hat{T}_i^{1/2}\right)Z\left(\frac{(\hat{\omega}-n)}{u\sqrt{2\hat{B}}}\hat{T}_i^{1/2}\right)\right],$$

$$F_{0e}=\left(\frac{\tau^{1/2}\hat{T}_e^{1/2}}{\sqrt{2}\mu^{1/2}}\left(\frac{\hat{\omega}}{u\sqrt{\hat{B}}}-\hat{V}_0\right)\right)Z\left(\frac{\tau^{1/2}\hat{T}_e^{1/2}}{\sqrt{2}\mu^{1/2}}\left(\frac{\hat{\omega}}{u\sqrt{\hat{B}}}-\hat{V}_0\right)\right)+\frac{\hat{V}_0'}{u\mu}\left[1+\left(\frac{\tau^{1/2}\hat{T}_e^{1/2}}{\sqrt{2}\mu^{1/2}}\left(\frac{\hat{\omega}}{u\sqrt{\hat{B}}}-\hat{V}_0\right)\right)Z\left(\frac{\tau^{1/2}\hat{T}_e^{1/2}}{\sqrt{2}\mu^{1/2}}\left(\frac{\hat{\omega}}{u\sqrt{\hat{B}}}-\hat{V}_0\right)\right)\right],$$

$$\Gamma(b)\equiv I_n(b)e^{-b},$$
$$\hat{B}\equiv(k_y\rho)^2,$$
$$\hat{\omega}\equiv\frac{\omega}{\Omega},$$
$$\hat{T}_i\equiv\frac{T_{i\perp}}{T_{i\|}},$$
$$\hat{T}_e\equiv\frac{T_{e\perp}}{T_{e\|}},$$
$$\tau\equiv\frac{T_{i\perp}}{T_{e\perp}},$$
$$\hat{V}_o'\equiv\frac{V_o'}{\Omega},$$
$$\hat{V}_o\equiv\frac{V_o}{v_{thi\perp}},$$
$$u\equiv\frac{k_\|}{k_y},$$
$$\mu\equiv\frac{M_i}{M_e}.$$

The zero-order expression for real frequency, in terms of the variables used in the computational treatment, is

$$\hat{\omega} \approx u\sigma\sqrt{\frac{B}{\tau\hat{T}_e}}. \qquad \text{G.2}$$

Appendix H The effect of varying the parameter B

The graphs in the ion acoustic mode analysis were generated by fixing the quantity B and varying u. For a proper treatment, however, both wavevector quantities should be scanned, and the peak growth rate should be determined from the two dimensional maximization. The purpose of this appendix is to justify holding B constant. Figure H.1 is a graph of growth rate versus real frequency for varying values of B in a plasma with $T_{i\perp}/T_{i\|} = 2$. Figure H.2 is a graph of growth rate versus real frequency for varying values of B in a plasma with $T_{i\perp}/T_{i\|} = 5$. Each curve is generated by scanning through u with a fixed value of B.

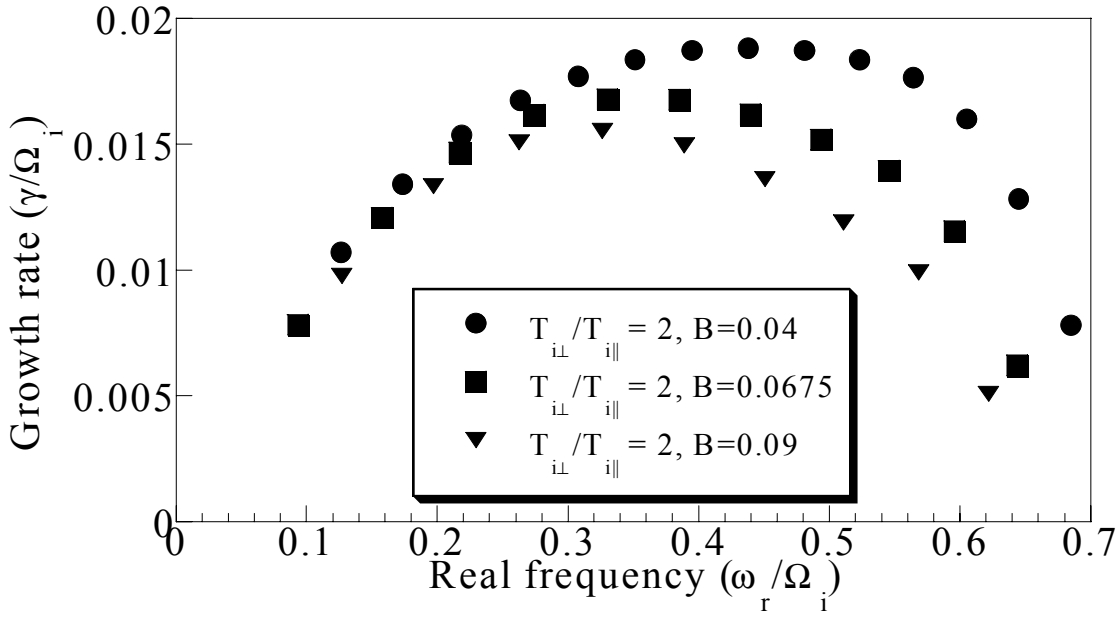

Figure H.1 Growth rate versus real frequency for varying values of B, $T_{i\perp}/T_{i\|} = 2$, $T_{i\perp}/T_{e\perp} = .3, M_i/M_e = 29392, V_o/v_{ith\perp} = 60, |V_o'|/\Omega = .5$.

Figure H.1 shows that maximizing over B results in a small shift in the real frequency at which the maximum growth rate occurs. More importantly, the shift resulting from maximizing over B is an increase in real frequency. Thus, the results of the ion acoustic instability analysis would be more exagerated if B were varied. This increase in shift is traded for simplicity in the analysis.

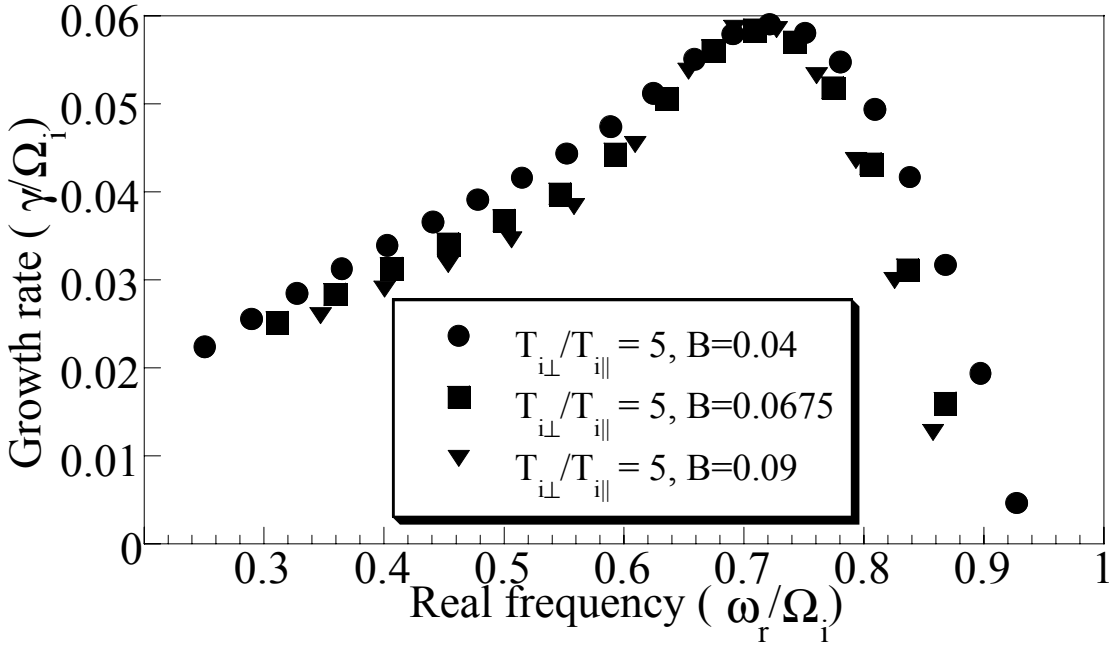

Figure H.1 Growth rate versus real frequency for varying values of B, $T_{i\perp}/T_{i||} = 2$, $T_{i\perp}/T_{e\perp} = .3, M_i/M_e = 29392, V_o/v_{ith\perp} = 60, |V_o'|/\Omega = .5$.

Figure H.1 shows that the effect of varying B is decreased with increasing $T_{i\perp}/T_{i||}$. Since maximizing over B would serve to increase the shift at lower values of $T_{i\perp}/T_{i||}$ and has no effect at higher values of $T_{i\perp}/T_{i||}$, maximizing over u only is justified.

Appendix I Derivation of simplified dispersion relation for ion acoustic mode

The purpose of this derivation is to obtain a simplified version of Equation (38) in the limits appropriate to describe the real frequency of an ion acoustic wave. Beginning with Equation (38) in the limit $(k\lambda_D)^2 \ll 1$, only n=0 terms are retained. That is,

$$\frac{T_{\perp i}}{T_{||i}} + \Gamma_n(b)\frac{T_{\perp i}}{T_{||i}}\left(\frac{\omega}{\sqrt{2}k_{||}v_{th||i}}\right)Z\left(\frac{\omega}{\sqrt{2}k_{||}v_{th||i}}\right) - \frac{T_{\perp i}V_o^{'}(x)}{T_{||i}\Omega u}\left(1+\left(\frac{\omega}{\sqrt{2}k_{||}v_{th||i}}\right)Z\left(\frac{\omega}{\sqrt{2}k_{||}v_{th||i}}\right)\right)+$$
$$\tau\frac{T_{\perp e}}{T_{||e}}\left[1+\left(\frac{\omega-k_{||}V_0(x)}{\sqrt{2}k_{||}v_{th||e}}\right)Z\left(\frac{\omega-k_{||}V_0(x)}{\sqrt{2}k_{||}v_{th||e}}\right)+\frac{V_0^{'}(x)}{u\mu\Omega}\left(1+\left(\frac{\omega-k_{||}V_0(x)}{\sqrt{2}k_{||}v_{th||e}}\right)Z\left(\frac{\omega-k_{||}V_0(x)}{\sqrt{2}k_{||}v_{th||e}}\right)\right)\right]=0\ . \quad \text{I.1}$$

Defining

$$\xi_{ion}=\frac{\omega}{\sqrt{2}k_{||}v_{th||i}};\ \xi_{elec}=\frac{\omega-k_{||}V_0(x)}{\sqrt{2}k_{||}v_{th||e}}, \quad \text{I.2}$$

Equation I.1 is rewritten,

$$\frac{T_{\perp i}}{T_{||i}} + \Gamma_n(b)\frac{T_{\perp i}}{T_{||i}}(\xi_{ion})Z(\xi_{ion}) - \frac{T_{\perp i}V_o^{'}(x)}{T_{||i}\Omega u}\left(1+(\xi_{ion})Z(\xi_{ion})\right)+$$
$$\tau\frac{T_{\perp e}}{T_{||e}}\left[1+(\xi_{elec})Z(\xi_{elec})+\frac{V_0^{'}(x)}{u\mu\Omega}\left(1+(\xi_{elec})Z(\xi_{elec})\right)\right]=0\ . \quad \text{I.3}$$

The real part of the asymptotic Plasma Dispersion Function expansion is used for the ion terms, and the real part of the power series expansion is used for the electron terms. Namely,

$$Z(\xi_{ion})=-\frac{1}{\xi_{ion}}-\frac{1}{2\xi_{ion}^3}+\ldots$$
$$Z(\xi_{elec})=-2\xi_{elec}+\ldots \quad \text{I.4}$$

Equation I.3 becomes

$$\frac{T_{\perp i}}{T_{||i}} + \Gamma_n(b)\frac{T_{\perp i}}{T_{||i}}\left(-1-\frac{1}{2\xi_{ion}^2}\right) - \frac{T_{\perp i}V_o^{'}(x)}{T_{||i}\Omega u}\left(1+\left(-1-\frac{1}{2\xi_{ion}^2}\right)\right)+$$
$$\tau\frac{T_{\perp e}}{T_{||e}}\left[1+-2\xi_{elec}^2+\frac{V_0^{'}(x)}{u\mu\Omega}\left(1+-2\xi_{elec}^2\right)\right]=0\ . \quad \text{I.5}$$

Since an ion acoustic wave is being described, $B \ll 1$. Thus $\Gamma(B) = I_o(B)e^{-B} \approx 1$. Recalling the definition of τ $(= T_{\perp i}/T_{\perp e})$, and multiplying by $T_{\|i}/T_{\perp i}$, Equation I.5 becomes

$$\left(-\frac{1}{2\xi_{ion}^2}\right) - \frac{V_o'(x)}{\Omega u}\left(-\frac{1}{2\xi_{ion}^2}\right) + \frac{T_{\|i}}{T_{\|e}}\left[1 - 2\xi_{elec}^2 + \frac{V_0'(x)}{u\mu\Omega}\left(1 - 2\xi_{elec}^2\right)\right] = 0 \ . \qquad \text{I.6}$$

Reinserting the definitions given by Equations I.2 and assuming that the particles' drift is much less than the parallel electron thermal speed, Equation I.6 is

$$\begin{aligned} 0 &= -\left(\frac{k_{\|}\mathrm{v}_{th\|i}}{\omega}\right)^2 + \frac{V_o'(x)}{\Omega u}\left(\frac{k_{\|}\mathrm{v}_{th\|i}}{\omega}\right)^2 + \\ &\frac{T_{\|i}}{T_{\|e}}\left[1 - \left(\frac{\omega}{k_{\|}\mathrm{v}_{th\|e}}\right)^2 + \frac{V_0'(x)}{u\mu\Omega}\left(1 - \left(\frac{\omega}{k_{\|}\mathrm{v}_{th\|e}}\right)^2\right)\right] \\ &= -\left(\frac{k_{\|}\mathrm{v}_{th\|i}}{\omega}\right)^2\left(1 - \frac{V_o'(x)}{\Omega u}\right) + \frac{T_{\|i}}{T_{\|e}}\left[-\left(\frac{\omega}{k_{\|}\mathrm{v}_{th\|e}}\right)^2\left(1 + \frac{V_0'(x)}{u\mu\Omega}\right) + 1 + \frac{V_0'(x)}{u\mu\Omega}\right] \end{aligned} \qquad \text{I.7}$$

Multiplying by ω^2,

$$-\left(k_{\|}\mathrm{v}_{th\|i}\right)^2\left(1 - \frac{V_o'(x)}{\Omega u}\right) + \frac{T_{\|i}}{T_{\|e}}\left(1 + \frac{V_0'(x)}{u\mu\Omega}\right)\omega^2 - \left(\frac{\omega}{k_{\|}\mathrm{v}_{th\|e}}\right)^2\left(1 + \frac{V_0'(x)}{u\mu\Omega}\right)\omega^2 = 0. \qquad \text{I.8}$$

The last term in Equation I.8 is negligible compared to the rest, so

$$\omega^2 \approx \left(k_{\|}\mathrm{v}_{th\|i}\right)^2 \frac{T_{\|e}}{T_{\|i}} \frac{\left(1 - \frac{V_o'(x)}{\Omega u}\right)}{\left(1 + \frac{V_0'(x)}{u\mu\Omega}\right)}. \qquad \text{I.9}$$

Defining $T_i = Mv_{thi}^2$ and assuming $\mu \gg 1$, Equation H.9 is

$$\omega \approx k_{\|}\sqrt{\frac{T_{\|e}}{M}\left(1 - \frac{V_o'(x)}{\Omega u}\right)}. \qquad \text{I.10}$$

The equivalent expression for the isotropic case [*Gavrishchaka et al*, 1998] is

$$\omega \approx k_{\|} \sqrt{\frac{T_e}{M}\left(1 - \frac{V_o^{'}(x)}{\Omega u}\right)}. \qquad \text{I.11}$$

Appendix J Effect of changing τ to compensate for a change in the electron temperature

The purpose of this appendix is to show the effect of changing the perpendicular ion to electron temperature ratio to compensate for the implied increase in electron temperature when the perpendicular ion temperature is increased. Figure J.1 is a plot of growth rate versus real frequency for plasmas of varying anisotropies. The isotropic case is presented for comparison. The other two curves represent ion acoustic instabilities in plasmas with $T_{\|i}/T_{\perp i} = 2$. The curve with the largest frequency upshift corresponds to an increase in anisotropy with no change in τ, while the curve with no upshift corresponds to a plasma in which τ was increased by the same factor as the anisotropy.

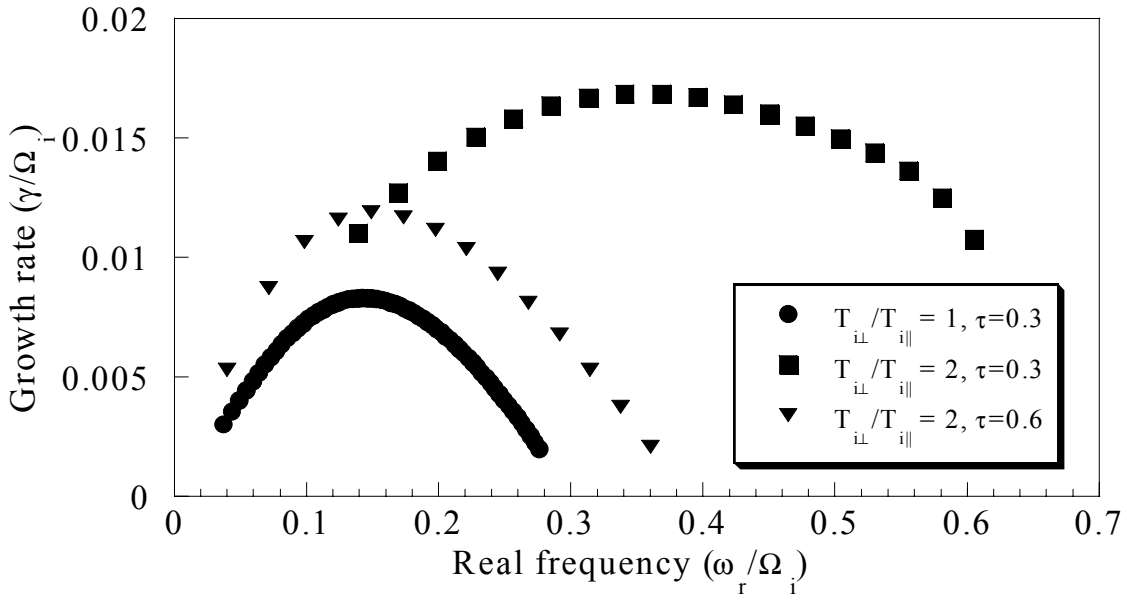

Figure J.1 Growth rate versus real frequency for plasmas of varying anisotropies